Introducing advanced MR imaging for personalized radiotherapy of glioblastoma

Master's thesis

Patrick Tang

Introducing advanced MR imaging for personalized radiotherapy of glioblastoma

P.L.Y. Tang
Student Number: 4330005
11 November 2021

Thesis in partial fulfillment of the requirements for the joint degree of
Master of Science in

Technical Medicine

Leiden University | Delft University of Technology | Erasmus University Rotterdam

Master thesis project (TM30004 | 35 ects)
Department of Radiotherapy | Erasmus MC Cancer Institute | Rotterdam, The Netherlands
Department of Radiology & Nuclear Medicine | Erasmus MC | Rotterdam, The Netherlands
January 2021 - November 2021

Supervisors
dr. A. Mendez Romero
dr. ir. E.A.H. Warnert
drs. J.P.M. Jaspers

Thesis committee members
prof. dr. M.S. Hoogeman (chair)
dr. A. Mendez Romero
dr. ir. E.A.H. Warnert
drs. J.P.M. Jaspers

Preface

As a child, I was intrigued by creativity and innovation, especially in the field of medicine. Apart from the time that eight-year-old me wanted to become a veterinarian (only because I heard my older sister mention something similar), I had always been keen to study medicine after high school. I dreamed of becoming a doctor who worked with the newest technology to help other people. As if it was meant to be, a new bachelor's programme, Clinical Technology, just started when I finished high school. Combining medicine, engineering and physics, Clinical Technology and its master's programme Technical Medicine provided a curriculum where I could unite my passion for technology, medicine and design.

During my internships, I became increasingly fascinated by oncological imaging. In this project, advanced imaging, which visualizes physiology rather than anatomy, is introduced to improve radiation treatment of glioblastomas. The introduction of advanced imaging is like perceiving a whole new dimension that was not visible before. Glioblastomas present themselves highly heterogeneously; therefore, I believe that an improved understanding of their pathophysiology is crucial for personalized treatment.

I would like to thank my supervisors for their valuable insights, patience and exceptional guidance during this project. Alejandra, even with your full schedule, you always made time for me when it was needed most. I will not forget the regular meetings we had in the evenings when we were writing the proposal for the Mosaïc programme. Esther, thank you so much for giving me the freedom in this project to develop my own ideas, while providing crucial input to keep me on the right track. Not only did your extensive feedback bring my project to a higher level, you were also there to give valuable advice for my personal and professional development. Jaap, I am extremely glad that you joined as one of my supervisors in this project. Your enthusiasm and expertise in radiation oncology helped me to understand the complexity of glioblastoma management and to recognize important considerations for this project.

I would also like to thank Fatemeh, Yulun and Karin. You were always willing to answer my (sometimes obvious) technical questions about the advanced imaging techniques or medical imaging file formats. Furthermore, I would like to thank Cleo, who has been responsible for a major part of my clinical experience during this internship. With your open attitude, constructive feedback and a similar sense of humour, my clinical internship has been both informative and enjoyable. Additionally, a special thanks to Jesper and Slávka for their great supervision and a warm welcome at Aarhus University Hospital. You have made my short-term scientific mission extremely insightful and valuable for this project.

Lastly, I would like to express my gratitute to my mom and dad. Thank you for always supporting me and I am proud to say it is you who inspired me to pursue my dreams.

Patrick Tang
Rotterdam, October 2021

Summary

Patients diagnosed with glioblastoma face poor prognosis, as the median survival from initial diagnosis is less than 15 months. Radiotherapy is considered to be one of the fundamentals of glioblastoma therapy and is given after maximum safe tumour resection or biopsy. Delineation of the gross tumour volume (GTV) and the clinical target volume (CTV) required for radiotherapy planning is performed on a combination of computed tomography and conventional, structural magnetic resonance (MR) imaging, which only visualize macroscopic features of the tumour. Due to the infiltrative nature of glioblastomas, the conventional CTV is typically defined as the GTV with an expansion of 1.5 cm. In this project, the aim was to introduce advanced MR imaging in order to visualize microscopic tumour infiltration and construct a personalized approach for CTV delineation to integrate the information provided by the advanced MR imaging. With this biological CTV, the 1.5 cm margin could be omitted and potentially lead to reduced radiation toxicity or improved local tumour control.

The advanced MR biomarkers APT, VSI and rCBV correlate to cell proliferation, vasodilatation and microvascular density, respectively. Brain maps of these biomarkers from four treated glioblastoma patients were introduced in MIM Maestro®, the software package used at the Department of Radiotherapy of the Erasmus MC Cancer Institute for target delineation. In addition, imaging used for radiotherapy, the corresponding delineations, i.e. GTV, CTV and organs at risk, and follow-up imaging that showed first progression according to the response assessment in neuro-oncology criteria were uploaded to MIM Maestro®.

To generate a biological CTV, a semi-automatic workflow was created that incorporates a region growing algorithm to delineate high-risk regions on the biomarker maps. Comparison of biological CTVs with the conventional CTVs showed a major reduction (ranging from 56.7% to 87.6%) in target size. Pattern of failure analysis revealed adequate coverage of the recurrence volume by the biological CTV. In three of the four patients, the biological CTV covered more than 95% of the recurrence volume. In the other patient, the coverage by the biological CTV was poor. This was partially due to the large spread of the recurrence volume.

In this master's thesis, a semi-automatic workflow is presented to take an initial step towards personalized radiotherapy for patients with glioblastoma. The introduction of advanced MR techniques was shown highly promising; future research should focus on optimization of the biological CTV generation and validation of the biomarkers in a larger cohort.

Contents

1

An Introduction to Glioblastoma

1.1 Glioblastoma: Epidemiology and etiology

With an age-adjusted incidence rate of 3.23 per 100000, glioblastomas are the most common primary malignant brain tumours and account for 48.6% of all malignant primary central nervous system (CNS) tumours.[1] They represent the most malignant and aggressive type of gliomas, a heterogeneous group of cancer predominantly arising from glial cells. The incidence rate is 1.6 times higher in men compared to women and glioblastomas are often seen at older ages (median age at diagnosis = 64 years).[2] Regarding ethnicity these tumours are significantly more frequently seen in Whites than other ethnic groups including Latinos, Blacks and Asians.[3, 4] The vast majority of glioblastomas are located supratentorial, most frequently situated in the frontal lobe.[5, 6]

Little is known about the etiology of gliomas. Past exposure to moderate-to-high doses of ionizing radiation is the only well-established risk factor associated with glioblastoma development. Among subjects of the Life Span Study, where life-long health effects following the atomic bombings of Hiroshima and Nagasaki are investigated, an increased incidence for all types of brain tumours was observed.[7] In addition, the risk of glioma development has been reported to be higher in children or infants that received ionizing radiation as treatment for tinea capitis or skin hemangioma or underwent diagnostic computed tomography (CT) scans.[8, 9] Not only does previous exposure to ionizing radiation increase the risk of gliomas in children, but in a cohort of adults that had received radiotherapy for pituitary adenoma an increased incidence of glioma was also observed.[10] As there is no known association between pituitary adenomas and gliomas, this increased risk is likely attributed to the ionizing radiation. Diagnostic use of ionizing radiation in adults, e.g. diagnostic X-rays during dental visits, is not associated with the development of future glioma.[11]

The presence of allergies or other atopic conditions (e.g. asthma and eczema) is inversely associated with gliomas.[12, 13] Individuals with a history of an atopic condition were observed to have a 30% lower risk in developing gliomas.[14, 15] Although it is hypothesized that a hyperactive immune system due to the presence of allergies or other atopic conditions might prohibit abnormal cell growth, a conclusive explanation for this inverse association has remained elusive. Furthermore, various rare hereditary disorders, including Lynch syndrome, neurofibromatosis type 1, Li-Fraumeni syndrome and tuberous sclerosis, are associated with an increased risk of glioma.[16] Smoking, alcohol consumption and diet show no association with glioma development.[17-20]

1.2 Classification of gliomas

Gliomas represent a heterogeneous tumour group that mostly arise from (precursor) glial cells, e.g. astrocytes and oligodendrocytes.[21] Glial cells have a great variety of functions; they can be responsible for the formation of myelin sheaths, maintain homeostasis or provide protection and physical support to neurons.[22] Formerly, classification of gliomas was solely based on histological properties, resulting in all gliomas with an astrocytic phenotype to be classified separately from those with an oligodendroglial phenotype.[23] As many studies have shed light on the involvement of various molecular markers to be of major importance for the prognosis and therapeutic strategy of patients with gliomas, molecular findings were incorporated in the 2016 World Health Organization (WHO) classification of tumours of the CNS.[24] This was the first time that the principle of diagnosis based solely on histology for CNS tumours was broken and a classification based on a combination of histology and molecular markers was introduced. Glioblastomas are graded the most malignant and aggressive type of glioma (i.e. grade IV) and arise from astrocytes. Additionally, since 2020, the updated guidelines provided by the European Association of Neuro-Oncology recognizes that glioblastomas are characterized by the absence of mutations in the isocitrate dehydrogenase (IDH) genes.[25] As IDH-mutation can have a major influence on

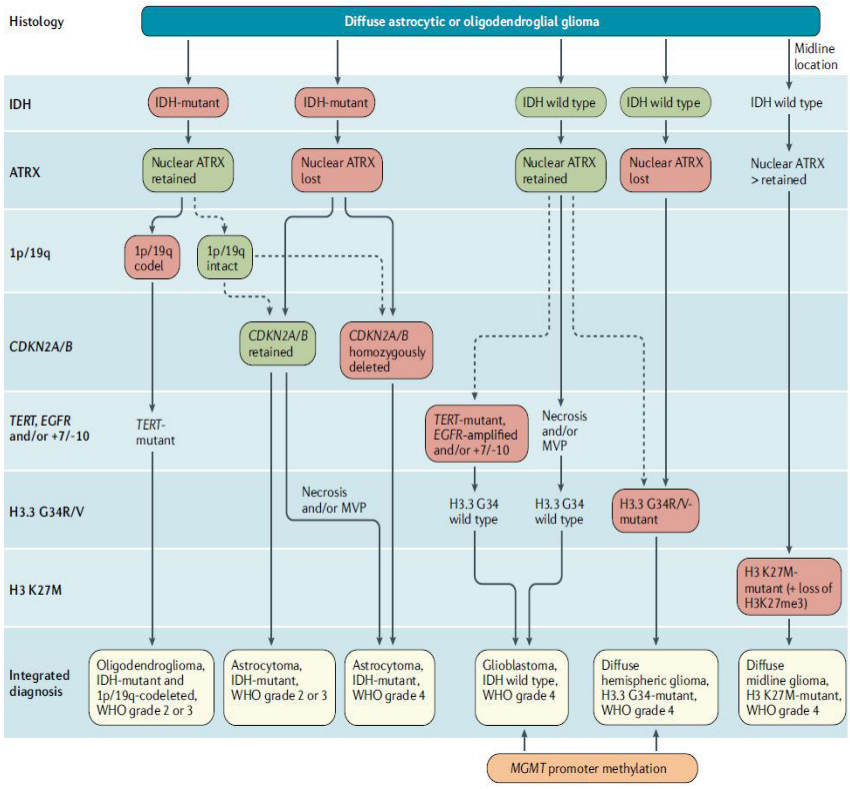

Fig. 1

Diagnostic algorithm for the integrated classification of the major diffuse gliomas in adults. According to this classification glioblastomas are characterized by the absence of mutations in the IDH genes and H3.3 G34R/V. [adapted from Weller et al.[25]]

recommended therapeutic strategy and prognosis, they proposed changing the term IDH-mutated glioblastoma (WHO grade IV) to IDH-mutated astrocytoma (WHO grade IV). Various other molecular biomarkers contribute to the classification of diffuse gliomas (i.e. gliomas with WHO grade II-IV) in adults. In addition to IDH-mutation status the absence of mutations of histone H3 genes is important for the diagnosis of glioblastoma. The 2020 classification proposed by the European Association of Neuro-Oncology for the majority of diffuse gliomas is included in *Fig. 1*.

1.3 Glioblastoma: Clinical presentation

Frequently, the clinical history of patients with glioblastoma is short; in a majority of cases symptoms are first experienced in less than three months before diagnosis.[26] Symptoms can vary depending on various factors including tumour size, tumour location and the degree of peritumoural edema.[27] The most common symptom patients with glioblastoma experience before diagnosis is headache followed by fatigue.[28, 29] Other commonly observed symptoms include nausea, focal deficits, cognitive decline and seizures. New onset seizures has the greatest positive predictive value of all individual symptoms.[29] Combinations of symptoms significantly increase the likelihood of an intracranial tumour being identified on diagnostic imaging.[30]

1.4 Diagnosis and imaging

The gold standard for diagnostic imaging of brain tumours is magnetic resonance (MR) imaging of the brain.[31] (Gadolinium-enhanced) T1-weighted MR imaging along with T2-weighted MR imaging and/or T2-weighted/fluid-attenuated inversion recovery (FLAIR) MR imaging are routinely acquired when a brain tumour is suspected. On contrast-enhanced T1-weighted MR imaging glioblastomas typically present themselves as a heterogeneous and irregular lesion with peripheral enhancement and a non-enhancing central area.[32] The peripheral enhancement is the result of accumulation of the contrast agent as the blood-brain barrier (BBB) is frequently seen to be disrupted in glioblastomas. The non-enhancing central area is caused by a necrotic center. On T2-weighted and T2/FLAIR MR imaging glioblastomas typically show a hyperintense mass surrounded by additional signal abnormality that corresponds to tumour infiltration or edema. A representative case of MR imaging of glioblastoma is shown in *Fig. 2*. The diagnosis of a glioblastoma can only be made final by pathological examination (e.g. after a biopsy).

1.5 Glioblastoma: Management

Glioblastomas are highly malignant and aggressive resulting in patients to have a 3-4 months median survival if untreated.[34] Current standard therapy of newly diagnosed glioblastomas requires a multidisciplinary approach and consists of maximal safe surgical resection followed by concurrent radiotherapy with temozolomide (TMZ) and, subsequently, adjuvant TMZ.[35] The aim of maximal safe surgical resection is to remove as much tumour as safely feasible, however, the infiltrative nature of glioblastomas obstructs complete resection of tumour tissue.[36] Concomitant chemoradiotherapy followed by adjuvant chemotherapy has the goal to target the remaining tumour cells and has shown to improve treatment outcome for glioblastoma patients when compared to patients who only receive postoperative radiotherapy.[37]

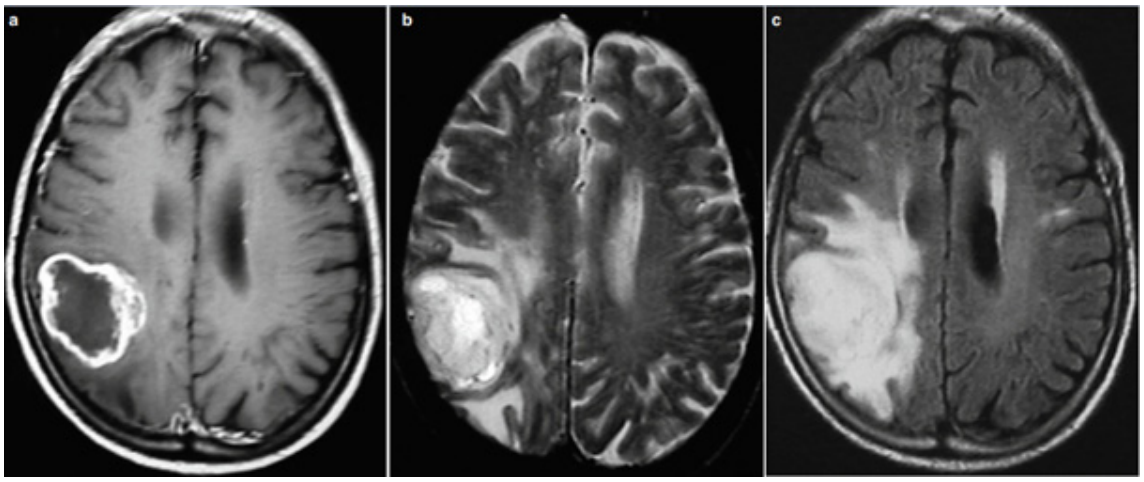

Fig. 2

MR imaging of a patient with a glioblastoma located in the right parietal lobe. The characteristic ring-enhancing lesion with a necrotic center can be seen on the contrast-enhanced T1-weighted MR image (a). Both the T2-weighted MR image (b) and the T2/FLAIR MR image (c) show hyperintensity beyond the ring-enhancing lesion visible on the contrast-enhanced T1-weighted image, indicating the presence of tumour infiltration or peritumoural edema. [Adapted from Drevelegas et al.[33]]

2

Radiotherapy for Glioblastoma

2.1 An introduction to radiotherapy

For more than a century, radiotherapy has been applied as an effective treatment for various types of cancer.[41] The goal of radiotherapy is to kill cancer cells or slow tumour growth with the use of ionizing radiation, which is a type of radiation that has sufficient energy to release electrons from atoms and molecules. The majority of cells within the human body carry deoxyribonucleic acid (DNA), a complex molecule composed of two polynucleotide chains that are connected by hydrogen bonds.[42] Within DNA all the genetic information of an organism is stored. Ionizing radiation can induce single-strand and/or double-strand breaks in DNA by affecting its structure either directly or indirectly.[43] The latter results from the production of free radicals that are created by the ionization of the water component within the cell. Both the direct and indirect effect of ionizing radiation on DNA can lead to the discontinuation of cell division and/or apoptosis, especially when double-stranded breaks occur.[44] As the effect of ionizing radiation is more profound in rapidly proliferating cells, ionizing radiation is particularly suitable for cancer treatment.[45]

2.2 The principles of external beam radiotherapy

Since its first therapeutic application, new insights and developments have resulted in numerous techniques being developed to apply ionizing radiation clinically. The preferred technique depends on many aspects including tumour characteristics, aim of the treatment and surrounding organs at risk. The most common approach used in clinical practice is external beam radiotherapy (EBRT). An external source of ionizing radiation is used to aim high-energy rays to a specific target volume within the human body. Nowadays, the linear accelerator (Linac) is often the device of choice for EBRT.[46] In the Linac electrons are accelerated towards a heavy metal target, e.g. tungsten, producing high-energy X-rays upon collision. The X-rays are directed to the target region and shaped conform the tumour by a multi-leaf collimator that has the aim to minimize the dose to surrounding healthy tissue. The gantry, i.e. the part of the Linac where the X-rays are directed to

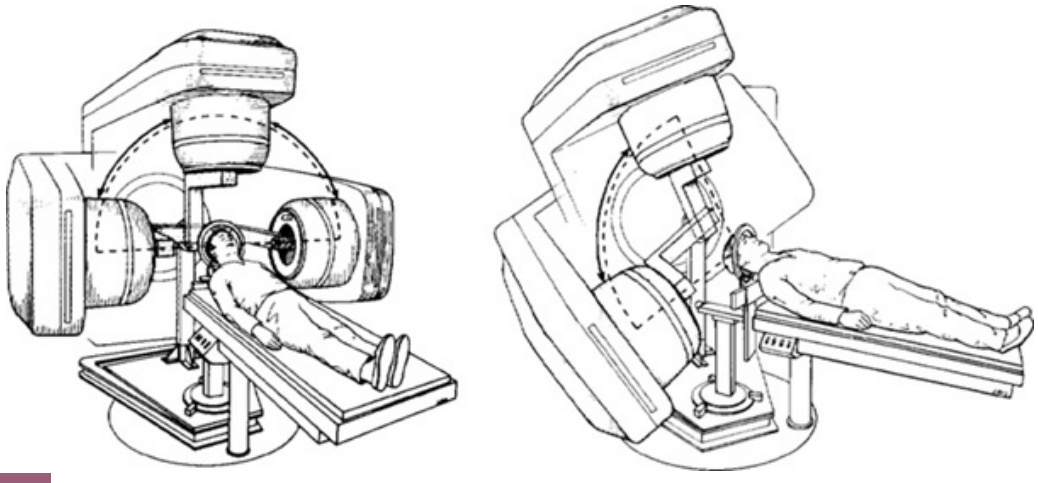

Fig. 3

The patient lies on a bed while the high-energy photons are directed to the tumour. Some Linacs can acquire cone-beam computed tomography scans perpendicular to the therapy beam to improve patient positioning (left). The gantry of a Linac can rotate around the patient to allow beam therapy from different angles (right). [Adapted from Friedman et al.[47]]

the tumour, can rotate around the patient to give radiation dose from different angles. By rotating the gantry and shaping the X-rays conform the tumour, the intent is to give sufficient radiation dose to the tumour while limiting harm to surrounding healthy tissue. An example of a Linac is shown in *Fig. 3.*

2.3 Radiation toxicity

The use of ionizing radiation as cancer treatment is accompanied with the risk of developing radiation toxicity.[48] The risk of developing radiation toxicity is closely related to a patient's absorbed dose, which is defined as the concentration of energy deposited in tissue as a result of exposure to ionizing radiation. Absorbed dose is expressed in gray (Gy); 1 Gy is equal to 1 Joule/kilogram. The manifestation of radiation toxicity can be acute or emerge at later stages and varies depending on a broad range of aspects, e.g. the location of absorbed dose.[49] Patients with prostate cancer who undergo radiotherapy, for example, have a higher risk of developing urinary obstruction as a consequence of radiation exposure, whereas patients who receive radiotherapy of the brain are more prone to present themselves with cognitive deterioration.[50, 51] Common generic symptoms of radiation toxicity after EBRT for cancer treatment include skin dermatitis, fatigue and nausea.[52] The risk of radiation toxicity can outweigh the benefits of radiotherapy as cancer treatment and result in the decision to settle for underdosing of the target or even eliminating radiotherapy as a treatment option. Radiotherapy planning, therefore, will always consist of a balance between the dose delivered to the tumour (probability of tumour control) and the dose delivered to the surrounding normal tissue or organs at risk (potential radiation toxicity).

2.4 The importance of target definition for radiotherapy

Ideally, radiotherapy would deliver radiation dose solely to regions that contain tumour tissue as ionizing radiation is accompanied with the risk of developing radiation toxicity. Over the past few decades, novel radiation techniques for EBRT have allowed for highly conformal dose distributions with improved target coverage and better sparing of healthy tissue.[53] Volumetric modulated arc therapy (VMAT) is a technique that delivers radiation to the patient from a full 360° beam angle by rotating the radiation source continuously. Treatment delivery of VMAT can be done with a Linac and relies upon simultaneous variation of three parameters: Gantry rotation speed, treatment aperture shape through the multi-leaf collimator and dose rate.[54] With VMAT the opportunity arises to achieve improved target volume conformity and better sparing of adjacent healthy tissue, particularly in complex concave shapes. Accurate target delineation, therefore, is crucial to exploit the full potential of VMAT.

In general, a total of three target volumes are defined for radiotherapy planning.[55] The first is the gross tumour volume (GTV), which encompasses the macroscopic extent of the tumour or the tumour bed if the patient has undergone surgery. The delineation of the GTV is often done on computed tomography (CT) combined with MR imaging. The second volume is the clinical target volume (CTV). The CTV contains the GTV, plus a margin to cover for microscopic disease. Although not fully visible on imaging, it is assumed that tumour is present within this margin and, therefore, should be treated adequately. Guidelines on the delineation of the CTV vary per tumour group as some tumours have a higher likelihood to develop microscopic spread of disease. Lastly, the planning target volume (PTV) encloses the CTV with an additional margin to allow for uncertainties in planning and treatment delivery, e.g. patient positioning. A schematic visualization of the GTV, CTV, PTV is shown in *Fig. 4.*

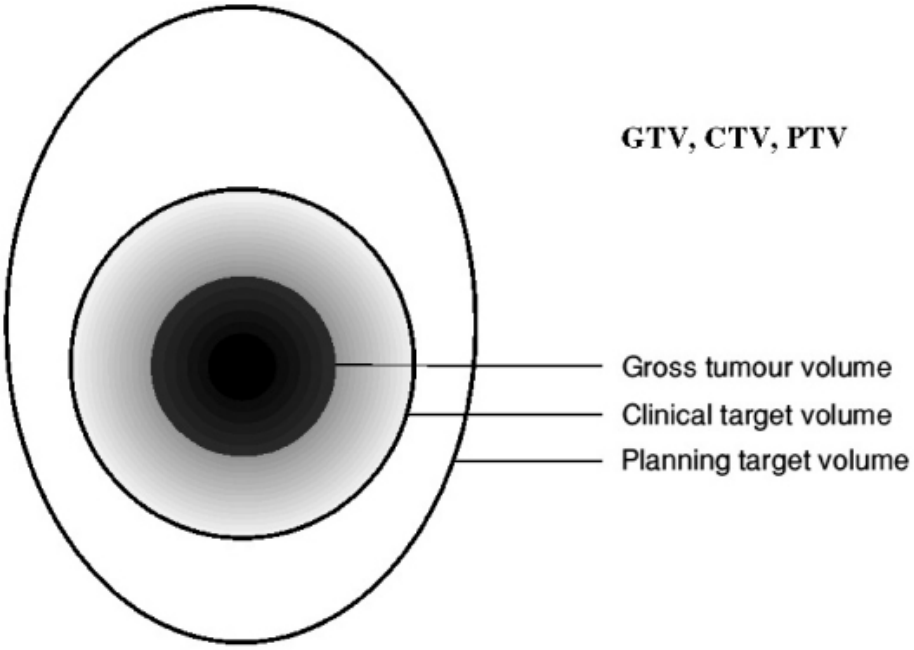

Fig. 4

A schematic overview of the volumes frequently delineated/generated for radiotherapy planning. The GTV is defined as macroscopic tumour visible on medical imaging, whereas the CTV additionally covers for microscopic disease. Finally, the PTV encloses the CTV to cover for geometric uncertainties. [Adapted from Burnet et al.[55]]

Apart from the three target volumes, organs or structures at risk of developing radiation toxicity when receiving excessive dose, are delineated as well.[56] The tolerance of ionizing radiation from these organs at risk is to be taken into account during radiotherapy planning. When the dose constraint of an organ at risk is exceeded in a radiotherapy plan, the radiation oncologist can opt to reduce the target dose or conclude radiotherapy to be infeasible.

2.5 External beam radiotherapy as treatment for glioblastomas

In the late 1970s it was shown that postoperative whole-brain radiotherapy (WBRT) could improve the survival for patients with high-grade glioma significantly, resulting in postoperative radiotherapy becoming part of the standard treatment of newly diagnosed glioblastoma.[57] Subsequently, comparison between WBRT and partial-brain irradiation demonstrated no advantage of WBRT regarding overall survival.[58] Partial-brain irradiation is preferred over WBRT to minimize radiation-induced complications like neurocognitive toxicity or leukoencephalopathy.

In current clinical practice, EBRT is given 3 – 5 weeks after surgery of newly-diagnosed glioblastoma.[25] Before radiotherapy is started, the procedure will be explained to the patient by a radiation oncologist. The procedure consists of four phases: Preparation, radiotherapy planning, treatment delivery and follow-up. In *Fig. 5* a schematic overview is given of the procedure.

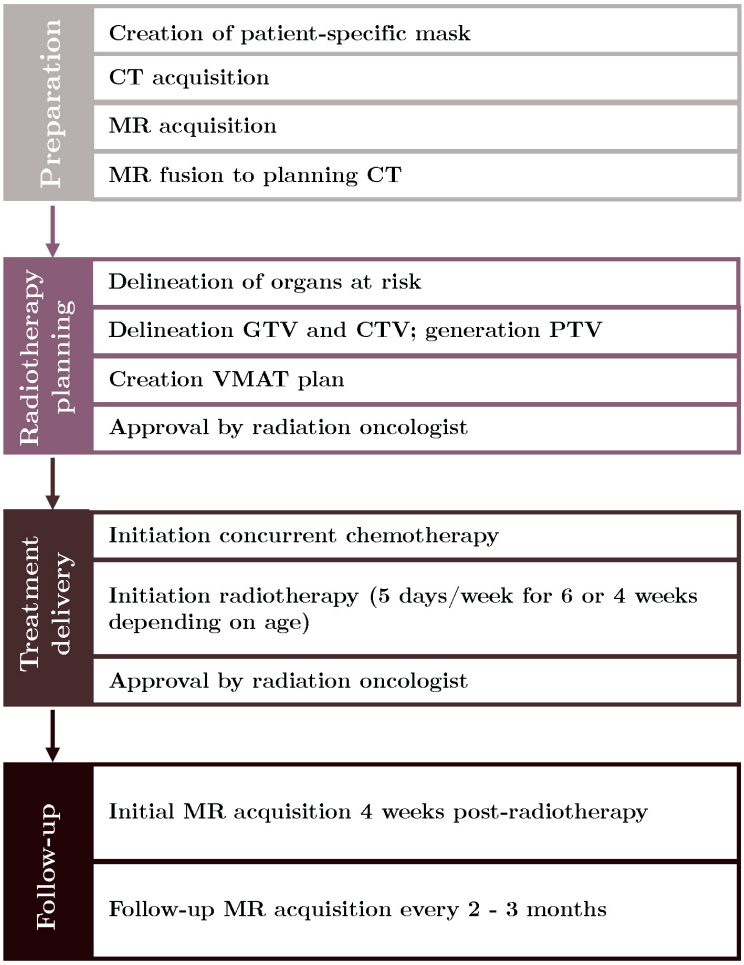

Fig. 5

A schematic overview of the radiotherapy procedure for patients with newly-diagnosed glioblastoma. The first stage (preparation) consists of the creation of a mask for immobilization and acquisition and fusion of the required imaging. The second stage (radiotherapy planning) involves the delineation and generation of the relevant structures and volumes and creation of a VMAT plan. In the third stage (treatment delivery) the patient receives both radiotherapy and chemotherapy. The final stage (follow-up) includes monitoring of the patient after radiotherapy.

2.5.1 Preparation

During preparation, a patient-specific thermoplastic mask is created to ensure accurate re-positioning.[59] The mask can be fixated to the bed to immobilize the patient's head. Subsequently, a CT-scan of the patient's brain (while fixated by the thermoplastic mask) is acquired for radiotherapy planning. MR imaging is acquired in addition to aid in delineation of the target volumes and organs at risk. Delineation on CT only has shown insufficient tumour coverage and can miss 20% of the target volume delineated on MR imaging.[60] Therefore, contrast-enhanced T1-weighted and T2-weighted/FLAIR imaging are often fused with the planning CT for radiotherapy planning.[61]

2.5.2 Radiotherapy planning

After the registration of the MR imaging to the planning CT is approved, delineation of the target volumes and organs at risk can be performed. Delineation of the organs at risk can be done manually or semi-automatically and include the optic nerves, optic chiasm, cochleas, retinas, lenses, eyes, lacrimal glands, pituitary, brain and brainstem.[61] Guidelines on delineation of the target volumes and the target dose of glioblastomas differ in two accustomed protocols, which are provided by the Radiation Therapy Oncology Group (RTOG) and the European Organisation for Research and Treatment of Cancer (EORTC).

The RTOG protocol recommends radiotherapy of glioblastoma to be performed in two phases.[62] The first phase comprises a total dose of 46 Gy to the target in 23 fractions of 2 Gy. The GTV in this phase encloses the resection cavity, (residual) contrast-enhancing areas on T1-weighted imaging post gadolinium and signal abnormalities on T2-weighted/FLAIR imaging. Subsequently, the CTV is defined as a 2 cm expansion of the GTV (2.5 cm when no peritumoural edema is visible on MR imaging) and is adjusted for anatomical barrier, e.g. the falx cerebri or the tentorium cerebelli. The PTV adds an additional margin of 0.3 - 0.5 cm to the CTV. In the second phase, an additional total dose of 14 Gy is given in seven fractions of 2 Gy to parts of the initial target. The GTV for this additional dose is defined as the contrast-enhancing area and the resection cavity, but does not include signal abnormalities on T2-weighted/FLAIR imaging. An isotropic expansion of 2 cm is applied to define the CTV and thereafter the PTV margin applied in the first phase is reused to define the PTV for the second phase.

The EORTC guidelines recommend a single-phase approach where the target receives 60 Gy in 30 fractions.[61] The GTV is defined as the resection cavity and any residual contrast enhancement. Additional information on T2-weighted/FLAIR imaging can be included in the delineation of the GTV. Formerly, the CTV was defined as a 2 cm isotropic expansion of the GTV with correction for anatomical barriers, however, recent guidelines state the feasibility of a reduced margin ranging between 1 and 2 cm to create the CTV.[25] Finally, the PTV is defined in similar fashion as the RTOG guidelines (0.3 – 0.5-cm around the CTV).

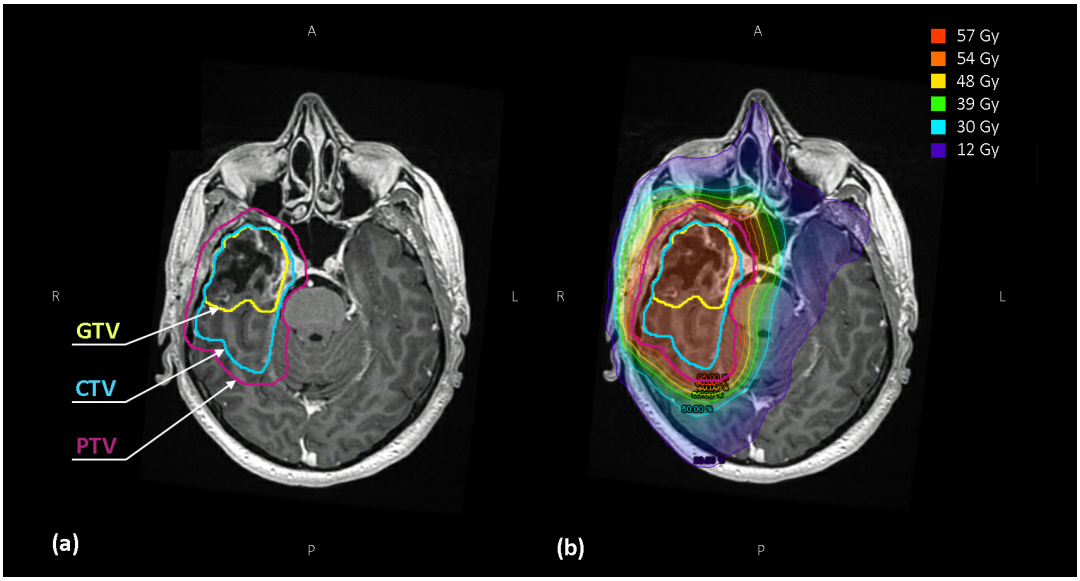

Fig. 6

Two axial views of a patient with a confirmed glioblastoma in the right temporal lobe after resection. Delineations of the GTV and CTV and generation of the PTV were performed with the aid of MR imaging; the CTV consists of a 1.5 cm expansion of the GTV and is corrected for anatomical barriers and organs at risk, e.g. the brainstem and the cerebellum (a). The VMAT plan allows for adequate target volume conformity (b).

At the Erasmus MC Cancer Institute *(Rotterdam, the Netherlands)*, radiotherapy planning of glioblastoma follows the principles of the EORTC consensus. As the vast majority of recurrences occur central, i.e. within the 95% isodose line of 60 Gy, the standard CTV margin at the Erasmus MC Cancer Institute is set at 1.5-cm.[63-65] Various studies on dose escalation, i.e. the use of radiation plans with a target dose higher than 60 Gy, have shown no major benefits on survival.[66, 67]

After delineation of the target volumes and organs at risk, a VMAT plan is created. In general, younger patients (under 65 years of age) are to receive a total target dose of 60 Gy in 30 fractions of 2 Gy, whereas elderly patients (65 years of age or older) will receive short-course radiotherapy (total target dose of 40 Gy in 15 fractions of 2.67 Gy).[25, 68] In *Fig. 6*, an example of the target volumes and radiotherapy planning is shown.

2.5.3 Treatment delivery

After approval of the radiotherapy plan by the radiation oncologist (in agreement with the medical physicist), the treatment can be initiated. The duration of the treatment is five days a week for six weeks for younger patients; each session the patient receives a fraction of 2 Gy to the target. Elderly patients will receive fractions of 2.67 Gy to the target for a duration of three weeks (five days per week). Simultaneously with the radiotherapy, a course of TMZ is initiated. Parallel treatment of radiotherapy and chemotherapy was shown to benefit overall survival.[37]

2.5.4 Follow-up

Although adjuvant chemotherapy is part of standard treatment of newly-diagnosed glioblastoma, MR imaging is acquired approximately 4 weeks after completion of radiotherapy to provide a baseline to monitor the further course of the disease. With initial intervals of 2 – 3 months neuroimaging is acquired to assess the status of the disease according to the Response Assessment in Neuro-Oncology (RANO) criteria.[69] Pseudo-progression, which is a post-radiotherapy phenomenon where damage to epithelial cells and increased inflammation present itself similar to tumour progression on conventional MR imaging, can complicate the detection of true tumour progression.[70] When progression is suspected during follow-up, potential treatment options are explored during multidisciplinary consultation.

3

Individualizing radiotherapy for glioblastomas

3.1 Microscopic tumour infiltration complicates radiotherapy

Radiotherapy is considered to be one of the fundamentals of glioblastoma therapy. A key characteristic of glioblastoma is its highly infiltrative nature, which is one of the root causes of curative treatment being nearly impossible.[71] As microscopic tumour infiltration cannot be visualized with CT or conventional MR techniques (i.e. T1 or T2/FLAIR imaging), the CTV requires a 1 – 2 cm expansion of the GTV in every direction. If microscopic tumour invasion could be visualized, the possibility arises to omit the isotropic approach and only include true tumour infiltration in the CTV. This could lead to better local tumour control and reduced radiation toxicity, which in turn can result in improved survival and quality of life for glioblastoma patients. The latter is equally important due to the extremely poor prognosis glioblastoma patients face.

3.2 Introducing advanced MR imaging

Structural MR imaging, e.g. T1-weighted or FLAIR imaging, has emerged as the imaging modality of choice for the diagnosis and monitoring of intracranial tumours. The use of advanced MR techniques, however, has remained limited. Whereas structural MR imaging offers detailed anatomic information, advanced MR techniques grant the ability to evaluate key pathophysiological features of glioblastomas. A broad range of advanced MR techniques have been developed and each technique targets a different physiological aspect, e.g. mitotic activity or angiogenesis.[72] Whereas conventional MR techniques lack the ability to visualize microscopic tumour invasion, some advanced MR techniques could have the potential to provide new information needed to identify tumour infiltration.

3.3 Thesis overview

This master's thesis has the main goal to take an initial step towards personalized radiotherapy for patients with glioblastoma by introducing advanced MR techniques. With advanced MR imaging it might be possible to visualize microscopic tumour infiltration or predict the location of future recurrence; the integration of advanced MR imaging for radiotherapy planning could therefore result in more accurate clinical target volume delineation and improve patient outcomes. The following subgoals were set for this project:

1. To explore the potential of advanced MR techniques and the corresponding imaging biomarkers to assess which (combination of) imaging techniques are most promising for personalized radiotherapy planning of glioblastomas. *(Chapter 4)*

2. To integrate advanced MR imaging into MIM Maestro®, the software package used at the Department of Radiotherapy of the Erasmus MC Cancer Institute *(Rotterdam, the Netherlands)*, for CTV delineation. *(Chapters 5 - 7)*

3. To develop a semi-automatic workflow for the generation of a biological CTV, i.e. a CTV based on advanced MR imaging rather than a 1.5 cm expansion. *(Chapters 8 - 9)*

4. To assess the potential of advanced MR imaging to reduce radiation toxicity and improve local tumour control by comparing the size and recurrence coverage of the conventional CTV and the biological CTV. *(Chapter 10)*

5. To propose future research and investigate promising directions in the field of personalized radiotherapy planning for glioblastoma patients. *(Chapters 11 – 12)*

First, a literature review is presented in *Chapter 4* outlining various advanced MR techniques and their potential for CTV delineation. Secondly, an overview of the included patients is provided in *Chapter 5*. The imaging from subjects from the iGene study, in which various advanced MR images were acquired preoperatively in patients with glioma, was used for this project. In *Chapter 6*, a pipeline is described to integrate advanced MR imaging into MIM Maestro®. The approach for image registration is narrated in *Chapter 7*. Subsequently, a semi-automatic workflow for the generation of a biological CTV in MIM Maestro using region growing is proposed in *Chapter 8* and *Chapter 9*. Assessment on size and coverage of recurrences was performed to evaluate the potential of the advanced MR imaging biomarkers for radiotherapy planning in *Chapter 10*. In *Chapter 11*, the outcomes of my short-term scientific mission at Aarhus University Hospital *(Aarhus, Denmark)* is presented. Short-term scientific missions are exchange visits funded by the COST Action, allowing researchers to gain new insights on a particular subject at another institute. At Aarhus University Hospital, a similar project has been initiated that incorporates an alternative advanced MR technique for radiotherapy of glioblastoma. Lastly, suggestions for future directions are proposed in *Chapter 12*.

4

The potential of advanced MR techniques for precision radiotherapy of glioblastoma: A review

The potential of advanced MR techniques for precision radiotherapy of glioblastoma multiforme: A review.

Patrick L.Y. Tang[1,2], Alejandra Méndez Romero[1],
Jaap P.M. Jaspers[1], Esther A.H. Warnert[2]

[1] *Department of Radiotherapy, Erasmus MC Cancer Institute, Rotterdam, The Netherlands.*

[2] *Department of Radiology & Nuclear Medicine, Erasmus MC, Rotterdam, The Netherlands.*

As microscopic tumour infiltration of glioblastomas is not visible on conventional MR imaging, an isotropic expansion of 1.5 cm around the visible tumour is applied to define the clinical target volume for radiotherapy. An opportunity to visualize microscopic infiltration arises with advanced MR imaging. In this review various advanced MR biomarkers are explored that could improve target volume delineation for radiotherapy of glioblastomas. Various physiological processes in glioblastomas can be visualized with different advanced MR techniques. Combining maps of oxygen metabolism ($CMRO_2$), relative cerebral blood volume (rCBV), vessel size imaging (VSI) and amide proton transfer (APT) can provide early information on tumour infiltration and high-risk regions of future recurrence. Oxygen consumption is increased six months prior to tumour progression being visible on conventional MR imaging. However, presence of the Warburg effect, marking a switch from an infiltrative to a proliferative phenotype, could result in $CMRO_2$ to appear unaltered in high-risk regions. Including information on biomarkers representing angiogenesis (rCBV and VSI) and cell proliferation (APT), can omit misinterpretation due to the Warburg effect. Future research should evaluate these biomarkers in radiotherapy planning to explore the potential of advanced MR techniques to individualize target volume delineation and reduce radiation-induced toxicity.

[Submitted to Magnetic Resonance Materials in Physics, Biology and Medicine (MAGMA)]

4.1 Introduction

Patients diagnosed with glioblastoma face poor prognosis, as the median survival from initial diagnosis is less than 15 months.[37] Current practice in management of glioblastoma comprises of maximum safe tumour resection or biopsy followed by postoperative chemoradiotherapy and adjuvant chemotherapy.[35] Delineation of the GTV and the CTV required for radiotherapy planning is performed on a combination of CT and conventional MR imaging only visualizing macroscopic features of the tumour.[61] Incorporating information on microscopic tumour invasion might con-

tribute to identification of future sites of relapse. A field size reduction based on this information could lead to smaller treatment volumes without sacrificing local control, potentially reducing the risk of radiation-induced toxicity. Over the past decade, advanced MR techniques have offered the ability to visualize pathophysiological properties of tumours. These properties can provide additional information on tumour infiltration, aggressiveness, treatment response and overall tumour behaviour. In this review, the aim is to evaluate promising advanced MR techniques that have potential to improve delineation of the CTV for individualized radiotherapy of glioblastomas.

4.1.1 Glioblastoma Management

Glioblastomas are the most common primary malignant brain tumours, accounting for almost 50% of all malignant primary CNS tumours.[1] The 2016 WHO classification of tumours of the CNS defines glioblastoma as a group of tumours that originates from astrocytes and displays an aggressive and infiltrative behaviour.[24] Additionally, since 2020, the updated guidelines provided by the European Association of Neuro-Oncology recognizes that glioblastomas are characterized by the absence of mutations in the IDH genes.[25] The prognosis of patients with glioblastoma varies depending on several factors including age, performance status and molecular biomarkers, e.g. MGMT promotor methylation status.[38, 39, 73] In general, however, the course of patients with glioblastoma is poor.[74, 75] Current standard treatment of glioblastomas consists of a multidisciplinary approach, where maximal safe surgical resection is followed by concurrent radiation with TMZ and then adjuvant chemotherapy with TMZ.[37]

4.1.2 The Role of Radiotherapy in the Treatment of Glioblastoma

As postoperative WBRT was shown to improve the survival for patients with high-grade glioma in the late 1970s, postoperative radiotherapy became part of the standard treatment of newly diagnosed glioblastomas.[57] Comparison between WBRT and partial-brain irradiation demonstrated no advantage of WBRT regarding overall survival.[58] Partial-brain irradiation is preferred over WBRT to minimize the risk of radiation-induced toxicity, e.g. cognitive impairment.

In the current clinical routine, target volume delineation for radiotherapy planning of glioblastoma is performed on a fusion of CT and MR imaging. Delineation on CT only has shown insufficient tumour coverage and can miss a significant part of the target volume delineated on MR imaging.[60] Therefore, contrast-enhanced T1-weighted and T2-weighted/FLAIR sequences are fused with the planning CT for radiotherapy planning. Microscopic tumour infiltration, which is a key characteristic of glioblastomas, however, cannot be fully visualized by these structural MR sequences. Hence, an additional standard expansion to the GTV is added to cover for nonvisible tumour invasion, creating the CTV.[76] Based on early studies on recurrence patterns and tumour infiltration the CTV initially consisted of the GTV with an isotropic expansion of 20 mm.[61] Analyses in several cohorts have shown that recurrence coverage and overall survival with smaller margins for the CTV are likely comparable to the margin of 20 mm.[64, 77-79] The majority of recurrences were observed to occur central, meaning a smaller margin could result in reduced radiation toxicity while achieving similar tumour control. The typical total dose given to the PTV is 60 Gy delivered in 2 Gy fractions administered five days per week for six weeks.[61] Various studies on dose escalation have shown no major benefits on survival.[66, 67]

4.2 Advanced MR Techniques to Assess Physiology in Glioblastoma

Various pathological processes in glioblastomas can be visualized with different advanced MR

techniques. In this section an overview is given of physiological processes present in glioblastoma and how (advanced) MR techniques can exploit these properties for tumour detection.

4.2.1 Blood-Brain Barrier Disruption: The Role of Contrast Agents

Inherent differences in T1 and T2 relaxation of different types of tissue allow for the excellent soft tissue signal contrast of MR imaging. Exogeneous contrast agents based on low-molecular-weight gadolinium are commonly used in neuro-oncology. These agents locally shorten the T1 relaxation times and allow for better contrast between regions with and without the contrast agent. The BBB in the healthy brain usually restricts the contrast agent to the vascular bed. Disruption of the BBB, e.g. caused by glioblastoma, can lead to accumulation of these agents in the interstitial spaces surrounding the leaky vasculature.[80] As shown in *Fig. 7*, accumulation can be seen as an increase in signal intensity on conventional T1-weighted MR imaging. This so-called contrast enhancement is currently used in clinical practice as a surrogate measure of malignancy.[81]

4.2.2 Vascular Permeability: The Role of Contrast Agents

The principles of dynamic contrast-enhanced (DCE) MR imaging are based on the exchange of gadolinium based contrast agents between the intravascular compartment and the interstitial tissue. By measuring the time course of the contrast agent as it diffuses from the blood pool into tissue information on flow and permeability of the vasculature can be obtained. DCE-MR imaging can be used to study vascular leakiness and has great potential to monitor changes in vascular permeability arising from antiangiogenic therapies.[82] An example of DCE-MR imaging can be seen in *Fig. 8*.

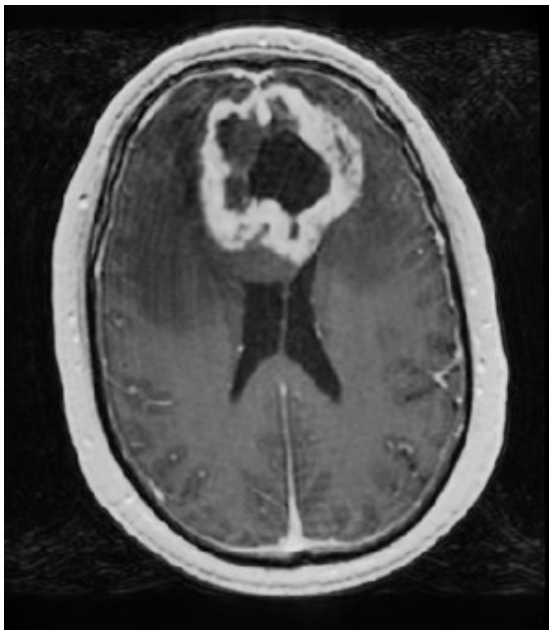

Fig. 7

Post gadolinium based contrast-enhanced T1-weighted axial image. A ring enhancing lesion, in this case a glioblastoma, can be seen. The peripheral enhancement is caused by accumulation of the contrast agent due to disruption of the BBB.

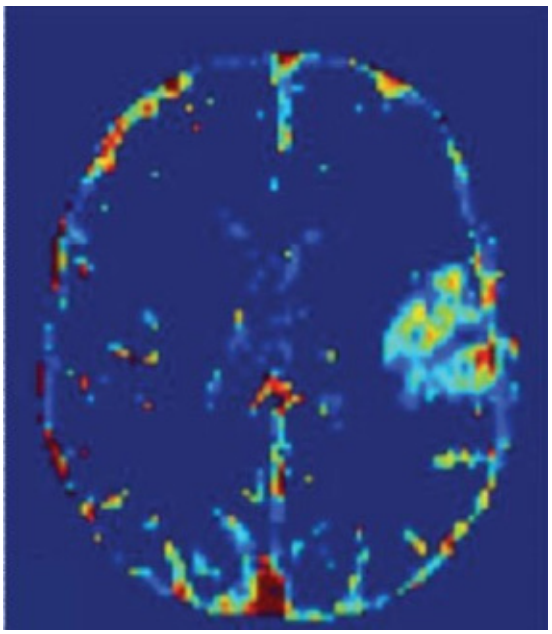

Fig. 8

The increase of signal intensity in the left parietal lobe suggests the presence of contrast agent. DCE-MR imaging can be used to study vascular permeability in tumours. [Adapted from Kalpathy-Cramer et al.[72]]

4.2.3 Angiogenesis: Exploiting the Magnetic Susceptibility of Contrast Agents

Malignant gliomas are characterized by a high degree of angiogenesis, resulting in increased neovasculature and vasodilatation.[83] Histologically, the abnormal number of tumour vessels can be measured by determination of the microvascular density.[84] This process, however, requires tissue sampling and can be time consuming.[85] Dynamic Susceptibility Contrast (DSC) MR imaging, where a time series of gradient echo images in which passage of a bolus of contrast agent is acquired, offers an alternative to histological assessment of microvascular density. Within gliomas the relative cerebral blood volume (rCBV), one of the perfusion parameters that can be examined using DSC-MR imaging, has been shown to correlate significantly with microvascular density.[86] An example of an rCBV map is provided in *Fig. 9*.

When performing DSC-MR imaging with a gradient and spin echo acquisition, the acquired images can also be used for vessel size imaging (VSI).[87] This technique was shown to estimate vessel size in good concordance with histological assessment of vessel diameters in human gliomas.[88] An example of VSI is given in *Fig. 10*.

As both neovascular activity and vasodilatation can be evaluated using DSC-MR imaging, this technique is a promising tool to assess the degree of angiogenesis within glioblastomas.

4.2.4 Angiogenesis: The Use of Magnetically Labelled Blood

An alternative parameter to assess vascular proliferation within glioblastoma is regional cerebral blood flow (CBF). Relative CBF has shown a positive correlation with rCBV as an increase in CBF can be observed in high-grade gliomas, see *Fig. 11*.[89] Arterial spin labelling (ASL) is a non-invasive MR technique used to measure CBF. By magnetically labelling the water molecules in arterial blood, which then flows into the brain, a tagged image of the brain can be acquired.

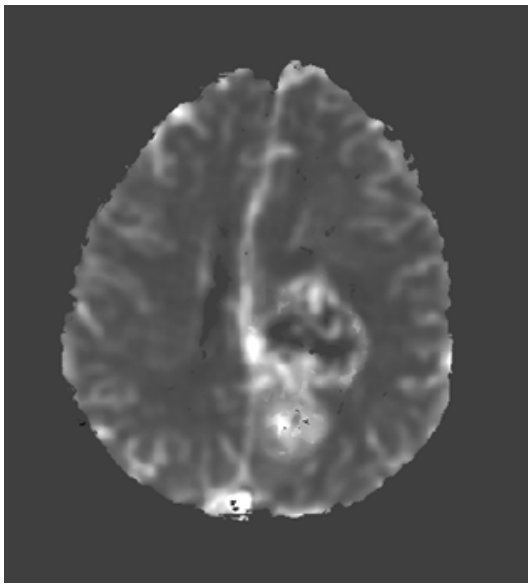

Fig. 9

Post gadolinium based contrast-enhanced T1-weighted axial image. A ring enhancing lesion, in this case a glioblastoma, can be seen. The peripheral enhancement is caused by accumulation of the contrast agent due to disruption of the BBB.

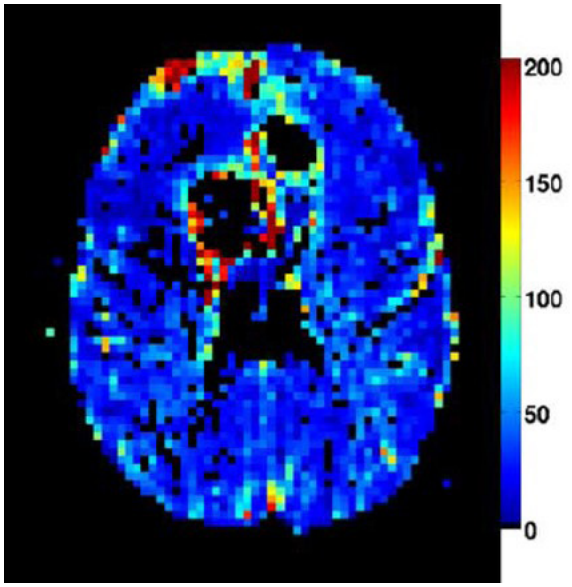

Fig. 10

A map displaying vessel size in a patient with glioblastoma. An increase of vessel diameters is observed in the area that corresponds with the ring enhancement seen on post-contrast T1-weighted imaging. The colour bar encodes the vessel size in μm [Adapted from Kellner et al.[88]]

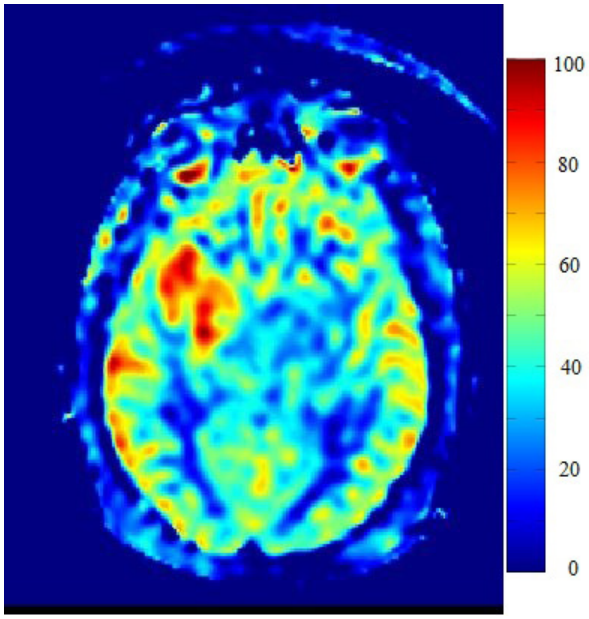

Fig. 11

ASL-CBF shows increased perfusion in a patient with a glioblastoma in the right frontotemporal lobe.

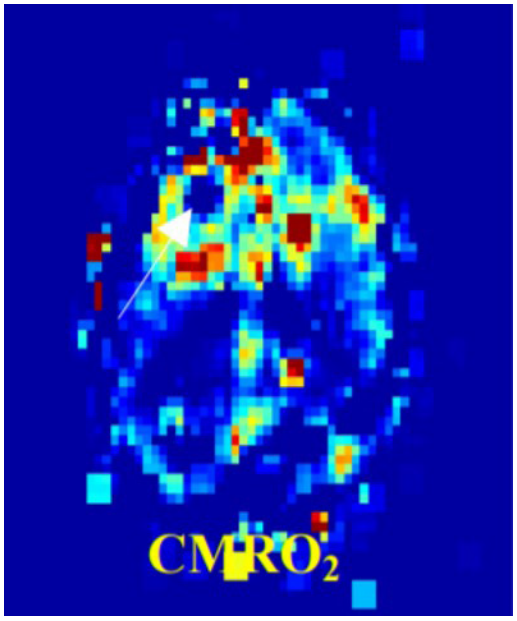

Fig. 12

A mapping of $CMRO_2$ of a patient with a glioblastoma in the right frontal lobe (white arrow). Oxygen consumption is increased in the peripheral region while no oxygen consumption is seen in the necrotic area of the tumour. [Adapted from Kim et al.[97]]

Subtraction between labeled and control images creates images with signal weighted by cerebral perfusion that via a kinetic model can be quantified to generate images of CBF.[90]

4.2.4 Oxygen Consumption: Exploiting the Sensitivity to Deoxygenated Blood

Angiogenesis in glioblastoma is characterized by dysfunctional microvascular proliferation resulting in hypoxic foci.[91] Subsequently, the hypoxic environment results in an altered cerebral metabolic rate of oxygen ($CMRO_2$), which is particularly observed in high-grade tumours compared to normal brain tissue.[92, 93] Functional MR imaging relies on the magnetic susceptibility of blood that depends on the oxygenation state of hemoglobin (Hb).[94] Quantitative Blood-Oxygen-Level Dependent (qBOLD) MR imaging is a functional MR method that is used to measure the oxygen extraction fraction (OEF) from the complex relationship between T2* and the Hb/deoxygenated Hb ratio.[95] Subsequently, combining information on the OEF with CBF, as is shown in *Fig. 12,* allows for mapping of the oxygen consumption, $CMRO_2$.[96]

4.2.5 Tumour Cellularity: Evaluating Diffusion of Water

High-grade gliomas show increased cellular density, which impedes free water diffusion.[98] Diffusion-weighted imaging (DWI) is an MR technique where free water molecular diffusion is measured. Gradient pulses are applied in such way that water molecules that do not move between pulse applications are refocused and generate signal. Water molecules that do move, lose their ability to generate signal. On DWI areas of restricted diffusion, therefore, appear bright, while

areas of free water motion appear dark. By varying the gradient strengths water molecules that diffuse with different speeds can be measured in different images. These resulting images can be used to calculate an apparent diffusion coefficient (ADC), with lower ADC values reflecting lower diffusion. Various pathophysiological properties of high-grade gliomas can influence ADC values. Necrosis, one of the characteristics of glioblastomas, shows higher ADC values as there is more free diffusion of water molecules. In solid tumour tissue the size of the extra-cellular space is limited by the increased cell density, lowering diffusion and thus ADC values *(see Fig. 13)*.[99] Therefore, DWI has the potential to be used as an indirect measurement of abnormal cellularity in glioblastomas.

4.2.6 Tumour Invasiveness: Evaluating Infiltration along White Matter Tracts

A key characteristic of glioblastomas is its extensive, diffuse infiltration of tumour cells. Diffusion tensor imaging (DTI) measures direction and magnitude of water diffusion based on data from a greater number (6 or more) of diffusion directions than DWI (3 directions). Water movement within white matter tracts is mainly restricted across the myelin sheaths, meaning diffusion is more prevalent parallel to myelinated nerve fibers opposed to transverse.[101] With information on the degree and the direction of diffusional anisotropy, insights into white matter tracts can be gained and utilized to provide tractography data *(see Fig. 14)*. Consequently, DTI offers information that might be useful in predicting invasive growth patterns of glioblastomas along white matter tracts.

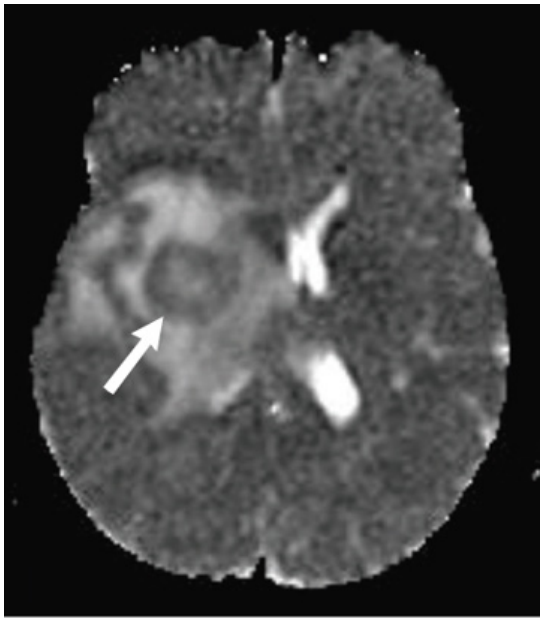

Fig. 13

Glioblastomas show decreased ADC values (white arrow) on the ADC map due to increased cell density. In the center of the tumour, the ADC values are higher. This is explained by the necrotic center that is characteristic for glioblastomas. [Adapted from Kao et al.[100]]

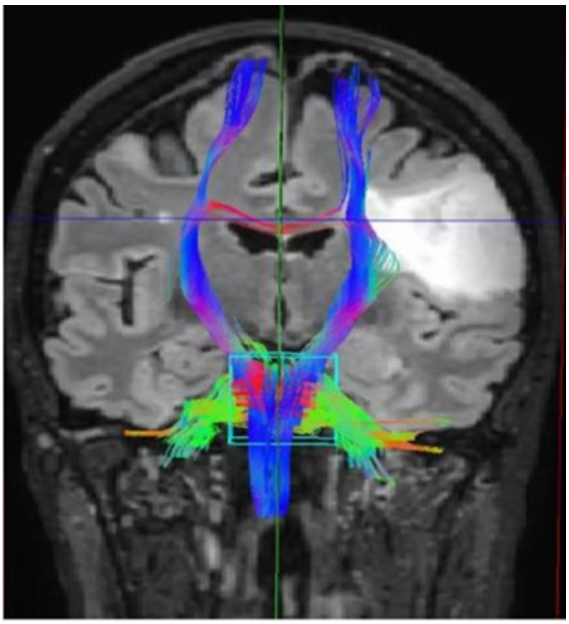

Fig. 14

This tractography image shows an intimate relationship of the right frontal mass with the corticospinal tract. [Adapted from Shukla et al.[102]]

4.2.7 Tumour Metabolism: Evaluating numerous Metabolites

Metabolites, the intermediate or end products of metabolism, play a crucial role in cell growth, development and reproduction. Reprogramming of cellular metabolism is considered one of the emerging hallmarks of cancer.[103] Conventional MR imaging relies on free protons, which are most abundant in water, to generate its signal. The signal, however, is also affected in a much lesser degree by protons bound to macromolecules. These bound protons have specific frequency variations. After suppression of the water signal, MR spectroscopy (MRS) can acquire data on separated frequency peaks, each representing a specific macromolecular component. Assessment of the peaks and ratios from various metabolites can provide information on a wide range of metabolic processes, such as energy metabolism, cell proliferation and necrotic tissue changes. Commonly used metabolites for MRS are N-acetyl aspartate (NAA), choline (Cho), creatine/phosphocreatine (Cr), lactate (Lac) and lipids (Lip).[104, 105] As metabolic changes may precede anatomic changes, MRS is a promising technique to determine early tumour development.[106] An example of MRS is shown in *Fig. 15*.

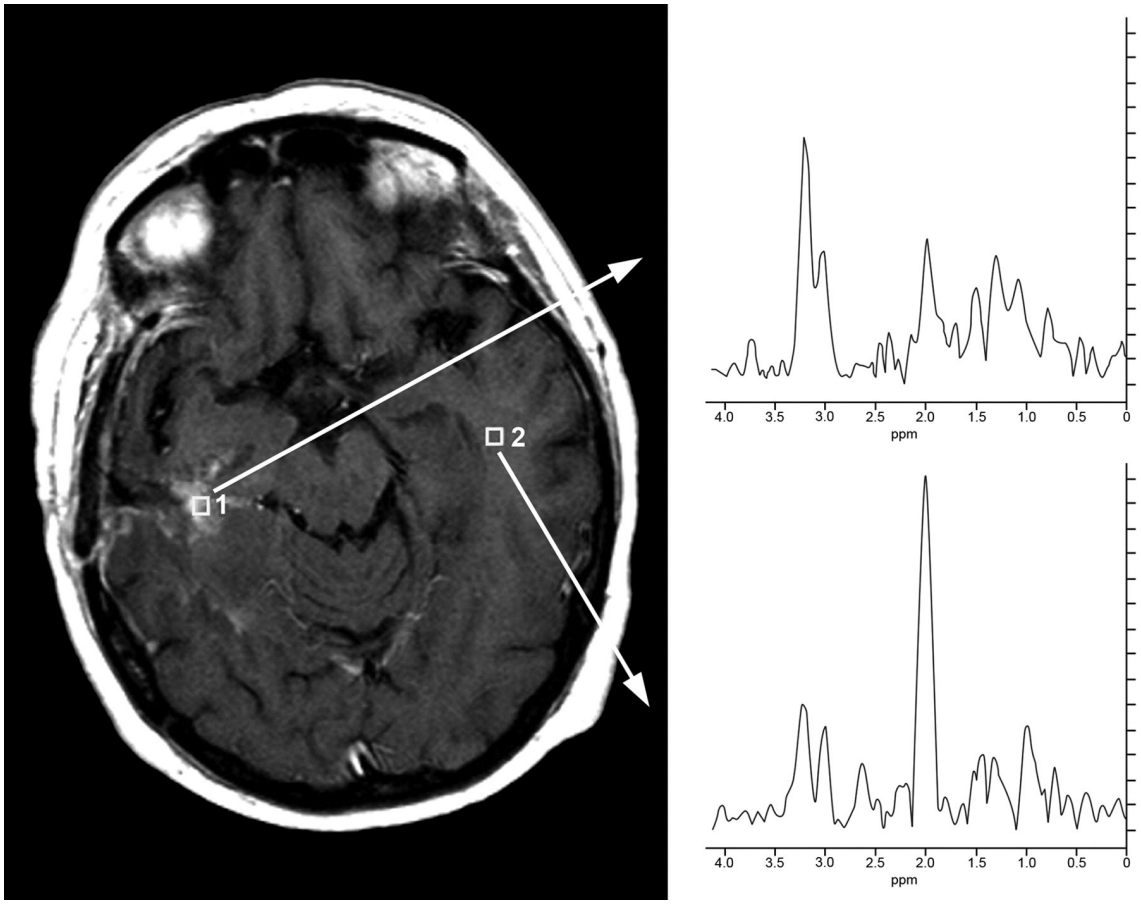

Fig. 15

Single-voxel MRS can be used to assess the concentration of metabolites in that voxel. The MRS spectrum in voxel 1 shows elevated choline (resonates at 3.2 ppm) and decreased NAA (resonates at 2 ppm), a characteristic of glioblastoma, when compared to the spectrum of voxel 2. [Adapted from Quon et al.[107]]

4.2.8 Cell Proliferation: Evaluating Protein Concentration

Sustained cell proliferation is one of the hallmarks of cancer.[108] Amide chemical exchange saturation transfer (CEST) imaging, also known as amide proton transfer (APT) CEST imaging, can be used to gain information on cell proliferation. In CEST the concept of saturation, i.e. a temporary state in which tissue shows no net magnetization, is exploited to achieve image contrast. By applying a radiofrequency pulse at the resonant frequency of a chemical species of interest, this chemical species can be targeted as it will show reduced signal due to the saturation effect. However, most chemical species are present in significant smaller quantities compared to water, meaning the signal change would be unnoticeable. Various chemical species, in the case of APT imaging amides (-NH), have a proton in its structure that is exchangeable with those of the free water pool. When saturated, the magnetic saturation of the amides will spontaneously be transferred to water over time, due to chemical exchange of the excited amide protons with non-excited water protons. The proton of the amides will thus be replaced with an unsaturated proton from water, which can in turn be saturated for another transfer. By continuously saturating the amides the continuous transfer of excited protons will lead to a buildup of saturation in water. This decrease in water signal can indirectly measure the concentration of amides in a target area.[109] The major known contributors to the APT signal are proteins and peptides.[110] A positive correlation is observed between APT signal intensity and Ki-67 labeling index (the cellular marker for proliferation).[111] Therefore, APT imaging might provide us with insights into cell proliferation to determine early tumour progression. An example of APT imaging is shown in *Fig. 16*.

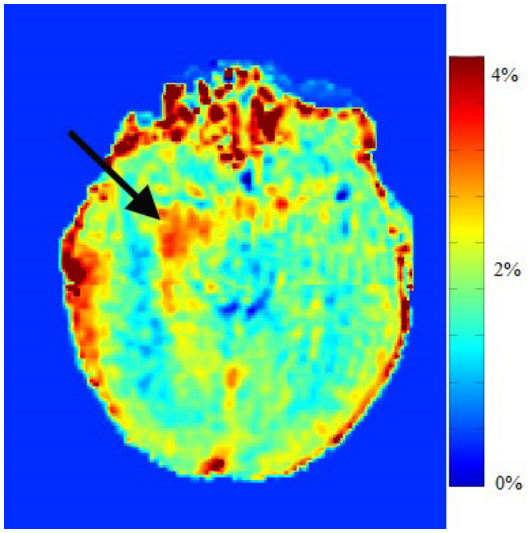

Fig. 16

APT shows an increased signal intensity in the tumour region (black arrow). This signal intensity is mainly caused by the increased concentration of proteins in this region.

4.3 Advanced MR Biomarkers in Gliomas

Biomarkers from advanced MR techniques have the potential to either visualize microscopic tumour infiltration or predict high-risk regions of future relapse. This information could be incorporated into radiotherapy planning to improve delineation of the CTV. In this section an overview is presented of trials that explore advanced MR biomarkers to visualize tumour infiltration or predict future recurrence sites.

4.3.1 Kinetic Parameters and Cerebral Blood Volume measured with DCE

Various DCE kinetic parameters in regions of tumour infiltration are shown to correlate to microvascular parameters that are involved in disruption of the BBB. In a biopsy study, *Keil et al. (2021)* explored the potential of DCE-MR imaging to predict vascular growth factor expression and neovascularization in 30 glioma patients.[112] In regions with vital tumour, tumour infiltration

and healthy brain tissue, 120 biopsies were taken to evaluate the parameters involved in BBB disruption with DCE kinetic parameters. Significant correlations were found not only in vital tumour tissue, but also, in a lesser degree, in the histologically confirmed infiltration zone highlighting the potential of DCE-MR imaging to visualize tumour infiltration.

Pattern of failure was evaluated in 52 glioblastoma patients who underwent DWI and DCE-MR imaging by *Wahl et al. (2018)*.[113] Progression during follow-up was seen in 33 patients. The median proportion of the recurrence volume (RV) within the region with elevated cerebral blood volume (CBV) was 22%, when combined with restricted diffusion the median proportion increased to 30%. Based on these results the authors implied that the majority of failures occur in volumes characterized by neither restricted diffusion nor increased perfusion. The median proportion of the overlapping volume (i.e. both restricted diffusion and enhanced perfusion) that developed progression during follow-up was 77%, indicating regions with restricted diffusion and enhanced perfusion are likely to develop progression in the future. This overlapping volume has been targeted in a phase II dose escalation study that showed significantly improved 12-month overall survival (92%) compared to historical control ($p = 0.03$).[114]

4.3.2 Relative Cerebral Blood Volume measured with DSC

The positive correlation of the degree of tumour infiltration in gliomas and rCBV is shown to predict tumour infiltration with a higher accuracy than various biomarkers acquired with MRS. In an image-guided biopsy study with 13 patients, *Hu et al. (2009)* demonstrated the potential of rCBV to distinguish tumour progression in high-grade gliomas (sensitivity = 91.7%, specificity = 100%).[115] This finding was supported by *Price et al. (2011)*, who presented a significant correlation between mean rCBV and the tumour proliferation index (MIB-1) in 10 patients with high-grade gliomas ($r = 0.66$, $p < 0.001$).[116] In four patients where biopsies went outside the region of contrast enhancement, the mean rCBV at the biopsy site was increased: In three patients the increased rCBV extended 1 cm from the edge of enhancement and in the other patient the biopsy was taken 2 cm from the enhanced area. In all four patients, the histology of these areas revealed regions of microscopic tumour invasion into normal appearing brain tissue. In subsequent research by the same research group a comparison of rCBV with various MRS biomarkers as predictor of tumour infiltration in glioblastomas was made ($n = 50$).[117] With a sensitivity and specificity of 82%, rCBV could predict tumour infiltration with better accuracy than all examined metabolite biomarkers.

In addition to the correlation with tumour infiltration, various studies have shown that increased rCBV can be an indication for high-risk regions of future relapse. *Stadlbauer et al. (2021)* demonstrated changes in rCBV at the site of recurrence 120 days prior to radiological recurrence.[118] From that timepoint a continuous increase was seen in rCBV before indications of progression on structural MR imaging could be seen. The feasibility of rCBV as predictive biomarker for progression was also supported by *Stecco et al. (2011)*, where both DTI parameters (ADC and FA) and perfusion (rCBV) were investigated in 17 patients.[119] Compared to the contralateral NAWM significantly higher rCBV values were seen on pretreatment imaging at the site where recurrence occurred during follow-up ($p < 0.001$). This was the case not only for volumes that showed enhancement on contrast-enhanced T1-weighted imaging before treatment, but also for volumes that did not show enhancement. In addition, a specific directional stripe-like pattern of rCBV increase in a region adjacent to contrast-enhancement was investigated in *Blasel et al. (2011)*.[120] In this study this extended increase of rCBV in a direction away from the tumour border was named the striate sign and observed in 42% of the cases between 2008 and 2009 at their institution (31 out of 77 histologically proven glioblastomas), see *Fig 17*. Sixteen patients with tumour recurrence were investigated retrospectively in this study. Four patients underwent second surgery where biopsy of the area of the striate sign revealed glioblastoma cell infiltration in all cases. The entire area of the striate sign showed contrast enhancement, indicating progression, in 15 out of 16 patients after 9 months. This study shows that the striate sign may depict future tumour progression and can extend far beyond the margins of contrast-enhancing tumour.

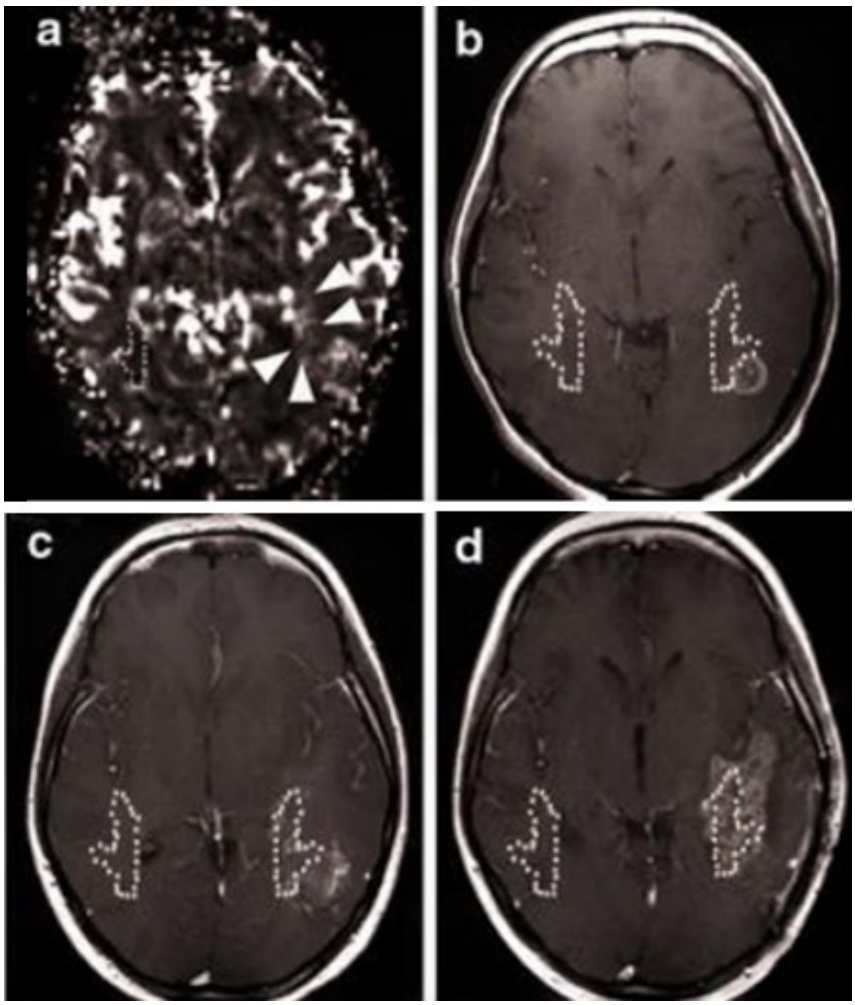

Fig. 17

On rCBV map (a) a specific directional stripe-like pattern that extended beyond the contrast-enhancing tumour rim, was visible (white arrows). Contrast-enhanced T1-weighted imaging of the baseline MR scan (b), and the three (c) and the six months (d) follow-up MR scan show that this extension (yellow delineation) was covered with contrast-enhancement in its entirety after six months. The delineation on the contralateral side mark a contralateral reference. [Adapted from Blasel et al.[120]]

4.3.3 Vessel Size measured with VSI

Vasodilatation, which is frequently observed in glioblastomas, can be accurately visualized with VSI. In a prospective stereotaxic biopsy study by *Kellner et al. (2015)*, vessel size index was proven to be related to histologically increased vessel diameters in human gliomas.[88] Although an overestimation of normal vessel size and an underestimation of grossly enlarged vessels was observed, a significant correlation for both mean and maximum vessel size with histologically measured diameters was seen *(see Fig. 18). Chakhoyan et al. (2019)* corroborated these findings, concluding that MR-based vessel size measures accurately reflect vessel caliber within high-grade gliomas, while traditional measures of rCBV are correlated with vessel density rather than vessel size.[87]

An increase in vessel size can be an indication of high-risk sites of future recurrence. Vessel

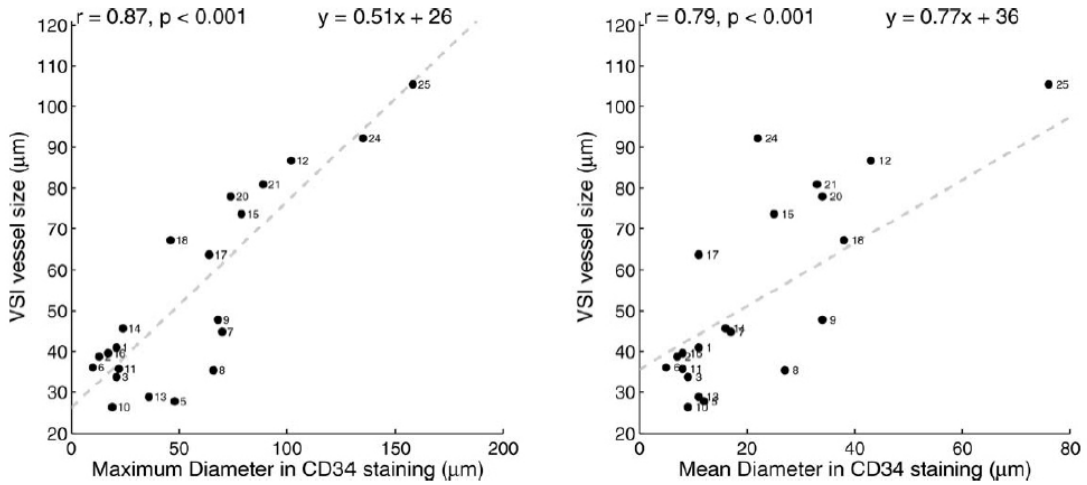

Fig. 18

Median vessel size estimated by VSI compared with the diameter obtained from CD34 staining. The correlation is shown for both the maximum (left) and the mean diameter (right). Although both significant, the maximum diameter shows a better correlation. [Adapted from Kellner et al.[88]]

size imaging was acquired by *Stadlbauer et al. (2021)* during the follow-up of 56 patients who received standard treatment for glioblastoma.[118] Approximately 120 days prior to radiological recurrence a decreasing vessel size index was observed for a duration of 80 days at the site of relapse. After this decrease, 40 days before radiological recurrence, the vessel size index was shown to continuously increase. As a continuous increase in mean vessel density was seen 120 days prior to radiological recurrence, the authors hypothesized that early neovascular activity was dominated by the formation of smaller vessels, which transformed into larger-lumen vessels during later phases of tumour vascular development.

4.3.4 CMRO2 measured with qBOLD and ASL

Altered oxygen consumption can identify regions that will form relapse up to 6 months later in glioblastoma patients. *Kim et al. (2011)* included ten healthy subjects and ten glioblastoma patients to compare cerebral oxygen consumption.[97] A significant increase of 59% in $CMRO_2$ was seen in contrast-enhancing tumour compared to healthy tissue. Peritumoural tissue showed an increased oxygen consumption of 27%. These findings were supported by *Stadlbauer et al. (2017)*, who observed an increased oxygen consumption in high-grade gliomas compared to both the contralateral and ipsilateral NAWM ($p < 0.001$) in 82 glioma patients.[121] The same research group evaluated physiologic MR imaging follow-up examinations of 56 glioblastoma patients who underwent standard treatment.[118] They found that $CMRO_2$ started to increase 190 days prior to relapse at the site of recurrence. At 60 days before relapse a maximum was reached, thereafter the $CMRO_2$ was observed to decrease. The tissue oxygen tension, which is influenced by $CMRO_2$ amongst others, started to decrease (i.e. hypoxia) 190 days before relapse, reaching a minimum value at 90 days prior to recurrence *(see Fig. 19)*.

4.3.5 Apparent Diffusion Coefficient measured with DWI

Biopsy studies have shown that DWI is not helpful for the distinction between glioma infiltration and peritumoural brain tissue. The correlation between tumour cellularity and ADC value, which

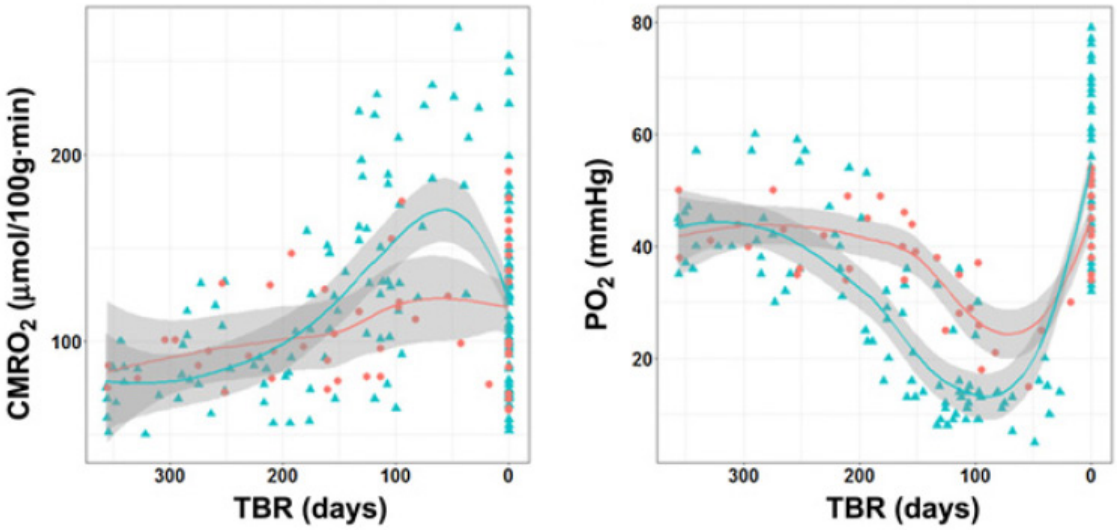

Fig. 19

Time courses of the biomarkers $CMRO_2$ (left) and oxygen tension (right) that occurred at the site prior to a local (cyan) or distant (red) recurrence of a glioblastoma. [Adapted from Stadlbauer et al.[118]]

can be derived from DWI, in solid tumour tissue has been histologically proven by *Kono et al. (2001)*.[122] The ADC in solid tumour tissue was found to be capable of predicting the degree of malignancy in gliomas. Signal intensities on DWI and ADC maps in peritumoural hyperintense areas on T2-weighted imaging, however, were not useful in determining the presence of peritumoural neoplastic cell infiltration. These findings were supported by *Pauleit et al. (2004)*, who concluded that distinction of tumour infiltration and adjacent edema or reactive gliosis in peritumoural tissue in individual patients with gliomas cannot be done using DWI.[123]

Pattern of failure analysis revealed that increased cell density can identify the site of recurrence at least 3 months before morphologic changes are visible on conventional MR imaging. *Gupta et al. (2011)* evaluated the correlation between low ADC values during treatment and recurrence location during follow-up.[124] Only in 67 of the 208 glioblastoma patients (32.2%) visibly detectable restricted diffusion was seen during treatment. 27 patients showed low ADC lesions and no contrast enhancement. At the site of restricted diffusion 23 patients (85.2%) developed contrast-enhancing tumour at a median of 3.0 months later. This is congruent with the findings of *Elson et al. (2015)*, who observed an overlap of pre-radiotherapy ADC hypointensity volumes with recurrences in 28 out of 32 (88%) cases.[125] The median progression-free survival in patients with ADC hypointensity was 3.2 months. *Pramanik et al. (2015)* showed that the use of pre-radiotherapy ADC maps to predict the location of late progression was inferior to the predictability for early progression.[126] For the 5 patients who progressed within 6 months post-radiotherapy, the median percentage of overlap between the pre-radiotherapy ADC hypointensity volume and the recurrent contrast-enhancing GTV was 78%, whereas 10 patients who progressed after 6 months had an overlap of 53%. *Wahl et al. (2018)* investigated the pattern of failure in 52 glioblastoma patients who underwent DWI and DCE-MR imaging.[113] For the 33 patients with radiographic progression during follow-up, the median proportion of the overlapping volume (i.e. the region that displayed both restricted diffusion and enhanced perfusion) that developed progression during follow-up was 77%. The median proportion of the RV within the region with restricted diffusion, however, was only 17%. When combined with the region with elevated CBV the median proportion increased to 30%. Based on these results the authors imply that volumes that display both restricted diffusion and enhanced perfusion harbor resistant disease that is likely to progress in the future, but most failures will spatially occur in volumes characterized by neither restricted diffusion nor increased

perfusion. At the same institute, *Kim et al. (2021)* conducted a phase II study in which patients with glioblastoma received dose intensification against regions with restricted diffusion and elevated perfusion resulting in improved overall survival.[114] *Chang et al. (2016)* used computational big-data modeling to evaluate the potential of ADC and FLAIR signal pre-radiotherapy to predict future recurrence.[127] Areas of future recurrence showed a 9.5% decrease in ADC value ($p < 0.001$) and a 9.2% decrease in signal intensity on FLAIR image ($p < 0.001$). Receiver operating characteristic (ROC) curves yielded areas under the curve (AUC) values of 0.566, 0.726 and 0.741 for ADC-only, FLAIR-only and a combined model respectively.

4.3.6 Anisotropic Diffusion measured with DTI.

In gliomas, regions with tumour infiltration can be identified with high sensitivity on DTI when information on the isotropic and anisotropic components of the diffusion tensor are split. To evaluate the potential of DTI to visualize tumour cell infiltration within peritumoural regions with increased T2-weighted signal intensity, *Tropine et al. (2004)* compared 20 patients with gliomas to 10 patients with meningiomas, in which no tumour infiltration is expected.[128] Comparison of the peritumoural regions showed no significant differences in fractional anisotropy (FA) values, suggesting reliable differentiation between infiltration and vasogenic edema based on DTI was not yet possible. These findings were in concordance with an image-guided biopsy study performed by *Price et al. (2006)*.[129] Preoperative DTI in 20 patients with gliomas were evaluated with the aim to use DTI to distinguish regions with tumour infiltration in NAWM from regions with normal brain tissue. The normalized FA values in this study could not distinguish infiltrated regions from normal brain tissue ($p = 0.27$). Areas beyond tumour enhancement with a normal anisotropic component and an isotropic component greater than 10% compared to contralateral NAWM, however, could identify tumour infiltration with a sensitivity of 98% and specificity of 81%.

Although tumour infiltration can be visualized with high sensitivity, DTI does not seem useful for prediction of areas of future relapse. The integration of DTI for radiotherapy treatment planning of patients with high-grade gliomas was first explored by *Jena et al. (2005)*.[130] DTI-based plans using a 1 cm margin added to an image-based high-risk volume were shown to reduce the size of the planning target volume when compared to the conventional planning target volume (mean 35%, range 18-46%). It is important to note that an isotropic CTV margin of 2.5 cm for the conventional radiotherapy planning was used in this study. A similar approach by *Berberat et al. (2014)* revealed a trend towards volume reduction using DTI, however, significance was not reached.[131] *Trip et al. (2019)* evaluated coverage of the RVs by DTI-based CTVs in forty glioblastoma patients who received standard treatment with CTV margins of 2 cm or less.[132] A slightly worse coverage of the RVs by the DTI-based CTVs was observed, with central recurrences in particular being covered less. The ability of DTI to predict locations of distant recurrence was explored by *Witulla et al. (2020)*, who saw a connection between fiber tracking and the distant RV in only 1 out of 7 patients.[133]

4.3.7 Cho/NAA ratio measured with MRS

Histologic evaluation of glioma tissue has shown the capability of MRS to distinguish tumour infiltration. *Croteau et al. (2001)* investigated the correlation of MRS metabolic ratios and the degree of tumour infiltration in 31 untreated glioma patients.[134] In 247 tissue samples a significant correlation of Cho/nCho ($p = 0.0372$) and Cho/NAA ($p = 0.0018$) was found with MIB-1, a cellular proliferation index indicating tumour infiltration. *Matsumura et al. (2005)* evaluated the correlation between Cho concentration and MIB-1 in 14 glioma patients with single-voxel MRS.[135] Although Cho concentration is believed to be elevated in glioma tissue, they only found a significant correlation for low-grade gliomas. This might be caused by the heterogeneous nature of high-grade gliomas, particularly for glioblastomas. Due to the large voxel size in single-voxel MRS, it is almost unavoidable to exclude all necrotic tissue during the selection of a voxel of interest.

Multi-voxel MRS has the potential to identify and delineate substantial tumour infiltration and high-risk regions for recurrence. The feasibility of target delineation with multi-voxel MRS was first explored by *Pirzkall et al. (2001)*.[136] On average, the volume delineated on MRS was 58% of the volume based on T2-weighted imaging. Metabolic active disease (i.e. regions with abnormal Cho/NAA ratios), however, was still observed to extent ipsilaterally beyond the T2-weighted delineation in 9 out of 12 patients with glioblastoma. On contrast-enhanced T1-weighted MR imaging the extension beyond the T1-weighted volume was not as great as was seen with grade III patients. *Cordova et al. (2016)* developed an imaging pipeline utilizing high resolution (0.1 cm^3 nominal voxel size) spectroscopic imaging to generate whole-brain metabolic maps and evaluated the correlation between MRS biomarkers and Sox2 density, a normalized metric of tumour infiltration, in tissue samples of 13 patients with glioblastoma.[137] Various metabolic markers showed significant correlations, but Cho/NAA exhibited the strongest association with tumour infiltration ($p < 0.0001$). During follow-up of these patients, 5 of the 13 patients had T1-weighted contrast-enhancing progression at the time of analysis. All patients showed T1-weighted contrast enhancing progression in regions that exhibited Cho/NAA abnormalities before radiotherapy was given *(see Fig. 20)*. A similar correlation between regions with increased Cho/NAA and recurrence site was also observed by *Park et al. (2007)* and *Czernicki et al. (2009)*.[138, 139]

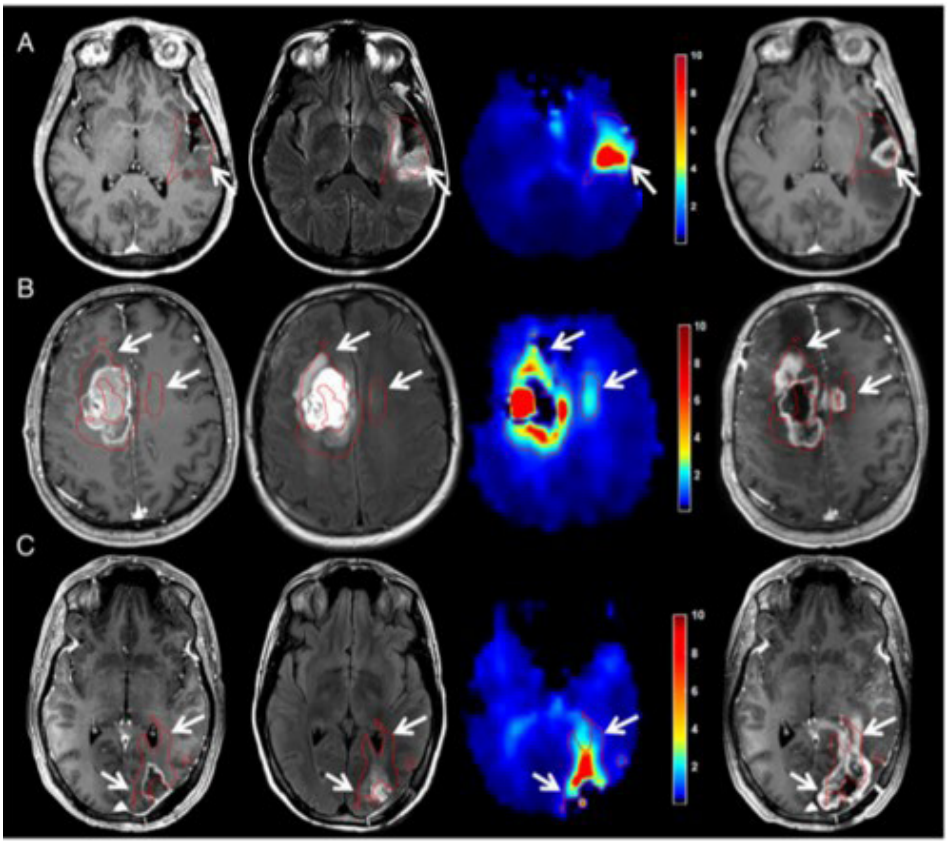

Fig. 20

Pre-radiotherapy Cho/NAA abnormalities were observed and delineated (red contour). Pre-RT imaging shows that increased Cho/NAA ratios on the Cho/NAA map (third column) extended beyond the GTV on T1-weighted contrast-enhancement (first column) and T2-weighted/FLAIR (second column). First recurrence on contrast-enhanced T1-weighted imaging after radiotherapy (fourth column) showed contrast-enhancing tumour development within the pre-radiotherapy increased Cho/NAA volume in 3 patients (A,B,C). [Adapted from Cordova et al.[137]]

4.3.8 Amide Concentration measured with APT CEST

APT CEST can be used to distinguish true glioma tissue from healthy tissue or post-treatment effects. Preclinical research by *Zhou et al. (2011)* first explored the potential of APT CEST to distinguish viable glioblastoma from post-treatment radiation necrosis.[140] Histologically confirmed regions with malignant tissue in 9 rats showed significantly higher APT signal intensity than regions with radiation necrosis or contralateral normal appearing white matter (NAWM) (both $p < 0.001$). *Sagiyama et al. (2014)* observed a significantly lower APT signal intensity in a group of mice treated with TMZ ($n = 6$) compared to a control group ($n=5$).[141] Histological evaluation determined no differences in cell density or apoptosis rate, however, a significantly lower Ki-67 labeling index was seen in the treated group ($p < 0.0001$). The correlation between APT signal intensity and the Ki-67 labeling index was confirmed in human gliomas by *Togao et al. (2013)* and *Jiang et al. (2019)*.[111, 142]

These biopsy studies and the ability of APT CEST to distinguish tumour tissue from treatment effects can be used to predict areas at risk for future tumour progression. *Mehrabian et al. (2018)* acquired APT CEST imaging at 3 Tesla (T) before, during and after chemoradiation therapy in 19 glioblastoma patients.[143] They found that APT CEST could predict future tumour progression as early as two weeks into treatment. The utility of APT CEST acquisition at 1.5T was examined in a prospective study ($n = 51$) by *Chan et al. (2021)*, who found significant differences in quantitative CEST parameters in patients who developed tumour progression within 6.9 months compared to those with late tumour progression.[144] These findings were supported by *Regnery et al. (2018)*, who found APT CEST imaging to yield significant predictors of early progression at 7T.[145]

An overview of the different biomarkers and corresponding advanced MR techniques is given in *Table 1.*

Biomarker	Advanced MR Technique	Physiological process	Reported time of observed alterations seen prior to relapse
Kinetic parameters and CBV	DCE-MR imaging	Vascular leakiness	n/a
rCBV	DSC	Angiogenesis	4 – 9 months
VSI	DSC (gradient *and* spin echo acquisition	Vasodilatation	1 month
$CMRO_2$	qBOLD and ASL	Oxygen consumption	6 months
ADC	DWI	Cellularity	3.0 – 3.2 months
Anisotropic diffusion	DTI	Invasiveness	n/a
Cho/NAA	MRS	Metabolism	4 – 5 months
Amide concentration	APT CEST	Cell proliferation	6.9 months

Table 1: An overview of the advanced MR biomarkers that have potential to visualize glioblastoma infiltration and predict regions of future recurrence.

4.4 Understanding glioblastoma development

Progression of glioblastoma is associated with hypoxic tumour microenvironment that is known to exist within glioblastomas. At cellular level the glioblastoma stem-like cells (GSC), a specific subpopulation of cells that display principal stem cell properties like self-renewal and differentiation, thrive in harsh microenvironmental niches.[146-148] Hypoxia and hypoxia-inducible factors (HIFs) play a critical role in creating the microenvironment that promotes cellular interactions and signaling pathways required for the survival and self-renewal of GSCs.[149] As GSCs are highly resistant to radiotherapy and chemotherapy, it is believed that survival of GSCs play a major role in the development of recurrence after treatment.[150-152]

Hypoxia is commonly observed in solid tumours, being a natural consequence of increased oxygen diffusion distance due to tumour expansion. In the early seventies, *Folkman et al. (1971)* first proposed that angiogenesis is vital for the progression of solid tumours beyond a size of a few mm^3, as tumour expansion demands an increase in supply of oxygen and nutrients.[153] Emerging evidence, however, shows that another mechanism called vessel co-option, can act as an alternative for tumour blood supply.[154] Vessel co-option is a process in which pre-existing vasculature is hijacked by tumour cells that form cuffs around microvessels. In a preclinical study, *Holash et al. (1999)* first demonstrated vessel co-option in gliomas to precede angiogenesis by up to 4 weeks *(see Fig. 21)*.[155] In this study, vessel co-option was shown to be associated with an upregulation of angiopoietin-2 (Ang-2), a growth factor that belongs to one of the main pathways involved in angiogenesis. The Ang-2 overexpression was associated with vascular endothelial cell apoptosis and vessel regression, which occurs in Ang-2 overexpression in the absence of vascular endothelial growth factor (VEGF).[156-158] Subsequently, this led to a temporary avascular tumour with increasing hypoxia, which in turn promotes induction of VEGF, a growth factor that promotes migration and proliferation of endothelial cells and stimulates sprouting of new blood vessels. This marks a switch from vessel co-option as the preferred mechanism of vascularization to angiogenesis. The process of angiogenesis will remain dominant due to the continuous presence of hypoxia and eventually lead to an abnormal vascular network with dilated vessels, abnormal perfusion and excessive leakiness. In addition to angiogenesis, it is believed that the hypoxic switch promotes another mechanism for neovascularization: vasculogenesis.[159] This process involves the mobilization, differentiation and recruitment of circulating bone marrow-derived cells for the de novo formation of tumour vasculature.

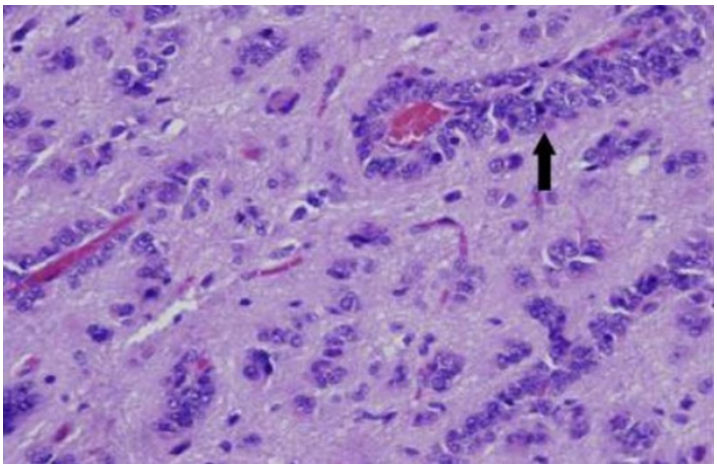

Fig. 21

Vessel co-option (black arrow) involves organization of tumour cells into cuffs around normal microvessels. [Adapted from Holash et al.[164]]

Glioblastoma cells can adopt and switch between an infiltrative phenotype, where cells migrate in a saltatory fashion, and a proliferative phenotype resulting in local tumour growth.[160] When a proliferative phenotype is adopted, altered metabolism in glioblastomas can result in rapid cell proliferation. In normal differentiated cells glucose is metabolized into pyruvate, which subsequently enters the tricarboxylic acid cycle to generate adenosine triphosphate (ATP) through a process called oxidative phosphorylation. ATP production is required for ATP hydrolysis, in which crucial energy is released for numerous cellular processes. Oxidative phosphorylation maximizes ATP production (36 mol ATP / mol glucose), with minimal production of lactate. However, when oxygen is limited, oxidative phosphorylation cannot occur and anaerobic glycolysis results in inefficient ATP production (2 mol ATP/ mol glucose) and the production of large amounts of lactate.[161] *Warburg et al. (1927)* observed that malignant cells tend to convert a majority of glucose to lactate, regardless of the presence of oxygen, resulting in less efficient ATP production (4 mol ATP / mol glucose) when compared to oxidative phosphorylation.[162] This process is called aerobic glycolysis or the Warburg Effect and is also observed in glioblastomas.[163] Although it is hypothesized that aerobic glycolysis can be beneficial for rapid cell proliferation due to the creation of additional cellular components (e.g. nucleotides, amino acids, and lipids) along with the production of ATP, a conclusive explanation for aerobic glycolysis in cancer cells has remained elusive.[161]

4.5 Discussion

This literature review explored the potential of advanced MR imaging to visualize microscopic tumour infiltration and predict future areas of relapse in patients with glioblastoma. Studies using various techniques that visualize tumour growth, vascularization and hypoxia show that advanced MR biomarkers can precede morphologic changes on conventional MR imaging and could be the initial step towards personalization of radiotherapy planning.

Although studies on multiple techniques have shown promising results, the integration of advanced MR imaging with radiotherapy planning in clinical practice remains limited. Careful consideration is taken regarding the introduction of these techniques into clinical practice, as it remains challenging how to incorporate the additional information resulting in either improved local tumour control or reduced radiation-induced toxicity.

Hypoxia and oxygen metabolism showed to be significantly altered approximately 6 months prior to tumour progression being visible on conventional MR imaging.[118] Including this biomarker in radiotherapy planning can provide early information on future sites of relapse compared to other biomarkers reviewed in this paper. As seen in *Fig. 19,* the oxygen tension and $CMRO_2$ show a turning point at 90 and 60 days before recurrence, respectively. This switch could be an indication of the Warburg effect, in which aerobic glycolysis becomes dominant and cell proliferation is upregulated. This is in concordance with findings of DWI trials that evaluated progression-free survival; significant hypercellularity was reported at a median of 3.0 or 3.2 months prior to recurrence.[124, 125] As a switch is observed during the course of tumour development and radiotherapy planning is performed on a single time-point, sole information on $CMRO_2$ or oxygen tension can result in overlooking potential sites of relapse. Depending on the time of acquisition the oxygen consumption could appear normal after the Warburg effect has become dominant.

A multiparametric approach, where multiple biomarkers were included, was shown to be superior to single-parameter predictive models.[119, 165, 166] Inclusion of biomarkers of perfusion-weighted imaging in addition to oxygenation could allow for a better understanding of the pathological processes in a region. Pattern of failure analysis showed that regions with increased perfusion acquired with DCE-MR imaging (and hypercellularity acquired with DWI) is likely to progress, however, the majority of failures were seen to occur at sites that did not display alterations on these MR techniques.[113] An increase in microvascular density can be seen 4 months before radiological recur-

rence, indicating upregulation of hypoxia-induced angiogenesis. In the early stages of angiogenesis it is believed that angiogenesis is dominated by the formation of smaller vessels, whereas the later stages show transformation of these vessels into larger-lumen vessels.[118] Including both rCBV, which correlates with microvascular density, and VSI with DSC can therefore provide complete information on the angiogenic process that occurs in tumour progression.

Combining perfusion and oxygen biomarkers allows for early indication of future sites of relapse while preventing misinterpretation due to the Warburg effect. A region with hypoxia or increased $CMRO_2$ without altered perfusion can indicate vessel co-option or a temporary avascular state, which is predictive for future upregulation of angiogenesis and relapse. When a region shows increased rCBV or VSI with normal $CMRO_2$, a switch from an infiltrative phenotype to a proliferative phenotype could have occurred.[118] In this case angiogenesis is upregulated and aerobic glycolysis is dominant indicating rapid cell proliferation and hence tumour growth.

In a preclinical study, *Baker et al. (2014)* showed that, in some cases, vessel co-option can persist through to later stages, with the absence of the switch to angiogenesis for tumour vascularization.[167] As vessel co-option is not measurable through rCBV or vessel size, another biomarker might be needed to prevent misinterpretation of oxygen biomarkers. Tumour growth can be directly or indirectly measured using various techniques. The Cho/NAA ratio was shown to correlate accurately with tumour infiltration, however, the heterogeneous nature of glioblastomas accompanied by a relatively poor signal-to-noise ratio and large voxel size of multi-voxel MRS makes this technique less suitable for delineation. The presence of (micro)necrosis within a voxel could result in a decreased Cho/NAA ratio. Techniques utilizing high resolution multi-voxel MRS have been explored, however, an acquisition time of 19 min was required. Measurements of hypercellularity with ADC mapping has been explored, showing significant hypercellularity to precede future tumour recurrence by 3 months. White matter tracking and the inclusion of DTI information for CTV delineation, however, showed rather disappointing results. Although APT CEST is a relatively novel technique and the application of the technique in large controlled trials is not yet explored, the studies presented in this review show promising results. Significant differences between groups that developed early progression (within 6.9 months) and late progression indicate the predictability for future sites of relapse to be superior to ADC maps. An additional benefit of APT CEST for radiotherapy is its ability to distinguish true tumour progression from pseudo-progression, which is a post-radiotherapy phenomenon where damage to epithelial cells and increased inflammation present itself similar to tumour progression on conventional MR imaging.[140, 168]

4.6 Conclusion

The potential of advanced MR imaging for the visualization of microscopic tumour infiltration and prediction of future relapse sites has been presented. Including information of oxygen ($CMRO_2$ or oxygen tension), perfusion (rCBV and VSI), proliferation (APT) biomarkers in radiotherapy planning could result in individualized CTV delineation, improved local tumour control and/or reduced radiation-induced toxicity.

5

Data retrieval

In *Chapter 4*, the potential of advanced MR techniques and their corresponding biomarkers to visualize microscopic tumour infiltration and high-risk regions of future relapse was explored. A combination of advanced biomarkers $CMRO_2$, VSI, rCBV and APT was hypothesized to be optimal for visualization of tumour infiltration and early prediction of sites of future relapse. Within the iGene study at the Erasmus MC, patients with gliomas underwent advanced MR imaging in addition to conventional MR imaging. The data from four glioblastoma patients from the iGene study was retrieved for this master's project. As qBOLD-MR imaging was not incorporated in the iGene scanning protocol, the biomarker $CMRO_2$ has been excluded from this project.

5.1 The iGene study

In the completed iGene study at the Erasmus MC *(Rotterdam, the Netherlands)*, forty patients undergoing standard therapy for newly-diagnosed gliomas received an adapted MR protocol preoperatively. In addition to conventional MR sequences (i.e. structural MR imaging like T1 postcontrast), various advanced MR sequences (DWI, ASL, APT CEST and DSC-MR imaging with simultaneous gradient and spin echo acquisition) were included in the protocol. An example of the timeline of a patient's trajectory in the iGene study is shown in *Fig. 22*.

For this master's project, data from glioblastoma patients with advanced MR imaging was required for the generation of a biological CTV based on advanced MR biomarkers. In *Chapter 4,* various advanced MR biomarkers were reviewed regarding their applicability in radiotherapy planning for gliomas. A combination of the biomarkers $CMRO_2$, VSI, rCBV and APT could provide early information on alterations in oxygen consumption, angiogenesis and cell proliferation while minimizing the risk of false negative results caused by the Warburg effect.

Eligible subjects from the iGene study were included for this master's project. As qBOLD-MR imaging was not included in the advanced MR protocol of the iGene study, $CMRO_2$ was excluded as a biomarker for the biological CTV in this project. In this chapter, an overview is given of the inclusion criteria, the approach for data retrieval and patient characteristics of the included subjects.

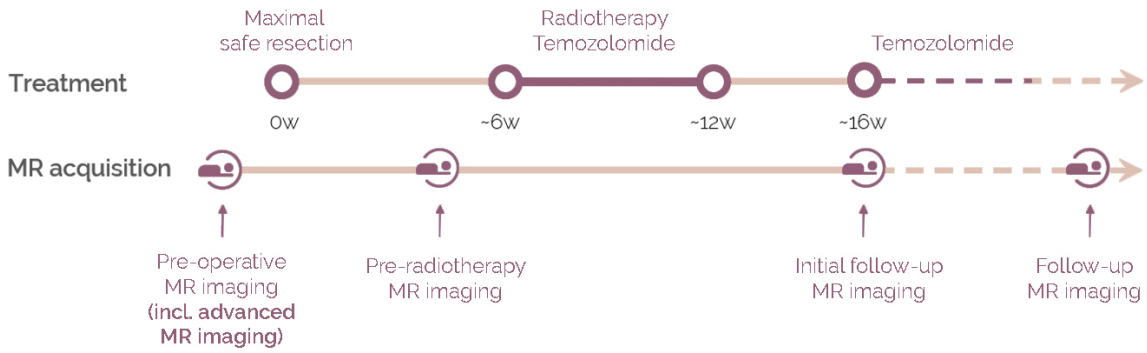

Fig. 22

A typical timeline of a patient in the iGene study who received standard treatment for newly-diagnosed glioblastoma. Advanced MR sequences were added to the protocol preoperatively, allowing the creation of APT, VSI and rCBV maps. During the other timepoints, i.e. pre-radiotherapy and follow-up, only structural MR imaging was included in the protocol.

5.2 Inclusion criteria and data retrieval

Patients from the iGene study who were diagnosed with a glioblastoma, confirmed by histological and molecular analysis, were included. Subjects were excluded when the patient did not receive radiotherapy or had no follow-up data available.

From the included patients, the data required for this project was acquired. First, the structural MR imaging and APT, VSI and rCBV maps from the preoperative MR session were retrieved. Secondly, the imaging and delineations for radiotherapy planning were obtained. This included the planning CT-scan, the structural MR imaging that was used as an aid for the delineations and the delineations of the GTV, CTV, PTV and the organs at risk. Lastly, the structural MR imaging from the MR session that showed first progression during follow-up according to the RANO criteria, was retrieved.[69] The MR sessions that showed first progression during follow-up was determined by an experienced neuroradiologist. A comprehensive overview of the retrieved data is provided in *Table 2.*

Treatment time-point	Imaging type	Maps or delineations
Preoperative	Conventional MR imaging	T1 + gd, T2/FLAIR
	Advanced MR imaging	APT, VSI, rCBV
Pre-radiotherapy	Planning CT scan	CT
	Conventional MR imaging	T1 + gd, T2/FLAIR
	Delineations of radiotherapy planning	GTV, CTV, PTV and organs at risk
Follow-up	Conventional MR imaging	T1 + gd, T2/FLAIR

Table 2: An overview of the imaging and delineations required for this project.

5.3 Patient characteristics

Six patients from the iGene study were eligible; two were excluded as they did not receive radiotherapy. Eventually, four patients matched the criteria for this project. A detailed overview of the patient characteristics is given in *Table 3.*

	Patient 1	Patient 2	Patient 3	Patient 4
Age at diagnosis	65	50	60	50
Sex	Male	Male	Male	Male
Tumour location	Left frontal lobe	Right medial temporal lobe	Right temporal lobe	Right temporal lobe
Resection/biopsy	Resection	Resection	Resection	Resection
MGMT status	Unknown	Methylated	Unmethylated	Unmethylated
Time until progression after finishing radiotherapy	10 months	1 month	8 months	4 months

Table 3: Patient characteristics of the four glioblastoma patients who were included in this project.

6

Integration of advanced MR imaging with MIM Maestro®

Chapter 5 narrates the data retrieval of four glioblastoma patients who underwent advanced MR imaging. From these patients, brain maps of the advanced MR biomarkers VSI, rCBV and APT were created with in-house developed scripts. In this chapter, a custom pipeline that was required to allow the introduction of the advanced MR biomarker maps in MIM Maestro® is presented.

6.1 Introduction

At the Department of Radiotherapy at the Erasmus MC Cancer Institute, fusion of the structural MR imaging to the planning CT and, subsequently, delineation of the target volumes and organs at risk for radiotherapy planning of glioblastoma is performed in a software named MIM Maestro® (MIM Software Inc.). MIM Maestro® provides a comprehensive set of tools for radiation oncology, e.g. automatic (deformable) registration, standardized integration of positron emission tomography or the calculation of dose-volume histograms.

Numerous imaging protocols that include advanced MR sequences have been developed, mainly for research purposes. Custom image analysis pipelines are frequently developed to generate a brain map of an advanced MR biomarker from the raw image acquired with the advanced MR sequence, e.g. a custom image analysis pipeline is used to create an APT map from APT CEST imaging. The generated biomarker maps are frequently stored in a Neuroimaging Informatics Technology Initiative (NifTI) format, which is commonly the file format of choice in neuroimaging research.[169] The NifTI file format is considered relatively simple and minimalistic making it more suitable for image processing and analysis. In clinical practice, however, Digital Imaging and Communication in Medicine (DICOM) has become the widely adopted standard for storage and transmission of medical imaging.[170] The DICOM standard groups and compresses a substantial amount of information into data sets resulting in the integration of imaging with numerous embedded tags. These tags contain information not only of the image data itself, but also patient specific data, e.g. date of birth or gender. MIM Maestro® only allows the introduction of imaging in DICOM format. As the imaging of the advanced MR biomarkers investigated in this project is stored in NifTI format, a conversion has to be performed. There is no standardized approach for a NifTI to DICOM conversion; the optimal approach depends on the purpose of the conversion. Different scanner manufacturers extend the DICOM standard differently resulting in incompatibilities between software that has been designed to work with only one particular subset of DICOM standards.[171] Depending on a specific software and its built-in DICOM standard, a DICOM image can appear erroneous displaying orientation flips or loss of data. Therefore, for this project, a custom conversion is required that can convert the advanced MR biomarker images to a DICOM standard that is compatible with MIM Maestro®.

6.2 Methods

A custom Python script was created that had the aim to convert NifTI files to the DICOM standard compatible with MIM Maestro®.

6.2.1 DICOM tags

The biomarker images (the APT, VSI and rCBV maps) were derived from raw advanced MR imaging using custom image analysis pipelines. Whereas the biomarker images were stored in NifTI format, the raw advanced MR images were stored according the DICOM standard. In the custom Python script, specified DICOM tags from the raw advanced MR images were copied and linked to the biomarker maps. Additionally, some tags were newly created. These DICOM tags had to be selected cautiously, as copying all DICOM tags or omitting specific tags would prohibit successful conversion.

6.2.2 Introducing a scaling constant

Furthermore, the DICOM standard does not allow the signal intensity of voxels to have non-integer values. The signal intensities of the voxels in the advanced MR images consist of point values; conversion to the DICOM standard would round signal intensities resulting in the loss of detailed information. An example of details of imaging data being lost due to the conversion is shown in *Fig. 23*. A common workaround for this issue is scaling of the NifTI image before conversion. Interpretation of imaging relies mainly on contrast between voxels rather than the signal intensity of voxels itself. It is with the information of surrounding voxels that conclusions can be drawn regarding diagnosis and treatment effects. By scaling the signal intensities of each voxel according *Eq. 1*, an image can be created with improved details when rounded while maintaining similar spatial contrast. Imagine two adjacent voxels in a NifTI image with signal intensities 1.342 and 1.145. Conversion to DICOM would round the signal intensities to integers, resulting in both voxels having a signal intensity of 1. By scaling the signal intensities before conversion, e.g. with a factor of 100, the voxels in the NifTI image would have a signal intensity of 134.2 and 114.5, respectively. Now, conversion to DICOM will again round the signal intensities to integers, but due to the scaling the voxels will have distinct signal intensities of 134 and 115. By introducing a scaling constant, the conversion to DICOM can be realized without the loss of significant spatial contrast. In the custom Python script for the conversion of the biomarker maps to DICOM, scaling constants were introduced before transforming all point values to integers. To find a suitable scaling constant for each biomarker, segmentations were made of the brain on the three biomarker maps of all patients. The mean signal intensity of each biomarker was calculated to identify the order of magnitude of the signal intensities of each biomarker. Based on these findings, a suitable scaling constant was chosen.

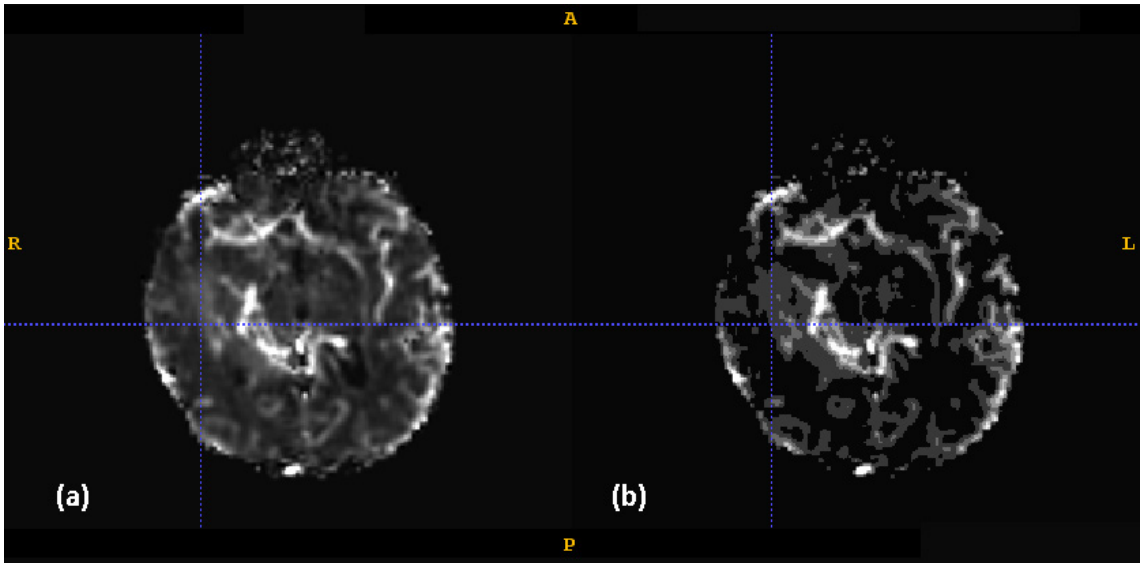

Fig. 23

The cursor is pointed at a voxel with signal intensity 1.217 in the original NifTI image of an rCBV map (a). Direct conversion of the NifTI image to the DICOM standard would result in losing detailed information, as the DICOM standard only allows voxels to have integers as signal intensities. The same voxel in the converted DICOM image, therefore, is rounded and has a signal intensity of 1 (b).

$$I_n(i,j,k) = I_o(i,j,k) * C \qquad \textit{Eq. 1}$$

Eq. 1: A new image (In) is created by multiplying the signal intensity of each voxel in the NifTI image (Io) by a scaling constant (C).

6.2.3 Validation strategy

Validation of the conversion was done by loading the output, i.e. the biomarker maps in the DICOM standard, of each patient into MIM Maestro®. Visual examination of the imaging in MIM Maestro® was performed to assess the presence of potential orientation flips. Additionally, a voxel-wise analysis that compared the input NifTI image and the output DICOM image was conducted in Python. Each voxel in the output image should have had the same signal intensity as the (scaled) input image to pass.

6.3 Results

The conversion of the biomarker maps to the DICOM standard of MIM Maestro® was performed for all four patients.

6.3.1 Creation of the DICOM header

Numerous DICOM tags were either copied from the raw advanced MR DICOM image or newly created for the creation of a DICOM header for the biomarker maps. Several crucial DICOM tags included Patient Name (0010,0010), Patient ID (0010,0020), Image Orientation (0020,0037) and Frame of Reference UID (0020,0052). A complete overview of the DICOM tags that were copied or newly created is given in *Appendix A*.

6.3.2 Image-processing before format conversion

The mean signal intensity within the brain segmentations was 0.0205, 0.0244 and 1.5655 for APT, VSI and rCBV, respectively. The mean signal intensities per patient can be found in *Appendix B*. APT signal intensities have been frequently reported in percentage [%] rather than the relative value.[111, 140] However, multiplying the APT signal intensities with 100 [%] is not enough to allow proper distinction when the intensities are rounded to integers. Therefore, the scaling constant for APT maps is set at 100.000 combining the notation of signal intensity in percentage and additionally multiplying by 1.000. The signal intensities of VSI indicate the vessel size diameter in mm. With a scaling constant of 1.000, VSI will be displayed in µm rather than mm. Lastly, rCBV does not have a unit; its scaling constant is set at 1.000 to ensure proper distinction when rounded. An overview of the scaling constants for each biomarker is given in *Table 4*.

6.3.4 Validation

All converted biomarker images (12/12) were loaded in MIM Maestro® successfully. Visual examination showed no orientation flips in all cases. An example of the advanced MR biomarker maps in the DICOM standard is shown in *Fig. 24*. Voxel-wise comparison between the input NifTI image after scaling and the output DICOM image of all biomarker maps revealed the conversion to create identical images in all cases (100%).

Biomarker	Initial signal intensity	Scaling constant	Rounded signal intensity after scaling
APT	0.0205	100.000	2050
VSI	0.0244	1.000	24
rCBV	1.5655	1.000	1566

Table 4: Scaling constants applied for the biomarkers.

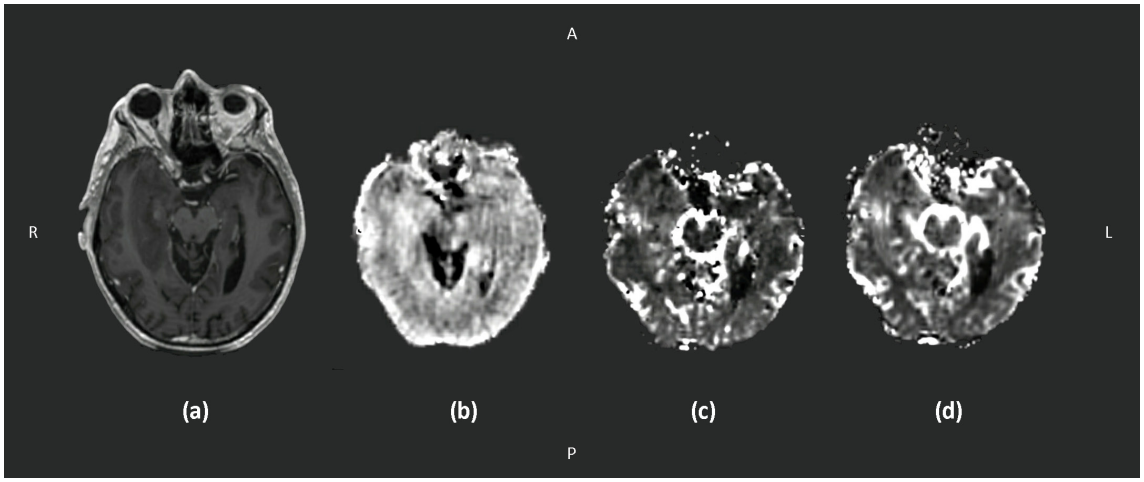

Fig. 24

(Advanced) MR imaging of one of the included patients acquired preoperatively. The T1 postcontrast (a) and converted APT (b), VSI (c) and rCBV (d) maps show similar orientations in MIM Maestro®. Note that the maps of the advanced MR biomarker maps only show information within the brain. This is part of the image analysis pipeline that is used to generate the biomarker maps from the raw MR data. As the converted advanced MR biomarker maps share the same value for Frame of Reference UID (0020,0052) as the T1 postcontrast, these images are linked to each other.

6.4 Limitations

The selection of scaling constants for each biomarker was based on improving the details after conversion while maintaining simplicity to convert signal intensities to meaningful measures. For example, the VSI scaling constant was chosen at 1000. Consequently, the majority of rounded signal intensities after conversion had an order of magnitude of 1 (i.e. within the range of 10^1 and 10^2). The other two biomarkers, APT and rCBV, had signal intensities with an order of magnitude of 3 (mostly ranging between 10^3 and 10^4), meaning more detailed information. Although a higher order of magnitude would provide more details, the value could become less intuitive to interpret.

6.5 Conclusion

In this chapter, a successful format conversion of the advanced MR biomarkers maps is presented. This conversion allows the integration of APT, VSI and rCBV maps in MIM Maestro® for radiotherapy planning.

7

Image registration

In *Chapter 5*, an overview was given of the collected data for this project. As the imaging was acquired at different timepoints, image registration was performed in MIM Maestro®. In this chapter, the procedure for the registration of the imaging is described.

7.1 Introduction

For this project, imaging from all four patients was retrieved at three different timepoints. First, the (converted) imaging from the MR session that included the advanced MR sequences was performed preoperatively. The second timepoint was pre-radiotherapy, where a planning CT (including radiotherapy delineations) and structural MR imaging was acquired. Lastly, the structural MR imaging of the follow-up session that showed first progression was retrieved. To compare the biomarker maps with the GTV, CTV and RVs, image registration was performed with the aim to transform all sets of data to the same coordinate system.

7.2 Registration

The T1-weighted postcontrast MR image from the preoperative, pre-radiotherapy and follow-up session were rigidly registered to the planning CT-scan using the fusion tool in MIM Maestro®. A radiation oncologist checked the registration and performed manual rigid correction if deemed necessary. Within each MR session, the images are co-registered, meaning they share the same frame of reference as the T1-weighted postcontrast MR image. Therefore, the other images, e.g. the advanced MR biomarker maps, are automatically registered to the planning CT-scan as well. A schematic overview of the registrations is given in *Fig. 25*. Finally, the registrations were adjusted (if necessary) and approved by another radiation oncologist.

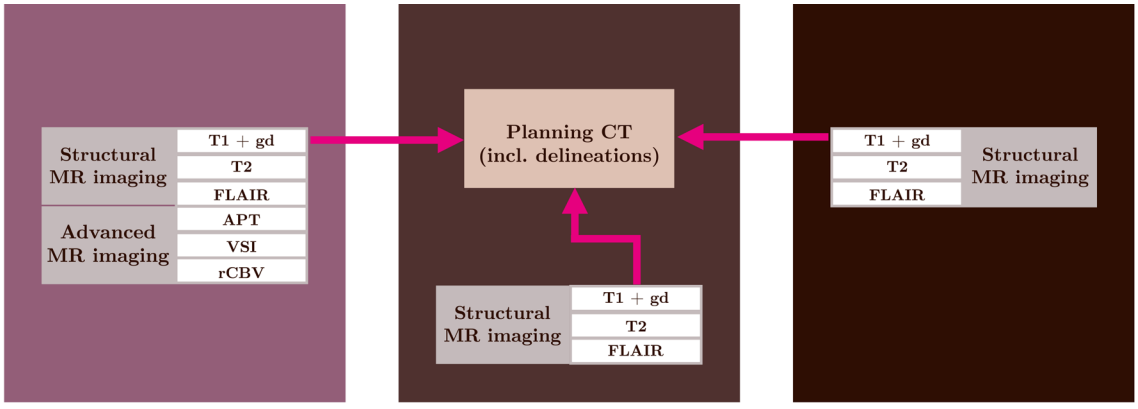

Fig. 25

An overview of the three timepoints and the transformations that were applied.

7.3 Discussion

The registration was performed for the imaging of all four patients and required manual rigid correction in all cases. As glioblastoma can grow rapidly and surgery can cause significant changes in the morphology of the brain, registration was challenging *(see Fig. 26)*. The option for deformable registration was explored, however, did not improve the outcome. Ideally, the advanced MR imaging was acquired pre-radiotherapy to minimize changes within the brain. In future studies that focus on introducing advanced MR techniques for radiotherapy planning, the acquisition of the advanced MR imaging should be done close to the planning CT acquisition. Now, discrepancies might occur between the high-risk regions on the preoperative advanced MR imaging and delineation of the biological CTV due to suboptimal registration. Nevertheless, the registrations performed for the four patients were found to be acceptable by two radiation oncologists.

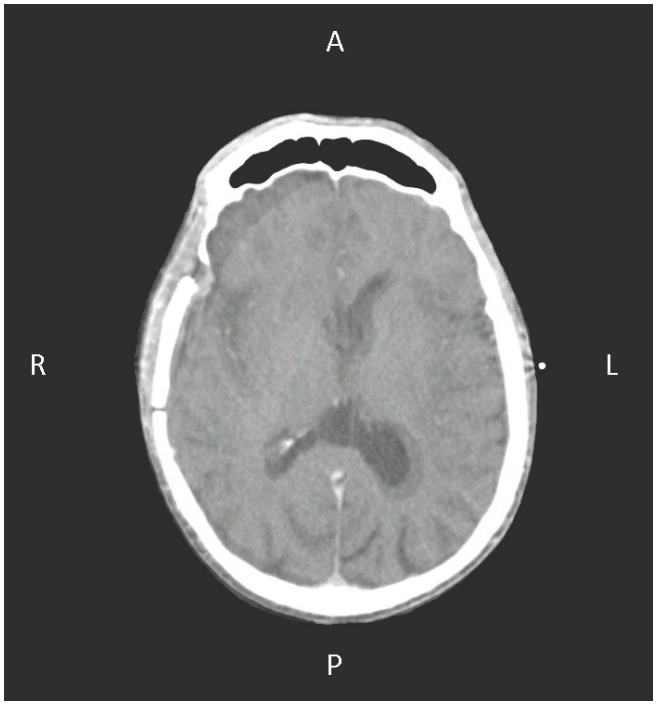

Fig. 26

A fusion of the preoperative T1-weighted postcontrast MR image to the planning CT scan (pre-radiotherapy) of one of the patients. The registration is suboptimal due to morphological changes within the brain after surgery (brain shift); correction of these changes is infeasible with rigid registration only.

8

Delineation of high-risk regions for future relapse

With the introduction of the biomarker maps in MIM Maestro®, the presence of increased cell proliferation, vasodilatation and microvascular density can be assessed. As explored in *Chapter 4*, these processes can precede morphological changes on conventional MR imaging and indicate significant tumour infiltration that is likely to develop into progression during follow-up. Therefore, a biological CTV would consist of the conventional GTV and regions with increased cell proliferation, vasodilatation and microvascular density. As these advanced MR biomarkers maps are not yet well-established in clinical practice, it can be difficult to interpret the advanced MR imaging and create a segmentation of the high-risk regions that are to be included in the biological CTV. In this chapter, a segmentation algorithm is introduced that can provide an initial segmentation of high-risk regions to aid in the delineation of the biological CTV.

8.1 Introduction

The vast majority of recurrences of glioblastomas are observed to occur local or close to the GTV.[63-65] Therefore, the hypothesis arises that hyperintense regions on the biomarker maps close to the GTV are more likely to contain significant tumour infiltration, whereas hyperintense regions further away could have other causes for the increased signal intensity. With this hypothesis, setting a threshold value within a margin from the GTV comes to mind for automatic segmentation of high-risk regions for future recurrence.

The biomarkers APT and VSI are derived using relatively novel techniques; therefore, research on optimal cutoff values to distinguish true tumour infiltration from healthy brain parenchyma is limited. For rCBV, numerous different cutoff values have been proposed.[115-117, 165] The broad range of values is a result from variations in techniques and image analysis pipelines at different institutes. An optimal cutoff value for rCBV (and APT and VSI) derived with the MR techniques and pipelines used in the Erasmus MC has yet to be investigated.

Nonetheless, closer visual examination of the biomarker maps does reveal suspicious regions within or close to the GTV *(see Fig. 27)*. As stated in *Chapter 6*, the interpretation of imaging relies mainly on context provided by contrast between voxels rather than voxel signal intensities itself. Although the imaging of only four patients is available in this project, a threshold value specific for these images could be proposed that covers the regions that appear hyperintense visually. However, with thresholding comes another problem as spatial contrast is also seen in the healthy brain, particularly on VSI and rCBV maps. Arteries, for example, can appear hyperintense on these maps as well *(see Fig. 28)*, making it difficult to only segment suspicious regions. Introducing an additional threshold or automatic tools to segment the arteries could be a viable solution, however, thresholding in general might not be the best approach for creating a biological CTV. It can be a useful tool for segmentation of the high-risk regions, but it is important to be mindful of the purpose of a CTV. It defines the volume that should be targeted with ionizing radiation and, ideally for VMAT, would have a convex shape to allow sufficient target coverage while limiting harm to surrounding

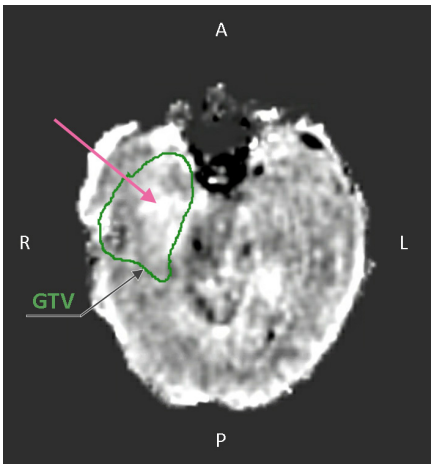

Fig. 27

An APT map of a patient with a glioblastoma in the right frontotemporal lobe. The GTV was delineated on conventional MR imaging. The APT map shows hyperintensity within and adjacent of the GTV, indicating increased cell proliferation (pink arrow).

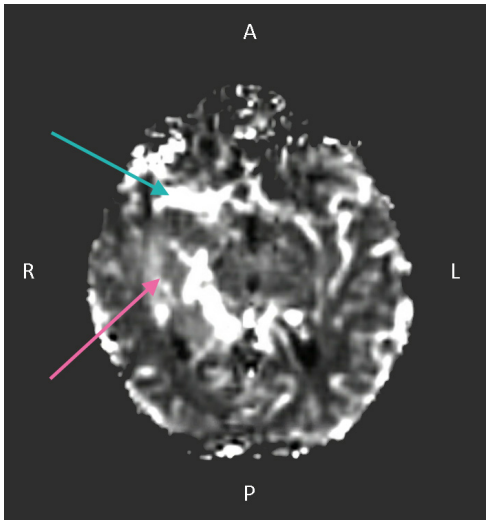

Fig. 28

The rCBV map of the same patient shown in Fig. 24. Structures that are present in the healthy brain can also be the cause of hyperintensity on these maps. The right middle cerebral artery (blue arrow) appears highly hyperintense. Although less profound, close to the tumour the rCBV seems to be increased as well (pink arrow).

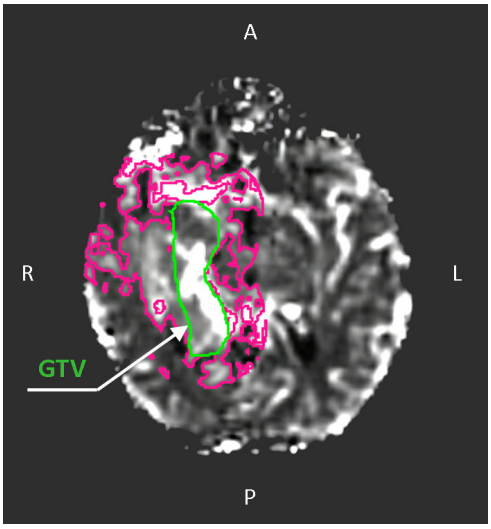

Fig. 29

Around the conventional GTV, voxels that were within a range of 1.5 cm from the GTV and had signal intensities above a chosen threshold were segmented as high-risk regions (pink contour). An additional threshold was selected to exclude voxels that were most likely included due to vascular structures rather than tumour pathophysiology. The irregular shape of the contour can complicate radiotherapy planning.

tissue. Thresholding does not take this aspect into account, as it is solely based on signal intensity of the voxels. The segmentations are less suitable for radiotherapy planning due to its complex shapes *(see Fig. 29)*.

An image segmentation method that might be more suitable for this project is region growing. This approach examines neighbouring voxels of an initial seed point and determines whether voxels should be included to a segmentation based on a set of parameters.[172] The advantage of the region growing algorithm is that its segmentation is expected to be more appropriate for radiotherapy planning. Additionally, as glioblastomas frequently recur locally, this algorithm fits this tumour type well as it indirectly takes distance into account.

8.2 Methods

The region growing algorithm incorporated in MIM Maestro® was used for this project.

8.2.1 The region growing algorithm

The algorithm requires three input parameters, the location of an initial seed point and a defined box as region of interest. The seed point is the voxel from which the algorithm will start growing. Based on the input parameters, i.e. a lower and upper threshold value and a tendril diameter, voxels adjacent to the seed point will be included in the growing contour. The algorithm searches within the defined box for voxels that are within the specified signal intensity range and are connected to the seed point by a path consisting of other voxels within the specified intensity range.

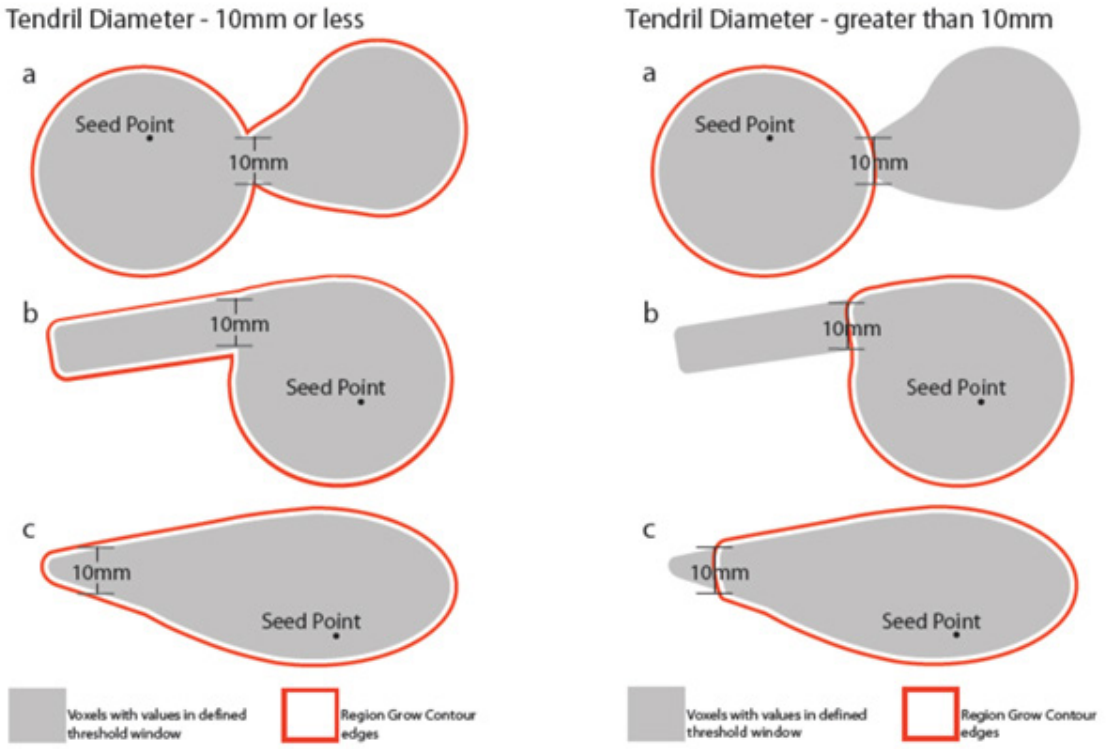

Fig. 30

The tendril diameter determines the tolerance for protrusion. Examples of three different shapes (a,b,c) with a link of 10 mm are given.

The tendril diameter prevents the contour from growing to neighbouring voxels when any dimension of contiguous voxels, as a group, is narrower than the tendril diameter. A larger value for the tendril diameter is more restrictive, and will, in general, result in a more convex contour shape. An illustrative explanation of the tendril diameter is given in *Fig. 30.*

8.2.2 Input parameters

Although optimal cut off values have yet to be explored, suspicious regions can be seen on the advanced biomarker maps. On each biomarker map a seed point was chosen manually within the suspicious region for each patient for the region growing algorithm. The box for the region of interest covered the entire brain in all cases. In an iterative manner, input parameters were selected that covered the suspicious region best for all four patients. Additionally, smoothening and morphological operations to fill holes were applied.

8.3 Results

The following input parameter values for each biomarker were found to cover the suspicious regions adequately in all four patients (see Table 5 - 7). An example of the APT high-risk contour in one patient is shown in *Fig. 31.*

	APT value in MIM Maestro®	APT value [%]
Lower threshold value	1 800	1.8
Upper threshold value	4 000	4.0
Tendril diameter	20	n/a
Fill holes	Strong	
Smoothening	Enabled	

Table 5: Input parameters selected for region growing of the high-risk contour on APT.

	VSI value in MIM Maestro®	VSI value [mm]
Lower threshold value	13	0.013
Upper threshold value	42	0.042
Tendril diameter	12	n/a
Fill holes	Strong	
Smoothening	Enabled	

Table 6: Input parameters selected for region growing of the high-risk contour on VSI.

	rCBV value in MIM Maestro®	rCBV value [-]
Lower threshold value	850	0.85
Upper threshold value	3200	3.2
Tendril diameter	12	n/a
Fill holes	Strong	
Smoothening	Enabled	

Table 7: Input parameters selected for region growing of the high-risk contour on rCBV.

8.4 Discussion

In this chapter, region growing is introduced as an assist for the delineation of the high-risk regions on the advanced MR biomarker maps. There are some limitations. The values for the input parameters of the algorithm were chosen based on visual coverage of hyperintense regions. This was an iterative process; however, a systematic approach that would assess different combinations of input parameters would be more accurate. Moreover, as the ultimate goal is to identify high-risk regions of future relapse, the systematic approach should have the aim to find the combination that covers the RV rather than hyperintense regions on the biomarker maps. Further examination

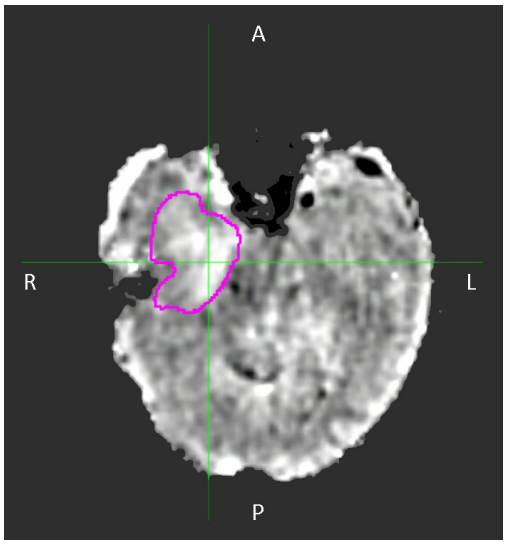

Fig. 31

The seed point (green cursor) was selected manually on the APT map. From there, the region growing algorithm was initiated with the input parameters provided in Table 5. The pink contour is the outcome of the algorithm that indicates the high-risk region for future recurrence based on APT information.

of optimal values for the input parameters has been excluded deliberately from this project, as this would have been based on only four patients. Future research should therefore include a larger cohort with acquisition of advanced MR biomarker maps to perform adequate parameter tuning.

Furthermore, region growing is a segmentation method that will not extend extremely far beyond the GTV. Therefore, if a first recurrence occurs distant, it is less likely to be included by the region growing algorithm. Nonetheless, the vast majority of recurrences occur within or close to the GTV. That is why the standard CTV yields a margin of 1.5 cm around the GTV. In addition, it is important to keep in mind that the purpose of the region growing algorithm is to provide an initial delineation. It is up to the radiation oncologist to customize the generated contours if deemed necessary.

9

Generation of the biological CTV

In *Chapter 8,* a region growing algorithm was introduced with the aim to assist in delineation of high-risk regions on the advanced MR biomarker maps. In this section, a semi-automatic workflow is presented that allows the generation of a biological CTV based on the high-risk regions contoured by the region growing algorithm.

9.1 Introduction

As this is the first time these advanced MR biomarker maps are introduced for radiotherapy planning in the Erasmus MC Cancer Institute, it can be difficult to fully understand the information the advanced MR imaging provides. This will come with further research and experience with these images. To ensure an intuitive and robust approach for the generation of a biological CTV, a workflow has been created in MIM Maestro®. This workflow incorporates automated seed point selection to ensure a suitable initial seed point is selected.

9.2 Seed point analysis

The region growing algorithm requires the selection of an initial seed point from which the algorithm will grow a contour. The seed point is a single voxel and must meet a set of requirements to ensure the algorithm to operate properly. Hypothetically, voxels have two major properties that can influence their suitability for becoming a seed point: The signal intensity and the location. Automatic seed point selection removes the possibility for choosing a wrong seed point. A seed point analysis is conducted to assess the requirements a voxel must have to be suitable as an initial seed point and to determine an optimal approach for automatic seed point selection.

9.2.1 Methods

It is hypothesized that a voxel must have a suitable signal intensity and location to succeed as seed point. First, the signal intensity has to be within the intensity range of the algorithm, i.e. the lower and the upper threshold. If the initial point falls outside the intensity range, the algorithm will fail. Secondly, the location has to be carefully chosen. The center of the GTV comes to mind, however, the voxel in the center of the GTV might have an insufficient signal intensity. This could be caused by noise or a resection cavity. Nonetheless, as the majority of recurrences occur locally, it is logical to have a seed point located within the GTV.

For the biomarker maps of each patient, a segmentation within the GTV was made of all suitable voxels based on signal intensity. For APT maps, for example, the lower and upper threshold used in the algorithm were 1800 and 4000, respectively. Within the GTV delineation, only voxels within that intensity range were included as possible seed points. Subsequently, the median signal intensity was found. Voxels with this specific signal intensity were selected as seed points for the seed point analysis. The median signal intensity is chosen as it is assumed that adjacent voxels have an intensity close to the median signal intensity. Thus, adjacent voxels have a higher probability to be included by the algorithm.

From the voxels with a median signal intensity, high-risk contours were created using the region growing algorithm and the input parameters described in *Chapter 8*. The generated contours from each seed point were compared to evaluate the effect of the location on the outcome of the algorithm. The amount of different volumes was explored; volumes were considered similar if the volumes had a dice similarity coefficient (DS) higher than 0.9. The volume that visually covered the high-risk region best was marked. Subsequently, each seed point was labelled with its corresponding volume. The Euclidean distance from each seed point to the GTV center was calculated to assess the effect of proximity to the GTV center on generated volume.

9.2.2 Results

For each patient, region growing was performed for all selected seed points on the three biomarker maps. An example of the generation of volumes on an APT map in the seed point analysis is shown in *Fig. 32.* In some cases, all seed points had the same outcome, e.g. the same volume or no volume. In other cases, seed points at different locations generated different outcomes. The outcomes for region growing on the APT maps is given in *Table 8* (a similar overview for VSI and rCBV can be found in *Appendix C*). In all cases (i.e. for each biomarker of each patient), the majority of seed points generated the volume that was marked to cover the high-risk regions best. Volumes that were considered similar (DS $>$ 0.9) had a DS of 1.0 in all cases, indicating 100% similarity.

Patient	Median signal intensity (APT)	Number of seed points	Generated volumes	Intervolume DS
1	2746	55	Vol. 1 (n=55)*	
2	2508	134	Vol. 1 (n=102)* Vol. 2 (n=15) No volume (n=17)	$DS_{Vol1,Vol2}$ = 0.033
3	2625	122	Vol. 1 (n=107)* Vol. 2 (n=1) No Volume (n=14)	$DS_{Vol1,Vol2}$ = 0.038
4	2410	109	No volume (n=109)*	

*Volume that visually covers the suspicious region best.

Table 8: An overview of the distribution of volumes on APT maps created during the seed point analysis.

Evaluation of the seed point locations and the corresponding volumes showed that seed points that had a median signal intensity and were located closest to the GTV center, generated the volume that covers the hyperintense region on the maps in 100% of the cases. The evaluation of the seed point locations for APT is shown in *Fig. 33.* The evaluation for VSI and rCBV are included in *Appendix D.*

9.2.3 Discussion

The seed point analysis revealed the feasibility of automated seed point selection. A voxel that has a median signal intensity of the voxels within the intensity range of the algorithm and is located close to the GTV center, is suitable as initial seed point and will generate a contour that covers the suspicious region on the advanced MR biomarker map. Seed points that generated an unwanted volume were mostly seen at the far edge of the GTV, indicating that the algorithm in these cases does not cover the central part.

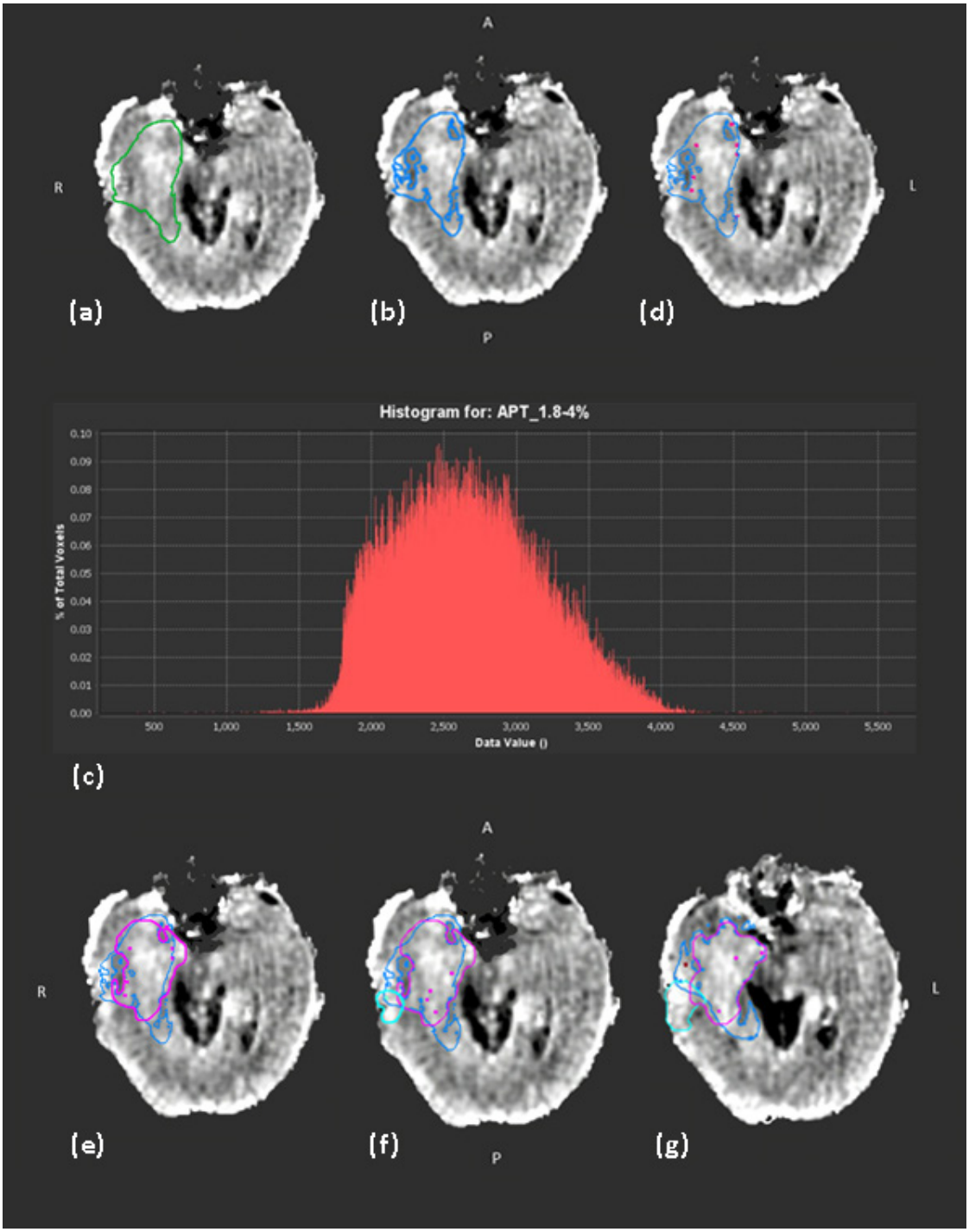

Fig. 32

The GTV (green contour) is located in the right frontotemporal lobe (a). A delineation is created of possible seed points within the GTV (blue contour) based on the intensity range, i.e. 1800 – 4000 for APT (b). From these voxels, the median signal intensity (i.e. 2625) is found (c). All possible seed points with a signal intensity of 2625 (pink seeds) are selected and used as initial seed point for the region growing algorithm (d). From 122 seed points, the algorithm generated the same volume (pink contour) from 107 different seed points (e), a different volume (cyan contour) from 1 seed point (f) and no volume from 14 seed points (brown seed) (g).

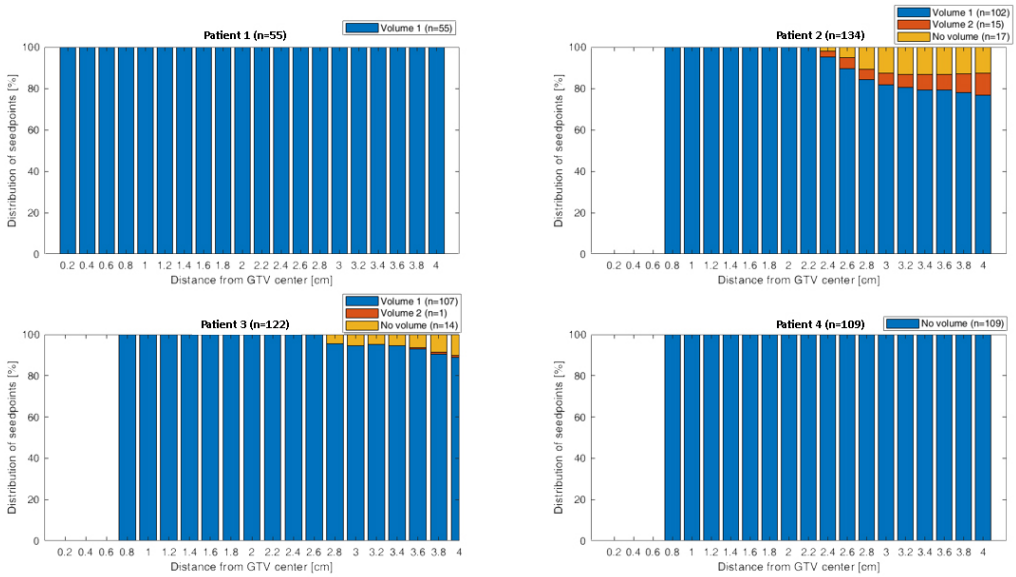

Fig. 33

The x-axis describes the distance of the seed points to the GTV center, whereas the y-axis describes the distribution of labelled seed points. In all four patients, it is shown that the seed points closest to the GTV center correspond to the marked volumes

Although this seed point analysis was performed on only four patients, all twelve cases (3 biomarkers per patient) showed the same results. It is important note that these advanced MR biomarker maps were acquired before surgery. In future research, it should be investigated if automatic seed point selection is also feasible by choosing a suitable seed point closest to the GTV center after surgery. Automatic seed point selection has the advantage of providing a robust and standardized approach for the generation of a biological CTV by minimizing inter- and intra-observer variations.

9.3 A semi-automatic workflow

MIM Maestro® offers the possibility to create workflows by automating step-by-step processes that involve complex, interactive analysis, displays and image-processing. Automated workflows can improve user-friendliness, ensure consistency and minimize the margin for human error. A semi-automatic workflow was created for the generation of a biological CTV in MIM Maestro®.

The workflow relies on the contouring of high-risk regions on APT, VSI and rCBV maps using a region growing algorithm. Before the workflow can be initiated, the advanced MR imaging has to be already registered to the planning CT-scan. In addition, a delineation for the GTV has to be already created. Only then, the workflow can be initiated. First, on the APT map a suitable initial seed point in the GTV for region growing is automatically found and selected as a seed point for region growing. Now, the radiation oncologist can enter the input parameters for the region growing algorithm. Custom templates for each biomarker have been created and can be used to select a specific combination of input parameters to limit the chance of human error and improve workflow efficiency. Thereafter, a checkpoint is reached where the radiation oncologist can adapt the contour on the biomarker map if deemed necessary. This process is repeated for the biomarkers VSI and rCBV, eventually yielding three contours of high-risk regions based on the advanced MR biomarker maps. The last part of the workflow combines the high-risk regions with the GTV to create a delineation of the biological CTV. A step-by-step user's manual is provided in *Appendix E.*

After the semi-automatic workflow, manual adjustment of the biological CTV can be performed to adjust for organs at risk or anatomical barriers. This is similar to the conventional approach for CTV delineation. Thereafter, the PTV can be created. A schematic overview of the workflow is shown in *Fig. 34*.

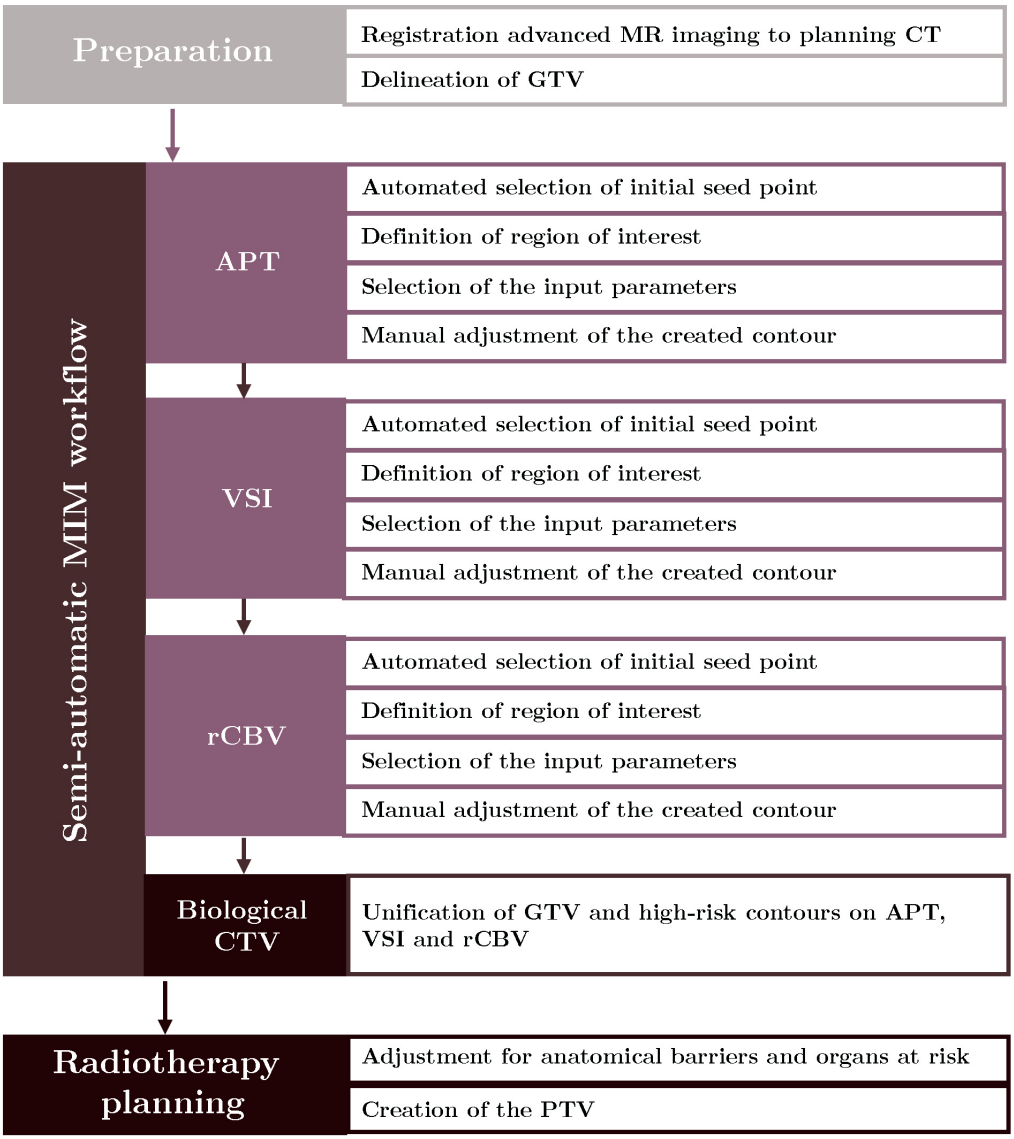

Fig. 34

The semi-automatic workflow in MIM Maestro® consists of four major steps.

9.4 Discussion

A semi-automatic workflow in MIM Maestro® is presented that creates an initial biological CTV delineation based on a region growing algorithm. The workflow incorporates checkpoints to allow interaction between the user during the creation of the biological CTV and only contains tools and functionalities from MIM Maestro® to ensure compatibility with the software. The latter consideration does have its drawback: The adaptability of functionalities and tools in MIM Maestro® is restricted, meaning possibilities for modifications are limited. MIM Maestro® does offer the option to create custom extensions using Java or Matlab programming languages. Extensions provide the freedom to perform image analyses or-processing otherwise not available in MIM Maestro®. Nevertheless, the semi-automatic workflow presented in this chapter works properly and does not require custom functionality. An extension, in this project, would only be beneficial if further research requires complex functionality not yet available in MIM Maestro®. The downside of the use of extensions in MIM Maestro® is the necessity of additional software and adequate frontend communication, complicating the workflow and reducing user-friendliness. MIM Maestro® offers numerous tools for image analyses and image processing, making the use of custom extensions in this project unnecessary.

10

Analysis of the biological CTV

With the data of four patients and the automated workflow described in *Chapter 9*, the added value of the biological CTV was explored. A remarkable reduction in size of the CTV was observed, while maintaining adequate coverage of the RVs.

10.1 Introduction

With the introduction of advanced MR imaging, the opportunity arises to personalize CTV delineation. Advanced biomarker maps provide additional information on tumour infiltration and high-risk regions of future relapse. These suspicious regions indicate altered physiology and encompassing these regions in addition to the GTV can produce a biological CTV. The introduction of a biological CTV can result in improved coverage of true tumour tissue while sparing more healthy tissue. At the moment, the typical CTV margin at the Erasmus MC Cancer Institute consists of a 1.5 cm expansion of the GTV. Generally, this margin is set in every direction due to the lack of information on tumour infiltration. Assuming the biological CTV only covers significant tumour tissue, a reduction in target size is expected compared to the conventional CTV. This can eventually lead to reduced radiation toxicity and thus improved quality of life. Furthermore, dose constraints for organs at risk can lead to the decision to underdose the target as the expected radiation toxicity could be too severe. With a biological CTV, there is a probability that the anticipated dose in organs at risk does not exceed the dose constraints, while it would in a radiotherapy plan with the conventional CTV. This could potentially lead to improved survival for this group of glioblastoma patients. Additionally, the advanced MR biomarker maps could provide novel insights in viable tumour tissue beyond the 1.5 cm margin. Including these regions to the biological CTV could result in improved coverage of tumour tissue and thus improved overall survival.

In this research, the aim was to explore the potential of a biological CTV that incorporates information from APT, VSI and rCBV maps for improved radiation treatment of glioblastomas

10.2 Methods

The four patients previously described in *Chapter 5* were included. The semi-automatic workflow described in *Chapter 9* was used to generate a biological CTV; manual adjustments during the workflow were prohibited. The input parameters for the region growing algorithm were similar to those reported in *Chapter 8*.

The size of the conventional CTV and the biological CTV were compared to assess the potential to reduce the risk on radiation toxicity. Furthermore, the tumour coverage by the GTV, biological CTV and the conventional CTV were compared by analysing the pattern of failure. The RV was delineated (by a radiation oncologist) on the MR imaging that first showed progression according to the RANO criteria.[69] Coverage of the RV could estimate the potential of the biological CTV to cover tumour infiltration.

To assess the resemblance of the contours of the individual biomarkers, the DS between the contours were calculated. Similar contours could imply that inclusion of only one of the maps is feasible, as the other maps would not provide any additional information. Furthermore, the RV was divided to evaluate the amount of coverage by each individual biomarkers. Delineations were made that classified the RV in three groups:

1. Covered by the GTV.
2. Covered by the biological CTV, but not the GTV.
3. Not coverd by the biological CTV.

The second group was separated further into the following groups:

2a. Covered by the contour of APT only.

2b. Covered by the contour of VSI only.

2c. Covered by the contour of rCBV only.

2d. Covered by the contours of APT and VSI.

2e. Covered by the contours of VSI and rCBV.

2f. Covered by the contours of APT and rCBV.

2g. Covered by the contours of APT, VSI and rCBV.

The separation and DS could provide insights into the potential of individual biomarkers to cover tumour tissue beyond the GTV.

Lastly, to estimate the performance of the semi-automatic workflow, a radiation oncologist manually delineated suspicious regions on the APT, VSI and rCBV maps without prior knowledge of the RV and the biological CTV generated by the workflow. The suspicious regions delineated by the radiation oncologist were united with the GTV to create a manually delineated biological CTV. This CTV was compared with the biological CTV generated by the semi-automatic workflow in terms of size and coverage of the RV to evaluate the performance of the semi-automatic workflow.

10.3 Results

The biological CTV for all four patients were created in MIM Maestro® using the semi-automatic workflow *(see Fig. 35)*. In all cases, the biological CTV was different from the conventional CTV. Furthermore, the RVs were delineated on the follow-up imaging.

10.3.1 Comparison between the biological CTV and the conventional CTV.

The biological CTV was smaller than the conventional CTV in all cases *(see Fig. 36)*. The observed size reduction was 82.6%, 56.7%, 58.8% and 65.1% for patient 1, patient 2, patient 3 and patient 4, respectively. In patient 4, the biological CTV was identical to the GTV, as the region growing algorithm did not identify suspicious regions on the APT, VSI and rCBV maps. A complete overview of the volume sizes is given in *Appendix F.*

In all four cases, the coverage of the RV by the biological CTV was smaller compared to the coverage by the conventional CTV. The biological CTV covered more than 95% of the RV in three of the cases. In patient 3, the coverage by the biological CTV was 57.3%. A comprehensive overview of the coverage by the GTV, biological CTV and conventional CTV is shown in *Table 9.*

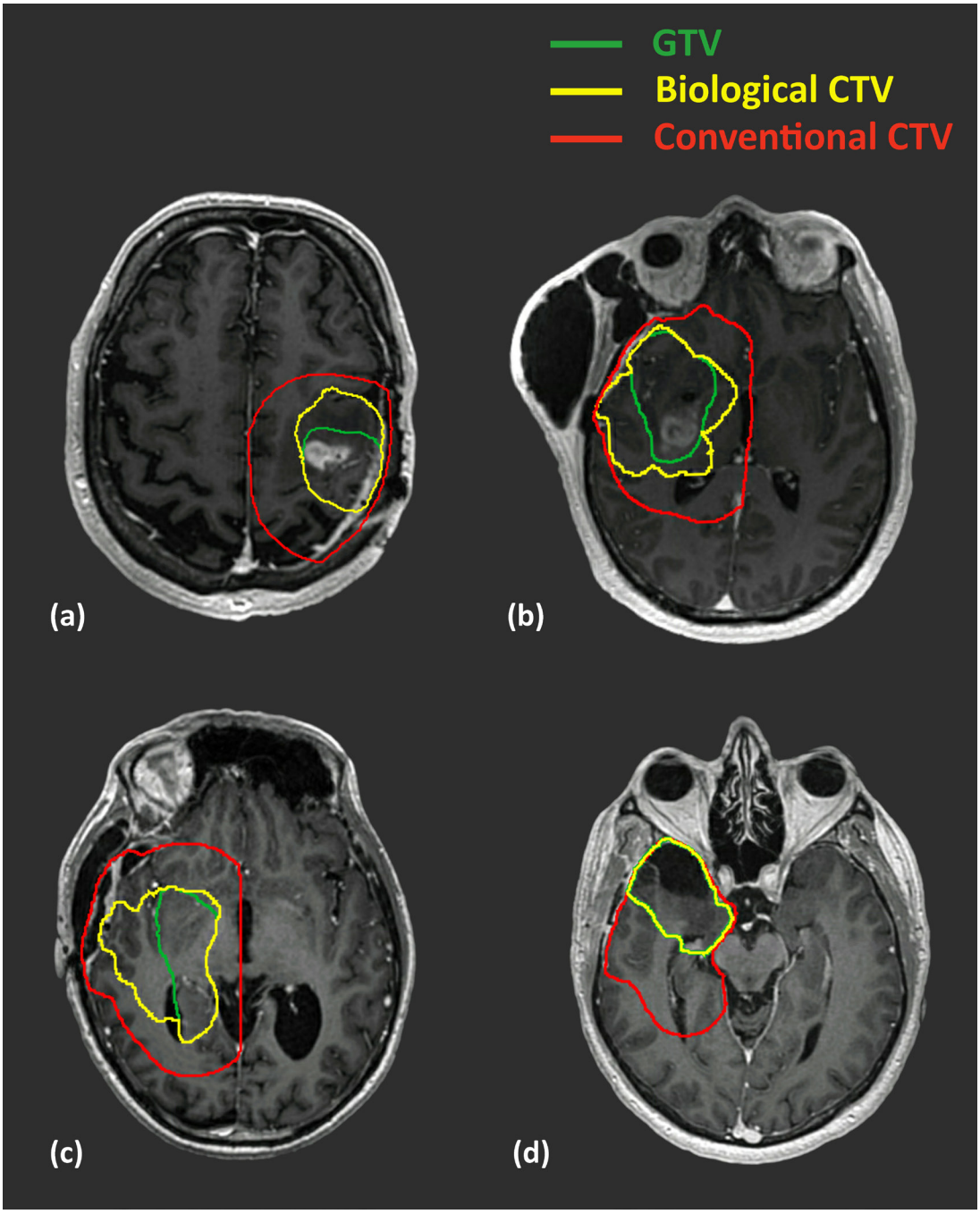

Fig. 35

The semi-automatic workflow generated a biological CTV different from the conventional CTV in all four subjects, i.e. patient 1 (a), patient 2 (b), patient 3 (c) and patient 4 (d). The contours are displayed on the T1-weighted MR image postcontrast that was used for radiotherapy planning and thus delineation of the GTV and the conventional CTV.

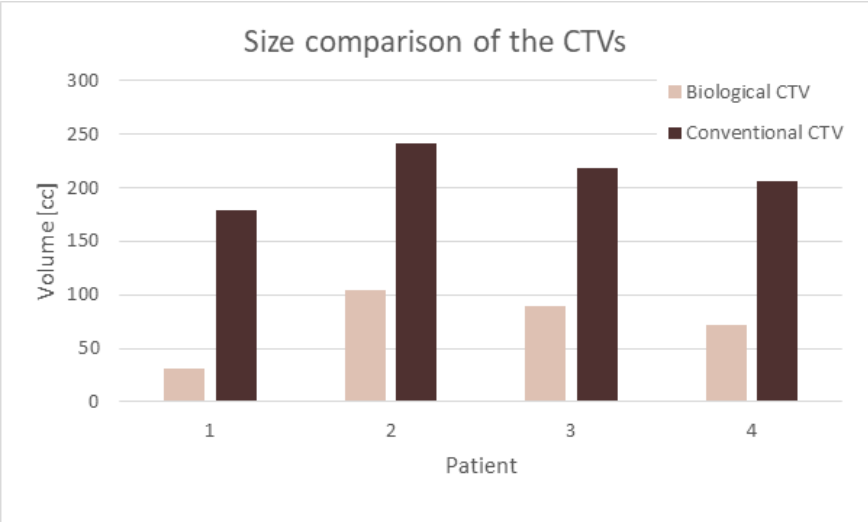

Fig. 36

A size comparison of the biological CTV and the conventional CTV of each patient. The generated biological CTV is smaller in every patient.

Patient	RV coverage by GTV [%]	RV coverage by biological CTV [%]	RV coverage by conventional CTV [%]	RV coverage difference between biological and conventional CTV [%]	Time until progression after finishing radiotherapy [months]
1	93.1	95.1	100	4.9	10
2	73.5	95.2	96.9	1.7	1
3	46.6	57.3	94.3	37.0	8
4	95.4	95.4	99.3	3.9	4

Table 9: An overview of the coverage of the RV by the GTV, biological CTV and the conventional CTV.

10.3.2 Analysis of the individual biomarkers.

Patient 1 had a biological CTV solely based on an APT contour, as the region growing algorithm found no suspicious regions on the VSI and rCBV maps. For patient 4, the biological CTV was similar to the GTV, as no contours were created on any biomarker map. The biological CTV of patients 2 and 3 were created from contours of all three biomarkers.

The DS between the contours from APT, VSI and rCBV maps were calculated for patients 2 and 3. The similarity was highest between the VSI and rCBV contours with a DS of 0.75 for patient 2 and a DS of 0.72 for patient 3. The DS between APT and VSI and APT and rCBV can be found in *Appendix G.*

In all cases, the majority of the RV was within the GTV. In patients 2 and 3, the RV outside the GTV was better covered by the APT and rCBV contours compared to the VSI contour. An example of the distribution of the RV coverage is given in *Fig. 37* and *Fig. 38.* A comprehensive overview of the coverage of each biomarker is given in *Appendix H.*

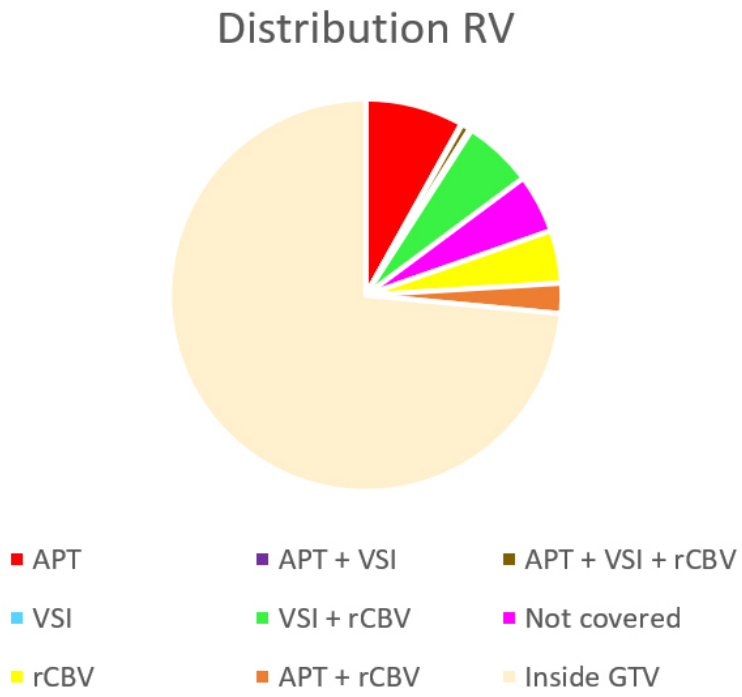

Fig. 37

A pie chart of the distribution of the RV coverage of Patient 2.

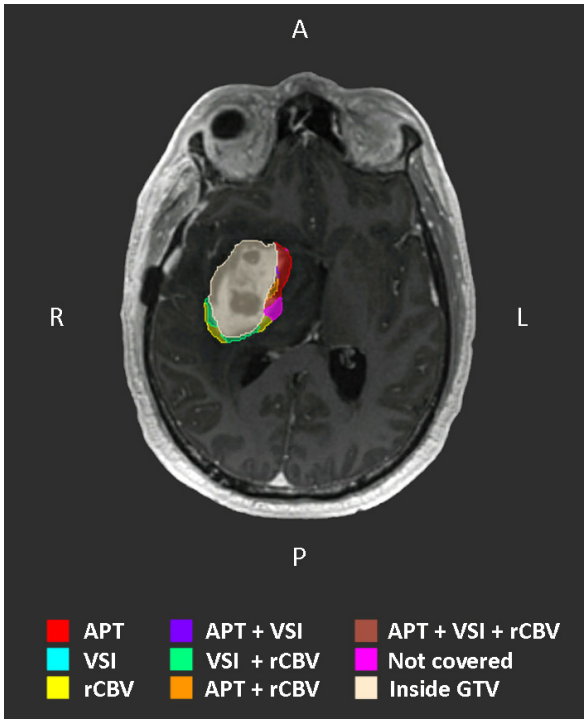

Fig. 38

An overlay of the distribution of the RV on the T1-weighted postcontrast MR image of Patient 2.

10.3.3 Comparison of the biological CTV generated with the workflow and manual delineation.

For each patient, a manual biological CTV was created by combining the GTV with the high-risk regions manually contoured by the radiation oncologist *(see Fig. 39)*. The DS of the manual biological CTV and the biological CTV created by the semi-automatic workflow ranged between 0.76 – 1.00. Varying per patient, the size of the manually delineated biological CTV was either smaller or larger than the biological CTV created with the workflow *(see Fig. 40)*. Improved coverage also varied per case. The observed difference of the coverage was never larger than 5%; a detailed overview of the coverage per case is provided in *Appendix I*.

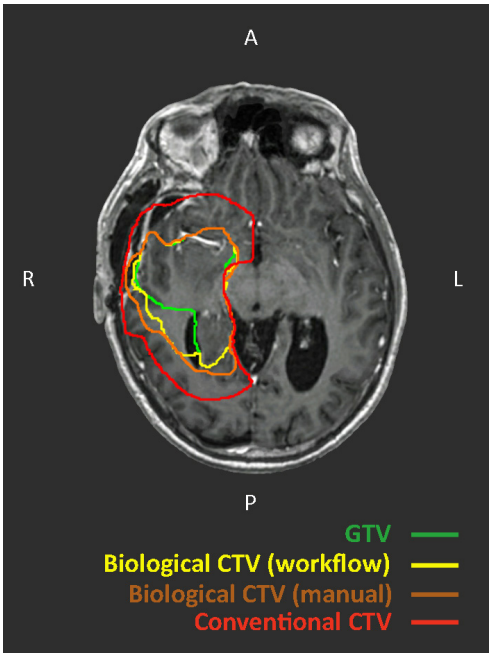

Fig. 39

The three CTVs on a T1-weighted post-contrast MR image of patient 3.

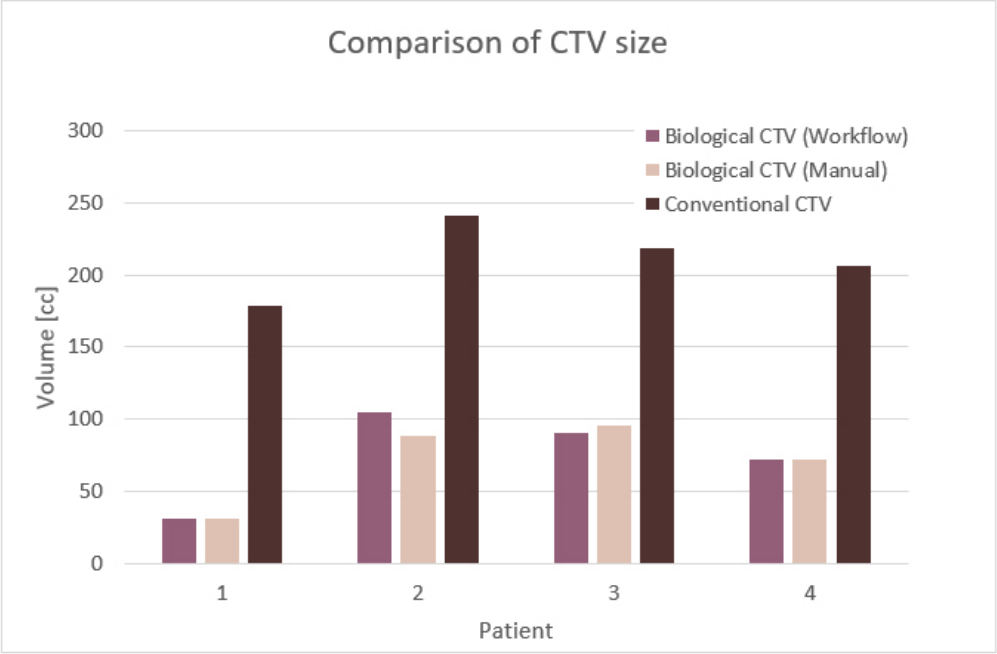

Fig. 40

A comparison of the size of the three CTVs per patient.

10.4 Discussion

In this chapter, the potential of advanced MR imaging and a biological CTV for improved radiotherapy for patients with glioblastomas is explored. The biological CTV that was created with a semi-automatic workflow in MIM Maestro®, showed a considerable reduction in size of the clinical target volume when compared with the conventional approach. In three of the four cases, the coverage of the RV by the biological CTV remained higher than 95%, indicating that the biological CTV would encompass pattern of failure adequately. In the other case, Patient 3, the coverage worsened considerably. It is important to note that the RV in this patient was extremely large when compared to the other patients *(see Fig. 41)*. The RV was almost twice the size of the GTV, while the RV in the other patients was abundantly smaller than the GTV. The observation of a relatively large RV could be caused by the fact that follow-up MR imaging had to be delayed. During follow-up, the patient's MR acquisition had to be terminated early due to the patient's clinical condition and thus be delayed. As glioblastomas are highly aggressive, the RV could have grown in size during the time the patient had to wait for new acquisition. As the biological CTV is significantly smaller than the conventional CTV, it is expected that the coverage of a RV that had the time to rapidly grow to a large volume, would be superior by a larger conventional CTV. Nonetheless, the other cases showed the potential of proper coverage by a biological CTV that significantly reduces the size of the target volume.

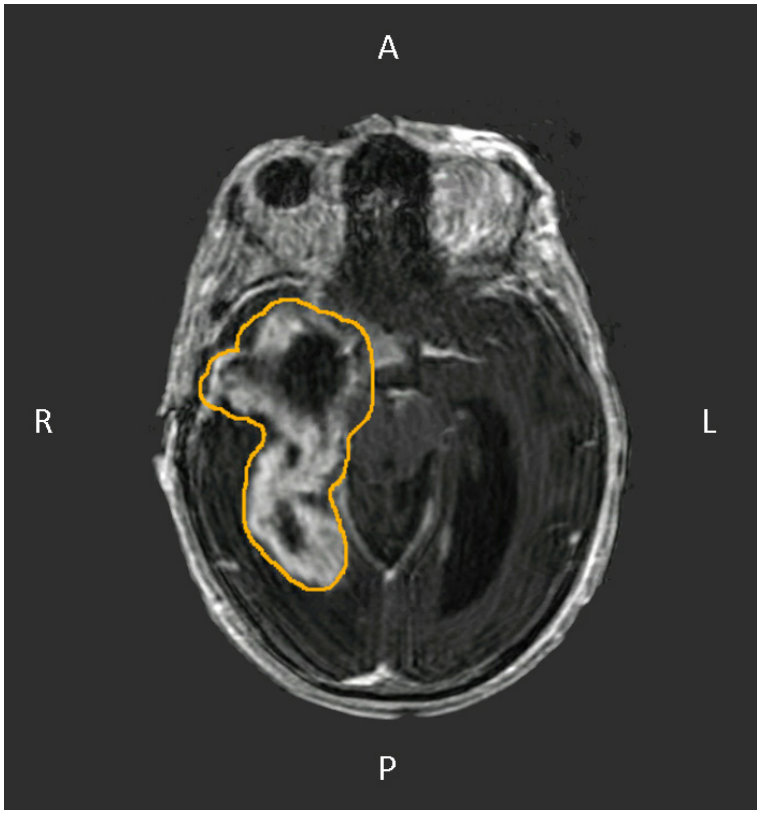

Fig. 41

The T1-weighted postcontrast MR image of Patient 3 shows a large contrast-enhancing RV (orange contour). The motion artefacts visible on this image are partially a result of the patient's clinical condition.

The time discrepancy between the advanced MR imaging acquired preoperatively and the radiotherapy delineations pre-radiotherapy could have caused spatial misalignment of the contours of high-risk regions. In some cases, mass effect or post-surgery brain shift made registration challenging. The possibility of deformable registration was explored, however, opted against after careful consideration with various experts. The rigid registration of the imaging was performed and supervised by two radiation oncologists to minimize the deviation caused by the time discrepancy.

The analysis of the contours of the individual biomarkers showed that the biomarkers APT, VSI and rCBV provide supplemental information for the biological CTV. Overlap in hyperintense regions on APT maps and hyperintense regions on vascular biomarker maps has not yet been explored in other research. Here, it is shown that these biomarkers individually highlight different regions around the GTV. Glioblastomas are notorious for their heterogeneity; the observation of different biomarkers providing important information fits this principle.[173, 174]

The APT, VSI and rCBV maps do not provide information on the whole brain. A region of interest had to be selected during the acquisition, causing imaging in craniocaudal direction of the brain beyond the tumour not to be imaged in the patients included in this project *(see Fig. 42)*. As the conventional CTV requires a 1.5 cm expansion of the GTV in every direction, it could be that the biological CTV does not include information on microscopic tumour infiltration in the craniocaudal axis as it is not visualized. Expanding the region of interest of MR image acquisition could be possible, but requires sacrifices on other criteria, e.g. the slice thickness or acquisition time. This should be done in careful consideration with both radiation oncologists and MR physicists to include all involves factors. The outcomes of this project were promising, however, might be improved by finding an optimal region of interest for image acquisition.

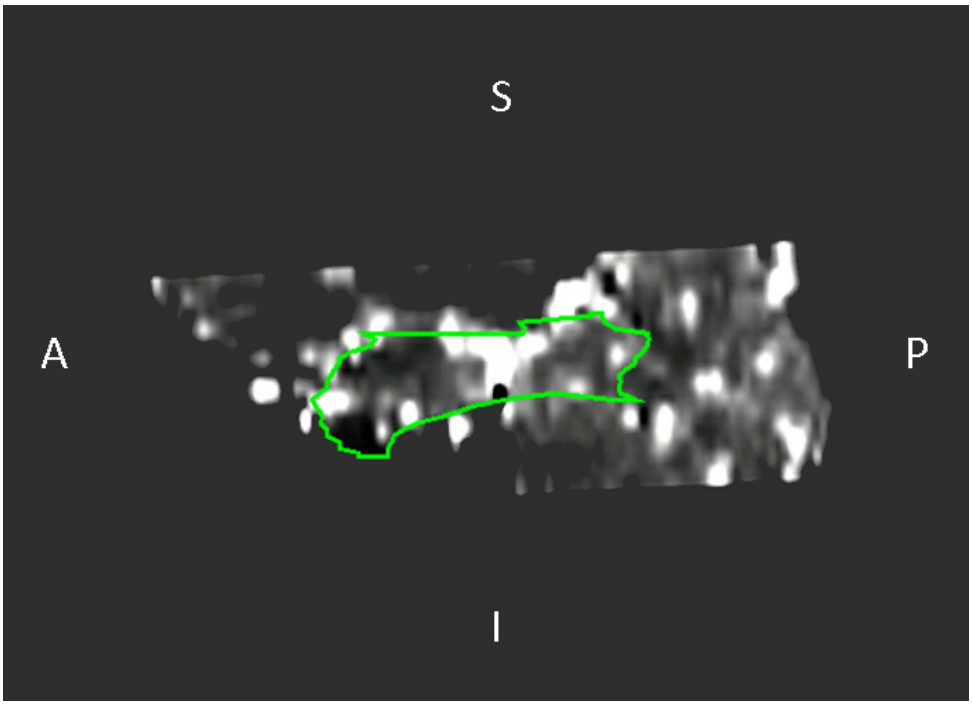

Fig. 42

A sagittal view of a VSI map of Patient 3. The region of interest was selected to ensure the gross tumour could be visualized in its entirety.

This project only included four patients, making a systematic approach for parameter tuning not practical. Instead, an iterative approach was chosen to visually find the input parameters for the region growing algorithm. This approach did yield information on how changes to the input parameters would affect the contouring of high-risk regions. The lower and upper threshold define the intensity range of the contour, making it feasible to exclude regions with normal physiology (like arteries). The tendril diameter is important to create conform delineations suitable for radiotherapy planning. Lower tendril diameters are less restrictive and thus result in a less spherical shape, making it more suitable for maps like VSI and rCBV: Exclusion of structures like arteries make it more difficult to create convex delineations, as vasculature is present throughout the whole brain. The input parameters that were chosen in this project have been a good starting point. With these input parameters, the region growing algorithm showed similar results regarding size and coverage of the RV compared to manual delineation of a biological CTV. Yet, the possibility for an optimal combination of input parameters should be explored.

Future research should therefore focus on exploring optimal input parameters for the semi-automatic workflow and further validation of the biological CTV in a larger cohort of patients. Further exploration of the coverage of the RV by the biological CTV could provide more evidence on the potential of personalized radiotherapy planning for glioblastomas. Ideally, a prospective study would be initiated that includes twenty-five glioblastoma patients who are to undergo standard therapy. This research is still in an early phase as the optimal input parameters have yet to be determined. Additionally, the incidence of glioblastoma is low, making inclusion difficult.[175] With the hypothesis that the algorithm works best on patients with local recurrences and assuming that approximately 10% of the recurrences are non-local, inclusion of twenty-five subjects would include twenty patients with local recurrences.[64, 65] Advanced MR acquisition should be done pre-radiotherapy instead of pre-operatively to minimize discrepancies caused by post-surgical effects. Follow-up should be done every 2 months, due to the fast growth rate of glioblastoma.[176] Before initiation of the study, possibilities should be explored with MR physicists to expand the region of interest of the advanced MR images with the goal to better visualize microscopic tumour infiltration along the craniocaudal axis. Additionally, as proposed in *Chapter 4,* the inclusion of $CMRO_2$ could be promising to further improve the biological CTV.

10.5 Conclusion

In this chapter, the potential of advanced MR imaging for improved radiotherapy of glioblastoma was highlighted. The possibility arises for improved quality of life and improved tumour control due to the large reduction of the CTV while maintaining adequate coverage of the RV. Not only can advanced MR biomarkers be a promising tool to visualize tumour infiltration when it is present, it also provides additional information when altered physiology around the GTV is absent.

11

Short-term scientific mission: Revisiting the tumour growth model

11.1 Introduction

At Aarhus University Hospital (Aarhus, Denmark), the utility of DTI is investigated to personalize CTV delineation of glioblastoma. As described in *Chapter 4*, DTI is an MR technique that utilizes the tensor of water diffusion to define the WMTs.[101] Various pathology studies have shown that glioma cells preferentially spread along the WMTs, highlighting the potential of DTI to predict tumour infiltration.[129, 177] In a phase 0 study by *Trip et al. (2019)*, forty glioblastoma patients were included at Aarhus University Hospital to evaluate the potential of integrating DTI into radiotherapy planning of glioblastoma.[132] With an in-house developed tumour growth model that incorporated DTI information, DTI-based CTVs were generated for the forty glioblastoma patients. The coverage of recurrences by the DTI-based CTV was worse overall, but a marginal improvement in coverage of satellites was observed. This study shed light on the potential of DTI to cover distant recurrences.

Only few research groups have explored the possibility to integrate advanced MR imaging with CTV delineation to improve radiotherapy of glioblastoma. Although the MR technique and approach investigated at Aarhus University Hospital are different from the ones examined in this master's project, exchanging knowledge could be beneficial to understand future directions and important considerations. Accordingly, a visit was made to Aarhus University Hospital with the aim to learn about the ongoing research on gliomas in Denmark and foster future collaborations. In addition, a project was initiated with the aim to explore the potential of improving the in-house developed tumour growth model to cover future satellites. *Trip et al. (2019)* used an isovolumetric approach to generate two DTI-based CTVs that incorporated a different weighting for anisotropy (γ).[132] A higher γ means a higher presumed probability of tumor spread along WMTs; the two DTI-based CTVs were generated with a γ=0 and γ=20. An increased understanding of the relationship between input variables in the model and the generated biological CTV can be valuable for future research that aims to include DTI information to visualize tumour infiltration. In this project, different combinations of input parameters for the tumour growth model were examined to explore the potential of improving the tumour growth model for coverage of distant recurrences.

11.2 Methods

As part of a short-term scientific mission funded by the COST Action (CA18206), a two-week visit at Aarhus University Hospital was conducted. First, the concepts of the in-house developed tumour growth model were explored. This included acquiring a basic understanding of the mathematical model and the approach for DTI-based CTV delineation. Subsequently, DTI-based CTVs were generated with different combinations of input parameters to explore the potential of optimization of the tumour growth model. From the same cohort as described in *Trip et al. (2019)*, patients who developed satellites during follow-up were included for this project.[132] Patients who presented themselves with multifocal disease before therapy were excluded. Segmentations were made of the satellites; when a patient developed multiple satellites, the satellites were delineated separately from each other. Additionally, segmentations of the gray matter, white matter, cerebrospinal fluid and anatomical boundaries (i.e. falx cerebri, tentorium cerebelli and brainstem) were obtained. The varying input parameters were γ and the white matter diffusion coefficient (D_w). The diffusion coefficient of gray matter (D_g) was kept constant; a higher D_w compared to D_g would model reduced gray matter infiltration meaning tumour infiltration is more likely to grow into white matter. The assumption was made that tumor cells did not spread into cerebrospinal fluid or through the anatomical boundaries. In the included patients, DTI-based CTVs with combinations of the following input parameters were generated: D_w = [0.2, 2, 10, 20, 50, 100, 150, 200] and γ = [0, 5, 10, 15, 20, 25, 50]. Hence, for each patient, 56 DTI-based CTVs were generated.

The coverage of the satellites by the DTI-based CTVs were evaluated for each patient and compared to the coverage by the conventional CTV to assess the added value of integration of DTI information for CTV delineation of glioblastoma.

11.3 Results

11.3.1 The concepts of the tumour growth model

By extending the Fisher-Kolmogorov mathematical model with DTI information, *Trip et al. (2019)* used a comparable approach as *Unkelbach et al. (2013)* for creating a tumour growth model that includes information on the WMTs.[132, 178] The Fisher-Kolmogorov mathematical model is based on a partial differential equation that estimates the spatial distribution of tumour cells in normal appearing regions of the brain. In this model, the tumour cell density drops exponentially with distance from the visible GTV. By extending the model with information acquired with DTI, the tumour cell density is not only determined by the distance from the GTV. D_w and D_g are scaling coefficients for white and gray matter diffusion, respectively. A D_w / D_g ratio higher than 1 models infiltration to grow more easily into white matter tissue. The γ, i.e. the anisotropy weighting parameter, indicates the degree of tumour infiltration that follows the WMTs. A higher γ would mean a higher presumed probability of tumor spread following the direction of the WMTs. Additionally, the tumour growth model assumes that infiltration cannot grow through anatomic boundaries or into the ventricles (cerebrospinal fluid). With these input parameters, the tumour growth model can mathematically construct a tumour cell density map. This map can also be perceived as a tumour probability map. The probability of a specific voxel to contain tumour tissue depends on the distance from the GTV, in which segmentation it resides (white matter, gray matter, cerebrospinal fluid or an anatomic boundary) and the direction of the WMTs. The tumour probability of voxels within the GTV is 100%, whereas the probabilities in the cerebrospinal fluid and anatomic boundaries is presumed to be 0%. The shape of the CTV is modified to match an isoline of the simulated tumour probability while the total volume is kept identical to volume of the conventional CTV.

11.3.2 Examining different combinations of input parameters

From the forty glioblastoma patients, eleven patients had developed satellites when progression was observed for the first time after treatment. Six patients had multifocal disease pretreatment and were excluded, resulting in further analysis to be performed on the remaining five patients. From these five patients, four patients had developed one satellite and one patient had developed two satellites.

In three satellites (from three patients), no difference was seen between the coverage of the satellite by the conventional CTV and the DTI-based CTV created with any combination. The satellite was either too far (0% coverage by any CTV) from or too close (100% coverage by all CTVs) to the GTV. Coverage of the remaining three satellites were better for the DTI-based CTV compared to the conventional CTV. The optimal combination of input parameters varied per satellite. One of the satellites was covered by the optimal DTI-based CTV for 65% compared to 0% by the conventional CTV. The input parameters for this DTI-based CTV were $D_w = 20$ and $\gamma = 50$. As can be seen in *Fig. 43,* the satellite occured on the contralateral side of the GTV. The other two satellites showed improved coverage by a DTI-based CTV with the optimal combinations of $D_w = 200$, $\gamma = 50$ (6% improved coverage compared to the conventional CTV) and $D_w = 0.2$, $\gamma = 50$ (25% improved coverage compared to the conventional CTV).

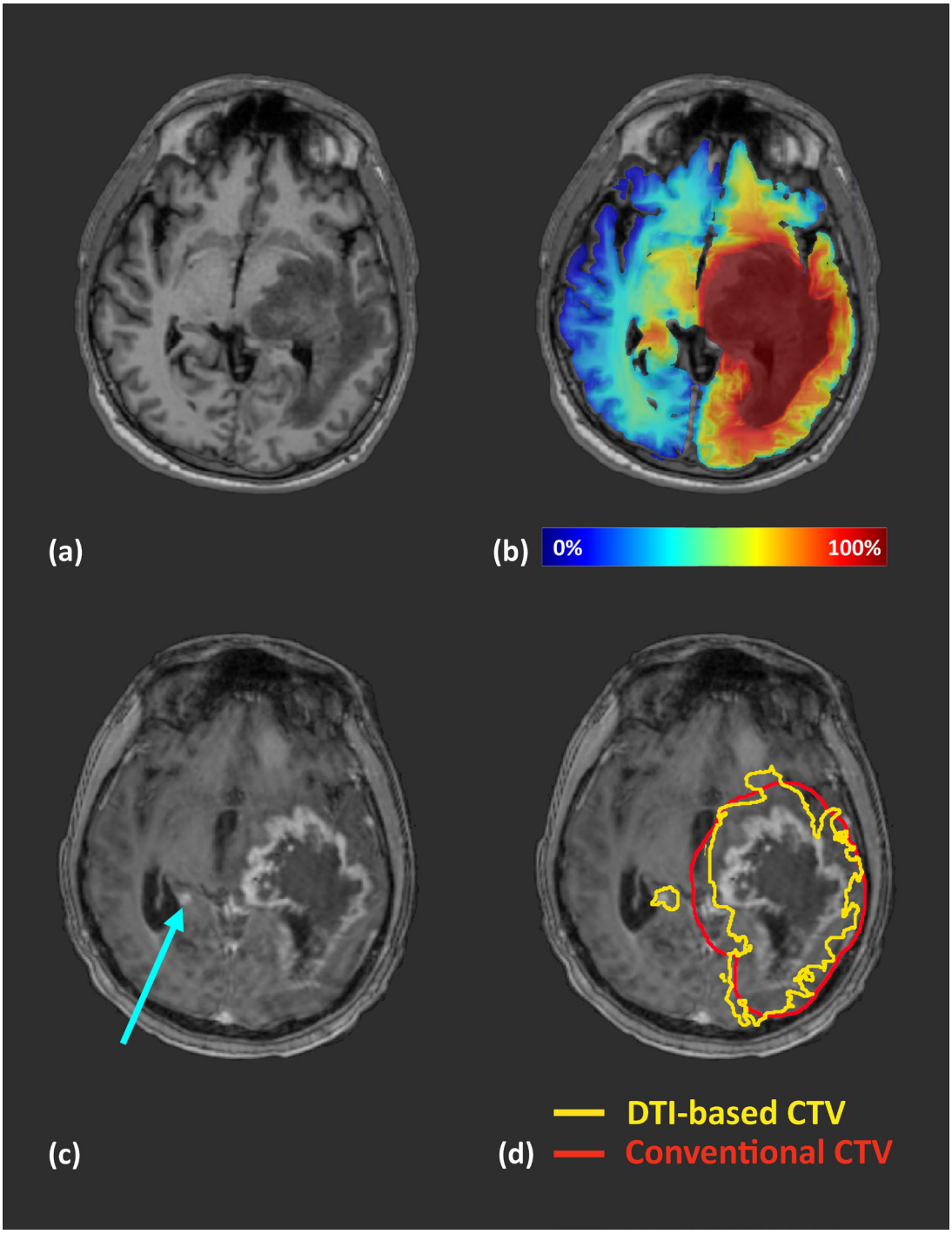

Fig. 43

On T1-weighted MR imaging acquired before radiotherapy, a glioblastoma (primarily located in the left parietal lobe) can be seen (a). Voxels within the GTV assigned 100% probability on the tumour probability map (b). Note that a high probability can also be observed in the contralateral side of the brain. This is most likely due to the WMTs that cross the corpus callosum. On follow-up imaging, a satellite (light blue arrow) can be seen aside from the recurrence that occurs locally (c). 65% of this satellite was covered by the DTI-based CTV ($Dw = 20$, $\gamma = 50$), whereas the conventional CTV did not cover part of the satellite (d).

11.4 Discussion

In this chapter, the tumour growth model developed at Aarhus University Hospital was revisited to explore the possibility for optimization. As the combinations of input parameters for the DTI-based CTV that covered the satellites best, varied per satellite, it is difficult to state an optimal combination. Nonetheless, the best coverage was observed in DTI-based CTVs with either a high value for D_w or for γ. This highlights the potential of DTI to predict the location of future satellites. The satellite that was shown in *Fig. 43*, was located on the contralateral side of the GTV; presumably, WMTs passing through the corpus callosum allowed for a major improvement of coverage by the DTI-based CTV. The high value for γ consolidates this presumption.

Only three satellites showed differences in coverage when using different combinations, the other satellites were either too close to or too far from the GTV. This small sample size limits the search for optimal input parameters for the tumour growth model. Therefore, future research should focus on finding optimal parameters in a larger cohort. Furthermore, the DTI-based CTVs created in this project had the same volume as the conventional CTV. With an isovolumetric approach, the opportunity arises to test the hypothesis that satellites would develop along the WMTs. When a DTI-based CTV were to be adapted in clinical practice, however, an isovolumetric approach would not be logical. Instead, the CTV delineation would preferably be generated based on the probability of voxels to be tumour tissue. Therefore, exploring optimal cutoff values of the tumour probability for inclusion in the DTI-based CTV could waive the isovolumetric approach and should be investigated in future research. Lastly, *Trip et al. (2019)* observed that local recurrences were covered worse by the DTI-based CTV compared to the conventional CTV.[132] As DTI-based CTV incorporates information from DTI and thus is more likely to grow along WMTs, the shape will be less convex and, therefore, it is anticipated that a DTI-based CTV would cover local recurrences less. As the vast majority of glioblastoma recurrences occur locally, DTI would be less suitable as an advanced MR technique for all glioblastomas.[63-65] Nevertheless, this chapter highlights the potential of DTI-based CTV delineation for those cases where satellites would occur after treatment. Future research should focus on identifying key characteristics of patients who had developed satellites during follow-up. Incorporating DTI information could be beneficial for this specific subgroup and potentially result in improved tumour control.

Revisiting the tumour growth model at Aarhus University Hospital has shed light on DTI and its value for CTV delineation of glioblastomas. The difference in approach for biological CTV delineation between Aarhus University Hospital and the one proposed in this master's project can be explained by the difference in information the MR techniques provide. The biomarkers investigated in this master's project (i.e. APT, VSI and rCBV) directly provide information on the presence of pathophysiological processes, e.g. hyperintense regions on APT imaging can indicate increased cell proliferation. With DTI, the location (and direction) of WMTs can be assessed. As image-guided biopsy studies have shown that glioblastoma infiltration preferentially grows along the WMTs, the research group at Aarhus University Hospital opts for a tumour growth model that assumes a higher tumour probability along WMTs.[129, 177]

As the presentation of glioblastomas is extremely diverse, there might be no ideal combination of advanced MR techniques for CTV delineation of all glioblastomas. This short-term scientific mission has shed light on the importance of identifying different advanced MR techniques for different subgroups.

12

Promising directions for the future

Glioblastomas present themselves highly heterogeneously; therefore, a better understanding of their pathophysiology is crucial for personalized treatment. The integration of molecular biomarkers in the classification of gliomas in 2016 shows the complexity of diagnosis and management of these malignancies.[24] Due to the poor prognosis of these patients, further efforts to improve survival or quality of life should be made. In this project, advanced MR techniques that visualize cell proliferation, vasodilatation and increased microvascular density, have shed light on the potential of adding information on pathophysiological processes to the current treatment of glioblastomas. Further research on the generation of the biological CTV and clinical outcomes are required to adapt advanced MR imaging into clinical practice.

In the future, personalized radiotherapy could be achieved with advanced MR imaging. As described in *Chapter 4*, the biomarkers explored in this project have great potential for the majority of glioblastoma patients. Other biomarkers, however, could provide additional information when looking at specific subgroup. Due to the heterogeneous patient group, personalized radiotherapy planning might require personalized advanced MR acquisition. Patients who have a better prognosis, e.g. younger age or with MGMT methylation, might benefit more from the addition of DTI information as they might be more prone to developing distant recurrences. rCBV is observed to be lower in non-enhancing gliomas than in contrast-enhancing gliomas.[179] Future insights might state that vascular biomarkers do not provide significant information for non-enhancing glioblastomas and, therefore, should not be included in the advanced MR protocol for these patients.

It is important to gain a better understanding of the pathophysiology in different subgroups and which advanced MR biomarkers could be beneficial to include for these patients. As different institutes have expertise on different advanced MR techniques, international cooperation is imperative. Advanced MR technology has great potential to alter the course for glioblastoma management and could eventually lead to a better prognosis for this devastating disease.

13

Conclusion

The aim of this master's thesis was to take an initial step towards integration of advanced MR imaging into radiotherapy planning of glioblastomas. The infiltrative nature of glioblastomas require the conventional CTV to be defined as a 1.5 cm expansion of the GTV. With advanced MR maps of the biomarkers APT, VSI and rCBV, the hypothesis arose that hyperintense regions on these maps indicate microscopic tumour infiltration and could be used to create a biological CTV.

In this project, a workflow is presented that incorporates the advanced MR imaging into MIM Maestro® and semi-automatically creates a biological CTV. Analysis of the biological CTV showed a considerable size reduction and adequate coverage of the RV.

In conclusion, the advanced MR techniques and the presented workflow show great potential for personalized radiotherapy of glioblastomas and should be further investigated. The introduction of advanced MR imaging into clinical practice could eventually lead to improved local tumour control and reduced radiation toxicity for patients with glioblastoma.

Bibliography

1. Ostrom QT, Patil N, Cioffi G, Waite K, Kruchko C, Barnholtz-Sloan JS. CBTRUS Statistical Report: Primary Brain and Other Central Nervous System Tumors Diagnosed in the United States in 2013–2017. Neuro-oncology. 2020;22(Supplement_1):iv1-iv96.
2. Thakkar JP, Dolecek TA, Horbinski C, Ostrom QT, Lightner DD, Barnholtz-Sloan JS, et al. Epidemiologic and molecular prognostic review of glioblastoma. Cancer Epidemiol Biomarkers Prev. 2014;23(10):1985-96.
3. Bohn A, Braley A, Rodriguez de la Vega P, Zevallos JC, Barengo NC. The association between race and survival in glioblastoma patients in the US: A retrospective cohort study. PLoS One. 2018;13(6):e0198581-e.
4. Ostrom QT, Cote DJ, Ascha M, Kruchko C, Barnholtz-Sloan JS. Adult Glioma Incidence and Survival by Race or Ethnicity in the United States From 2000 to 2014. JAMA Oncol. 2018;4(9):1254-62.
5. Adams H, Chaichana KL, Avendaño J, Liu B, Raza SM, Quiñones-Hinojosa A. Adult cerebellar glioblastoma: understanding survival and prognostic factors using a population-based database from 1973 to 2009. World neurosurgery. 2013;80(6):e237-43.
6. Simpson JR, Horton J, Scott C, Curran WJ, Rubin P, Fischbach J, et al. Influence of location and extent of surgical resection on survival of patients with glioblastoma multiforme: results of three consecutive Radiation Therapy Oncology Group (RTOG) clinical trials. International journal of radiation oncology, biology, physics. 1993;26(2):239-44.
7. Preston DL, Ron E, Tokuoka S, Funamoto S, Nishi N, Soda M, et al. Solid Cancer Incidence in Atomic Bomb Survivors: 1958–1998. Radiation Research. 2007;168(1):1-64.
8. Wrensch M, Minn Y, Chew T, Bondy M, Berger MS. Epidemiology of primary brain tumors: current concepts and review of the literature. Neuro-oncology. 2002;4(4):278-99.
9. Pearce MS, Salotti JA, Little MP, McHugh K, Lee C, Kim KP, et al. Radiation exposure from CT scans in childhood and subsequent risk of leukaemia and brain tumours: a retrospective cohort study. Lancet. 2012;380(9840):499-505.
10. Tsang RW, Laperriere NJ, Simpson WJ, Brierley J, Panzarella T, Smyth HS. Glioma arising after radiation therapy for pituitary adenoma. A report of four patients and estimation of risk. Cancer. 1993;72(7):2227-33.
11. Wrensch M, Miike R, Lee M, Neuhaus J. Are prior head injuries or diagnostic X-rays associated with glioma in adults? The effects of control selection bias. Neuroepidemiology. 2000;19(5):234-44.
12. Turner MC, Krewski D, Armstrong BK, Chetrit A, Giles GG, Hours M, et al. Allergy and brain tumors in the INTERPHONE study: pooled results from Australia, Canada, France, Israel, and New Zealand. Cancer causes & control : CCC. 2013;24(5):949-60.
13. Amirian ES, Zhou R, Wrensch MR, Olson SH, Scheurer ME, Il'yasova D, et al. Approaching a Scientific Consensus on the Association between Allergies and Glioma Risk: A Report from the Glioma International Case-Control Study. Cancer Epidemiol Biomarkers Prev. 2016;25(2):282-90.
14. Linos E, Raine T, Alonso A, Michaud D. Atopy and Risk of Brain Tumors: A Meta-analysis. JNCI: Journal of the National Cancer Institute. 2007;99(20):1544-50.
15. Chen C, Xu T, Chen J, Zhou J, Yan Y, Lu Y, et al. Allergy and risk of glioma: a meta-analysis. European Journal of Neurology. 2011;18(3):387-95.
16. Ostrom QT, Bauchet L, Davis FG, Deltour I, Fisher JL, Langer CE, et al. The epidemiology of glioma in adults: a "state of the science" review. Neuro-oncology. 2014;16(7):896-913.
17. Hochberg F, Toniolo P, Cole P, Salcman M. Nonoccupational risk indicators of glioblastoma in adults. J Neurooncol. 1990;8(1):55-60.
18. Holick CN, Giovannucci EL, Rosner B, Stampfer MJ, Michaud DS. Prospective study of cigarette smoking and adult glioma: dosage, duration, and latency. Neuro-oncology. 2007;9(3):326-34.
19. Braganza MZ, Rajaraman P, Park Y, Inskip PD, Freedman ND, Hollenbeck AR, et al. Cigarette smoking, alcohol intake, and risk of glioma in the NIH-AARP Diet and Health Study. British Journal of Cancer. 2014;110(1):242-8.
20. Huncharek M, Kupelnick B, Wheeler L. Dietary cured meat and the risk of adult glioma: a meta-analysis of nine observational studies. Journal of environmental pathology, toxicology and oncology : official organ of the International Society for Environmental Toxicology and Cancer. 2003;22(2):129-37.
21. Jiang Y, Uhrbom L. On the origin of glioma. Upsala Journal of Medical Sciences. 2012;117(2):113-21.
22. Jäkel S, Dimou L. Glial Cells and Their Function in the Adult Brain: A Journey through the History of Their Ablation. Frontiers in Cellular Neuroscience. 2017;11(24).
23. Louis DN, Ohgaki H, Wiestler OD, Cavenee WK, Burger PC, Jouvet A, et al. The 2007 WHO classification of tumours of the central nervous system. Acta neuropathologica. 2007;114(2):97-109.
24. Louis DN, Perry A, Reifenberger G, von Deimling A, Figarella-Branger D, Cavenee WK, et al. The 2016 World Health Organization Classification of Tumors of the Central Nervous System: a summary. Acta neuropathologica. 2016;131(6):803-20.
25. Weller M, van den Bent M, Preusser M, Le Rhun E, Tonn JC, Minniti G, et al. EANO guidelines on the diagnosis and treatment of diffuse gliomas of adulthood. Nature Reviews Clinical Oncology. 2021;18(3):170-86.
26. Rasmussen BK, Hansen S, Laursen RJ, Kosteljanetz M, Schultz H, Nørgård BM, et al. Epidemiology of glioma: clinical characteristics, symptoms, and predictors of glioma patients grade I-IV in the the Danish Neuro-Oncology Registry. J Neurooncol. 2017;135(3):571-9.
27. Salo J, Niemelä A, Joukamaa M, Koivukangas J. Effect of brain tumour laterality on patients' perceived quality of life. Journal of neurology, neurosurgery, and psychiatry. 2002;72(3):373-7.
28. Yuile P, Dent O, Cook R, Biggs M, Little N. Survival of glioblastoma patients related to presenting symptoms, brain site and treatment variables. Journal of Clinical Neuroscience. 2006;13(7):747-51.
29. Ozawa M, Brennan PM, Zienius K, Kurian KM, Hollingworth W, Weller D, et al. The usefulness of symptoms alone or combined for general practitioners in considering the diagnosis of a brain tumour: a case-control study using the clinical practice research database (CPRD) (2000-2014). BMJ Open. 2019;9(8):e029686.

30. Posti JP, Bori M, Kauko T, Sankinen M, Nordberg J, Rahi M, et al. Presenting symptoms of glioma in adults. Acta neurologica Scandinavica. 2015;131(2):88-93.
31. Villanueva-Meyer JE, Mabray MC, Cha S. Current Clinical Brain Tumor Imaging. Neurosurgery. 2017;81(3):397-415.
32. Abd-Elghany AA, Naji AA, Alonazi B, Aldosary H, Alsufayan MA, Alnasser M, et al. Radiological characteristics of glioblastoma multiforme using CT and MRI examination. Journal of Radiation Research and Applied Sciences. 2019;12(1):289-93.
33. Imaging of Brain Tumors with Histological Correlations. AJNR: American Journal of Neuroradiology. 2003;24(9):1921-.
34. Omuro A, DeAngelis LM. Glioblastoma and other malignant gliomas: a clinical review. Jama. 2013;310(17):1842-50.
35. Stupp R, Hegi ME, Mason WP, van den Bent MJ, Taphoorn MJ, Janzer RC, et al. Effects of radiotherapy with concomitant and adjuvant temozolomide versus radiotherapy alone on survival in glioblastoma in a randomised phase III study: 5-year analysis of the EORTC-NCIC trial. The Lancet Oncology. 2009;10(5):459-66.
36. Lara-Velazquez M, Al-Kharboosh R, Jeanneret S, Vazquez-Ramos C, Mahato D, Tavanaiepour D, et al. Advances in Brain Tumor Surgery for Glioblastoma in Adults. Brain Sci. 2017;7(12):166.
37. Stupp R, Mason WP, van den Bent MJ, Weller M, Fisher B, Taphoorn MJ, et al. Radiotherapy plus concomitant and adjuvant temozolomide for glioblastoma. The New England journal of medicine. 2005;352(10):987-96.
38. Bell EH, Pugh SL, McElroy JP, Gilbert MR, Mehta M, Klimowicz AC, et al. Molecular-Based Recursive Partitioning Analysis Model for Glioblastoma in the Temozolomide Era: A Correlative Analysis Based on NRG Oncology RTOG 0525. JAMA Oncol. 2017;3(6):784-92.
39. Wee CW, Kim IH, Park C-K, Kim JW, Dho Y-S, Ohka F, et al. Validation of a novel molecular RPA classification in glioblastoma (GBM-molRPA) treated with chemoradiation: A multi-institutional collaborative study. Radiotherapy and Oncology. 2018;129(2):347-51.
40. Ballman KV, Buckner JC, Brown PD, Giannini C, Flynn PJ, LaPlant BR, et al. The relationship between six-month progression-free survival and 12-month overall survival end points for phase II trials in patients with glioblastoma multiforme. Neuro-oncology. 2007;9(1):29-38.
41. Bernier J, Hall EJ, Giaccia A. Radiation oncology: a century of achievements. Nature reviews Cancer. 2004;4(9):737-47.
42. Watson JD, Crick FHC. Molecular Structure of Nucleic Acids: A Structure for Deoxyribose Nucleic Acid. Nature. 1953;171(4356):737-8.
43. Baskar R, Dai J, Wenlong N, Yeo R, Yeoh K-W. Biological response of cancer cells to radiation treatment. Front Mol Biosci. 2014;1:24-.
44. Tounekti O, Kenani A, Foray N, Orlowski S, Mir LM. The ratio of single- to double-strand DNA breaks and their absolute values determine cell death pathway. Br J Cancer. 2001;84(9):1272-9.
45. Prise KM, Schettino G, Folkard M, Held KD. New insights on cell death from radiation exposure. The Lancet Oncology. 2005;6(7):520-8.
46. Grau C, Defourny N, Malicki J, Dunscombe P, Borras JM, Coffey M, et al. Radiotherapy equipment and departments in the European countries: final results from the ESTRO-HERO survey. Radiotherapy and oncology : journal of the European Society for Therapeutic Radiology and Oncology. 2014;112(2):155-64.
47. Friedman WA, Bova FJ. Linear accelerator radiosurgery for arteriovenous malformations. Journal of neurosurgery. 1992;77(6):832-41.
48. FitzGerald TJ, Bishop-Jodoin M, Laurie F, Lukez A, O'Loughlin L, Sacher A. Treatment Toxicity: Radiation. Hematology/Oncology Clinics of North America. 2019;33(6):1027-39.
49. De Ruysscher D, Niedermann G, Burnet NG, Siva S, Lee AWM, Hegi-Johnson F. Radiotherapy toxicity. Nature Reviews Disease Primers. 2019;5(1):13.
50. Matta R, Chapple CR, Fisch M, Heidenreich A, Herschorn S, Kodama RT, et al. Pelvic Complications After Prostate Cancer Radiation Therapy and Their Management: An International Collaborative Narrative Review. European Urology. 2019;75(3):464-76.
51. Lawrence YR, Li XA, el Naqa I, Hahn CA, Marks LB, Merchant TE, et al. Radiation dose-volume effects in the brain. International journal of radiation oncology, biology, physics. 2010;76(3 Suppl):S20-S7.
52. Wang K, Tepper JE. Radiation therapy-associated toxicity: Etiology, management, and prevention. CA: A Cancer Journal for Clinicians. 2021;71(5):437-54.
53. Teoh M, Clark CH, Wood K, Whitaker S, Nisbet A. Volumetric modulated arc therapy: a review of current literature and clinical use in practice. Br J Radiol. 2011;84(1007):967-96.
54. Otto K. Volumetric modulated arc therapy: IMRT in a single gantry arc. Medical physics. 2008;35(1):310-7.
55. Burnet NG, Thomas SJ, Burton KE, Jefferies SJ. Defining the tumour and target volumes for radiotherapy. Cancer imaging : the official publication of the International Cancer Imaging Society. 2004;4(2):153-61.
56. Mir R, Kelly SM, Xiao Y, Moore A, Clark CH, Clementel E, et al. Organ at risk delineation for radiation therapy clinical trials: Global Harmonization Group consensus guidelines. Radiotherapy and Oncology. 2020;150:30-9.
57. Walker MD, Alexander E, Jr., Hunt WE, MacCarty CS, Mahaley MS, Jr., Mealey J, Jr., et al. Evaluation of BCNU and/or radiotherapy in the treatment of anaplastic gliomas. A cooperative clinical trial. Journal of neurosurgery. 1978;49(3):333-43.
58. Shapiro WR, Green SB, Burger PC, Mahaley MS, Jr., Selker RG, VanGilder JC, et al. Randomized trial of three chemotherapy regimens and two radiotherapy regimens and two radiotherapy regimens in postoperative treatment of malignant glioma. Brain Tumor Cooperative Group Trial 8001. Journal of neurosurgery. 1989;71(1):1-9.

59. Sweeney R, Bale R, Vogele M, Nevinny-Stickel M, Bluhm A, Auer T, et al. Repositioning accuracy: comparison of a noninvasive head holder with thermoplastic mask for fractionated radiotherapy and a case report. International journal of radiation oncology, biology, physics. 1998;41(2):475-83.
60. Fiorentino A, Caivano R, Pedicini P, Fusco V. Clinical target volume definition for glioblastoma radiotherapy planning: magnetic resonance imaging and computed tomography. Clinical and Translational Oncology. 2013;15(9):754-8.
61. Niyazi M, Brada M, Chalmers AJ, Combs SE, Erridge SC, Fiorentino A, et al. ESTRO-ACROP guideline "target delineation of glioblastomas". Radiotherapy and oncology : journal of the European Society for Therapeutic Radiology and Oncology. 2016;118(1):35-42.
62. Cabrera AR, Kirkpatrick JP, Fiveash JB, Shih HA, Koay EJ, Lutz S, et al. Radiation therapy for glioblastoma: Executive summary of an American Society for Radiation Oncology Evidence-Based Clinical Practice Guideline. Practical radiation oncology. 2016;6(4):217-25.
63. Chang EL, Akyurek S, Avalos T, Rebueno N, Spicer C, Garcia J, et al. Evaluation of peritumoral edema in the delineation of radiotherapy clinical target volumes for glioblastoma. International journal of radiation oncology, biology, physics. 2007;68(1):144-50.
64. Gebhardt BJ, Dobelbower MC, Ennis WH, Bag AK, Markert JM, Fiveash JB. Patterns of failure for glioblastoma multiforme following limited-margin radiation and concurrent temozolomide. Radiation oncology (London, England). 2014;9:130.
65. Minniti G, Amelio D, Amichetti M, Salvati M, Muni R, Bozzao A, et al. Patterns of failure and comparison of different target volume delineations in patients with glioblastoma treated with conformal radiotherapy plus concomitant and adjuvant temozolomide. Radiotherapy and oncology : journal of the European Society for Therapeutic Radiology and Oncology. 2010;97(3):377-81.
66. Tsien C, Moughan J, Michalski JM, Gilbert MR, Purdy J, Simpson J, et al. Phase I three-dimensional conformal radiation dose escalation study in newly diagnosed glioblastoma: Radiation Therapy Oncology Group Trial 98-03. International journal of radiation oncology, biology, physics. 2009;73(3):699-708.
67. Badiyan SN, Markovina S, Simpson JR, Robinson CG, DeWees T, Tran DD, et al. Radiation therapy dose escalation for glioblastoma multiforme in the era of temozolomide. International journal of radiation oncology, biology, physics. 2014;90(4):877-85.
68. Perry JR, Laperriere N, O'Callaghan CJ, Brandes AA, Menten J, Phillips C, et al. Short-Course Radiation plus Temozolomide in Elderly Patients with Glioblastoma. New England Journal of Medicine. 2017;376(11):1027-37.
69. Wen PY, Macdonald DR, Reardon DA, Cloughesy TF, Sorensen AG, Galanis E, et al. Updated Response Assessment Criteria for High-Grade Gliomas: Response Assessment in Neuro-Oncology Working Group. Journal of Clinical Oncology. 2010;28(11):1963-72.
70. Chaskis C, Neyns B, Michotte A, De Ridder M, Everaert H. Pseudoprogression after radiotherapy with concurrent temozolomide for high-grade glioma: clinical observations and working recommendations. Surgical Neurology. 2009;72(4):423-8.
71. Sahm F, Capper D, Jeibmann A, Habel A, Paulus W, Troost D, et al. Addressing diffuse glioma as a systemic brain disease with single-cell analysis. Archives of neurology. 2012;69(4):523-6.
72. Kalpathy-Cramer J, Gerstner ER, Emblem KE, Andronesi O, Rosen B. Advanced magnetic resonance imaging of the physical processes in human glioblastoma. Cancer research. 2014;74(17):4622-37.
73. Li J, Wang M, Won M, Shaw EG, Coughlin C, Curran WJ, Jr., et al. Validation and simplification of the Radiation Therapy Oncology Group recursive partitioning analysis classification for glioblastoma. International journal of radiation oncology, biology, physics. 2011;81(3):623-30.
74. Weller M, Tabatabai G, Kästner B, Felsberg J, Steinbach JP, Wick A, et al. MGMT Promoter Methylation Is a Strong Prognostic Biomarker for Benefit from Dose-Intensified Temozolomide Rechallenge in Progressive Glioblastoma: The DIRECTOR Trial. Clinical cancer research : an official journal of the American Association for Cancer Research. 2015;21(9):2057-64.
75. Krex D, Klink B, Hartmann C, von Deimling A, Pietsch T, Simon M, et al. Long-term survival with glioblastoma multiforme. Brain. 2007;130(10):2596-606.
76. Lo SS, Sahgal A, Slotman BJ, Mansur DB, Khouri A, Sloan AE, et al. What is the most appropriate clinical target volume for glioblastoma? CNS Oncology. 2013;2(5):419-25.
77. Paulsson AK, McMullen KP, Peiffer AM, Hinson WH, Kearns WT, Johnson AJ, et al. Limited margins using modern radiotherapy techniques does not increase marginal failure rate of glioblastoma. American journal of clinical oncology. 2014;37(2):177-81.
78. Piroth MD, Galldiks N, Pinkawa M, Holy R, Stoffels G, Ermert J, et al. Relapse patterns after radiochemotherapy of glioblastoma with FET PET-guided boost irradiation and simulation to optimize radiation target volume. Radiation oncology (London, England). 2016;11:87.
79. McDonald MW, Shu HK, Curran WJ, Jr., Crocker IR. Pattern of failure after limited margin radiotherapy and temozolomide for glioblastoma. International journal of radiation oncology, biology, physics. 2011;79(1):130-6.
80. Jain RK, di Tomaso E, Duda DG, Loeffler JS, Sorensen AG, Batchelor TT. Angiogenesis in brain tumours. Nature reviews Neuroscience. 2007;8(8):610-22.
81. Ellingson BM, Bendszus M, Boxerman J, Barboriak D, Erickson BJ, Smits M, et al. Consensus recommendations for a standardized Brain Tumor Imaging Protocol in clinical trials. Neuro-oncology. 2015;17(9):1188-98.
82. Pitman KE, Bakke KM, Kristian A, Malinen E. Ultra-early changes in vascular parameters from dynamic contrast enhanced MRI of breast cancer xenografts following systemic therapy with doxorubicin and liver X receptor agonist. Cancer Imaging. 2019;19(1):88.

83. Kickingereder P, Brugnara G, Hansen MB, Nowosielski M, Pflüger I, Schell M, et al. Noninvasive Characterization of Tumor Angiogenesis and Oxygenation in Bevacizumab-treated Recurrent Glioblastoma by Using Dynamic Susceptibility MRI: Secondary Analysis of the European Organization for Research and Treatment of Cancer 26101 Trial. Radiology. 2020;297(1):164-75.
84. Birner P, Piribauer M, Fischer I, Gatterbauer B, Marosi C, Ambros PF, et al. Vascular patterns in glioblastoma influence clinical outcome and associate with variable expression of angiogenic proteins: evidence for distinct angiogenic subtypes. Brain pathology (Zurich, Switzerland). 2003;13(2):133-43.
85. Hansen S, Grabau DA, Rose C, Bak M, Sørensen FB. Angiogenesis in breast cancer: a comparative study of the observer variability of methods for determining microvessel density. Laboratory investigation; a journal of technical methods and pathology. 1998;78(12):1563-73.
86. Sadeghi N, D'Haene N, Decaestecker C, Levivier M, Metens T, Maris C, et al. Apparent diffusion coefficient and cerebral blood volume in brain gliomas: relation to tumor cell density and tumor microvessel density based on stereotactic biopsies. AJNR American journal of neuroradiology. 2008;29(3):476-82.
87. Chakhoyan A, Yao J, Leu K, Pope WB, Salamon N, Yong W, et al. Validation of vessel size imaging (VSI) in high-grade human gliomas using magnetic resonance imaging, image-guided biopsies, and quantitative immunohistochemistry. Scientific Reports. 2019;9(1):2846.
88. Kellner E, Breyer T, Gall P, Müller K, Trippel M, Staszewski O, et al. MR evaluation of vessel size imaging of human gliomas: Validation by histopathology. Journal of Magnetic Resonance Imaging. 2015;42(4):1117-25.
89. Hakyemez B, Erdogan C, Ercan I, Ergin N, Uysal S, Atahan S. High-grade and low-grade gliomas: differentiation by using perfusion MR imaging. Clinical radiology. 2005;60(4):493-502.
90. Buxton RB, Frank LR, Wong EC, Siewert B, Warach S, Edelman RR. A general kinetic model for quantitative perfusion imaging with arterial spin labeling. Magn Reson Med. 1998;40(3):383-96.
91. Beppu T, Kamada K, Yoshida Y, Arai H, Ogasawara K, Ogawa A. Change of Oxygen Pressure in Glioblastoma Tissue Under Various Conditions. Journal of Neuro-Oncology. 2002;58(1):47-52.
92. Hoffmann SH, Radbruch A, Bock M, Semmler W, Nagel AM. Direct (17)O MRI with partial volume correction: first experiences in a glioblastoma patient. Magma (New York, NY). 2014;27(6):579-87.
93. Paech D, Nagel AM, Schultheiss MN, Umathum R, Regnery S, Scherer M, et al. Quantitative Dynamic Oxygen 17 MRI at 7.0 T for the Cerebral Oxygen Metabolism in Glioma. Radiology. 2020;295(1):181-9.
94. Ogawa S, Lee TM, Kay AR, Tank DW. Brain magnetic resonance imaging with contrast dependent on blood oxygenation. Proceedings of the National Academy of Sciences of the United States of America. 1990;87(24):9868-72.
95. He X, Yablonskiy DA. Quantitative BOLD: mapping of human cerebral deoxygenated blood volume and oxygen extraction fraction: default state. Magn Reson Med. 2007;57(1):115-26.
96. Yablonskiy DA, Sukstanskii AL, He X. Blood oxygenation level-dependent (BOLD)-based techniques for the quantification of brain hemodynamic and metabolic properties - theoretical models and experimental approaches. NMR Biomed. 2013;26(8):963-86.
97. Kim H, Catana, C., Mouridsen, K., Bolar, D., Gerstner, E.R., Batchelor, T.T., Jain, R.K., Rosen, B.R., Sorensen, A.G., editor Evaluation of relative CMRO2 from BOLD and CBF changes in hyperoxia: Significant increase of oxygen consumption rate in glioblastoma. Proc Intl Soc Mag Reson Med 19; 2011.
98. Sugahara T, Korogi Y, Kochi M, Ikushima I, Shigematu Y, Hirai T, et al. Usefulness of diffusion-weighted MRI with echo-planar technique in the evaluation of cellularity in gliomas. Journal of magnetic resonance imaging : JMRI. 1999;9(1):53-60.
99. Durand-Muñoz C, Flores-Alvarez E, Moreno-Jimenez S, Roldan-Valadez E. Pre-operative apparent diffusion coefficient values and tumour region volumes as prognostic biomarkers in glioblastoma: correlation and progression-free survival analyses. Insights Imaging. 2019;10(1):36-.
100. Kao H-W, Chiang S-W, Chung H-W, Tsai FY, Chen C-Y. Advanced MR Imaging of Gliomas: An Update. BioMed Research International. 2013;2013:970586.
101. Beaulieu C. The basis of anisotropic water diffusion in the nervous system - a technical review. NMR Biomed. 2002;15(7-8):435-55.
102. Shukla G, Alexander GS, Bakas S, Nikam R, Talekar K, Palmer JD, et al. Advanced magnetic resonance imaging in glioblastoma: a review. Chinese clinical oncology. 2017;6(4):40.
103. Hanahan D, Weinberg Robert A. Hallmarks of Cancer: The Next Generation. Cell. 2011;144(5):646-74.
104. Zhu H, Barker PB. MR spectroscopy and spectroscopic imaging of the brain. Methods Mol Biol. 2011;711:203-26.
105. Oz G, Alger JR, Barker PB, Bartha R, Bizzi A, Boesch C, et al. Clinical proton MR spectroscopy in central nervous system disorders. Radiology. 2014;270(3):658-79.
106. Park I, Mukherjee J, Ito M, Chaumeil MM, Jalbert LE, Gaensler K, et al. Changes in pyruvate metabolism detected by magnetic resonance imaging are linked to DNA damage and serve as a sensor of temozolomide response in glioblastoma cells. Cancer research. 2014;74(23):7115-24.
107. Quon H, Brunet B, Alexander A, Murtha A, Abdulkarim B, Fulton D, et al. Changes in Serial Magnetic Resonance Spectroscopy Predict Outcome in High-grade Glioma During and After Postoperative Radiotherapy. Anticancer Research. 2011;31(10):3559.
108. Hanahan D, Weinberg RA. The hallmarks of cancer. Cell. 2000;100(1):57-70.
109. van Zijl PCM, Lam WW, Xu J, Knutsson L, Stanisz GJ. Magnetization Transfer Contrast and Chemical Exchange Saturation Transfer MRI. Features and analysis of the field-dependent saturation spectrum. Neuroimage. 2018;168:222-41.
110. Zhou J, Lal B, Wilson DA, Laterra J, van Zijl PCM. Amide proton transfer (APT) contrast for imaging of brain tumors. Magn Reson Med. 2003;50(6):1120-6.

111. Togao O, Yoshiura T, Keupp J, Hiwatashi A, Yamashita K, Kikuchi K, et al. Amide proton transfer imaging of adult diffuse gliomas: Correlation with histopathological grades. Neuro-oncology. 2013;16.
112. Keil VC, Gielen GH, Pintea B, Baumgarten P, Datsi A, Hittatiya K, et al. DCE-MRI in Glioma, Infiltration Zone and Healthy Brain to Assess Angiogenesis: A Biopsy Study. Clinical neuroradiology. 2021.
113. Wahl DR, Kim MM, Aryal MP, Hartman H, Lawrence TS, Schipper MJ, et al. Combining Perfusion and High B-value Diffusion MRI to Inform Prognosis and Predict Failure Patterns in Glioblastoma. International journal of radiation oncology, biology, physics. 2018;102(4):757-64.
114. Kim MM, Sun Y, Aryal MP, Parmar HA, Piert M, Rosen B, et al. A Phase 2 Study of Dose-intensified Chemoradiation Using Biologically Based Target Volume Definition in Patients With Newly Diagnosed Glioblastoma. International journal of radiation oncology, biology, physics. 2021;110(3):792-803.
115. Hu LS, Baxter LC, Smith KA, Feuerstein BG, Karis JP, Eschbacher JM, et al. Relative Cerebral Blood Volume Values to Differentiate High-Grade Glioma Recurrence from Posttreatment Radiation Effect: Direct Correlation between Image-Guided Tissue Histopathology and Localized Dynamic Susceptibility-Weighted Contrast-Enhanced Perfusion MR Imaging Measurements. American Journal of Neuroradiology. 2009;30(3):552.
116. Price SJ, Green HA, Dean AF, Joseph J, Hutchinson PJ, Gillard JH. Correlation of MR relative cerebral blood volume measurements with cellular density and proliferation in high-grade gliomas: an image-guided biopsy study. AJNR American journal of neuroradiology. 2011;32(3):501-6.
117. Price SJ, Young AMH, Scotton WJ, Ching J, Mohsen LA, Boonzaier NR, et al. Multimodal MRI can identify perfusion and metabolic changes in the invasive margin of glioblastomas. Journal of magnetic resonance imaging : JMRI. 2016;43(2):487-94.
118. Stadlbauer A, Kinfe TM, Eyüpoglu I, Zimmermann M, Kitzwögerer M, Podar K, et al. Tissue Hypoxia and Alterations in Microvascular Architecture Predict Glioblastoma Recurrence in Humans. Clinical cancer research : an official journal of the American Association for Cancer Research. 2021;27(6):1641-9.
119. Stecco A, Pisani C, Quarta R, Brambilla M, Masini L, Beldì D, et al. DTI and PWI analysis of peri-enhancing tumoral brain tissue in patients treated for glioblastoma. Journal of Neuro-Oncology. 2011;102(2):261-71.
120. Blasel S, Franz K, Ackermann H, Weidauer S, Zanella F, Hattingen E. Stripe-like increase of rCBV beyond the visible border of glioblastomas: site of tumor infiltration growing after neurosurgery. Journal of Neuro-Oncology. 2011;103(3):575-84.
121. Stadlbauer A, Zimmermann M, Kitzwögerer M, Oberndorfer S, Rössler K, Dörfler A, et al. MR Imaging-derived Oxygen Metabolism and Neovascularization Characterization for Grading and IDH Gene Mutation Detection of Gliomas. Radiology. 2017;283(3):799-809.
122. Kono K, Inoue Y, Nakayama K, Shakudo M, Morino M, Ohata K, et al. The Role of Diffusion-weighted Imaging in Patients with Brain Tumors. American Journal of Neuroradiology. 2001;22(6):1081.
123. Pauleit D, Langen K-J, Floeth F, Hautzel H, Riemenschneider MJ, Reifenberger G, et al. Can the apparent diffusion coefficient be used as a noninvasive parameter to distinguish tumor tissue from peritumoral tissue in cerebral gliomas? Journal of Magnetic Resonance Imaging. 2004;20(5):758-64.
124. Gupta A, Young RJ, Karimi S, Sood S, Zhang Z, Mo Q, et al. Isolated diffusion restriction precedes the development of enhancing tumor in a subset of patients with glioblastoma. AJNR American journal of neuroradiology. 2011;32(7):1301-6.
125. Elson A, Paulson E, Bovi J, Siker M, Schultz C, Laviolette PS. Evaluation of pre-radiotherapy apparent diffusion coefficient (ADC): patterns of recurrence and survival outcomes analysis in patients treated for glioblastoma multiforme. Journal of Neuro-Oncology. 2015;123(1):179-88.
126. Pramanik PP, Parmar HA, Mammoser AG, Junck LR, Kim MM, Tsien CI, et al. Hypercellularity Components of Glioblastoma Identified by High b-Value Diffusion-Weighted Imaging. International journal of radiation oncology, biology, physics. 2015;92(4):811-9.
127. Chang PD, Chow DS, Yang PH, Filippi CG, Lignelli A. Predicting Glioblastoma Recurrence by Early Changes in the Apparent Diffusion Coefficient Value and Signal Intensity on FLAIR Images. American Journal of Roentgenology. 2016;208(1):57-65.
128. Tropine A, Vucurevic G, Delani P, Boor S, Hopf N, Bohl J, et al. Contribution of diffusion tensor imaging to delineation of gliomas and glioblastomas. Journal of Magnetic Resonance Imaging. 2004;20(6):905-12.
129. Price SJ, Jena R, Burnet NG, Hutchinson PJ, Dean AF, Peña A, et al. Improved delineation of glioma margins and regions of infiltration with the use of diffusion tensor imaging: an image-guided biopsy study. AJNR American journal of neuroradiology. 2006;27(9):1969-74.
130. Jena R, Price SJ, Baker C, Jefferies SJ, Pickard JD, Gillard JH, et al. Diffusion tensor imaging: possible implications for radiotherapy treatment planning of patients with high-grade glioma. Clinical oncology (Royal College of Radiologists (Great Britain)). 2005;17(8):581-90.
131. Berberat J, McNamara J, Remonda L, Bodis S, Rogers S. Diffusion tensor imaging for target volume definition in glioblastoma multiforme. Strahlentherapie und Onkologie. 2014;190(10):939-43.
132. Trip AK, Jensen MB, Kallehauge JF, Lukacova S. Individualizing the radiotherapy target volume for glioblastoma using DTI-MRI: a phase 0 study on coverage of recurrences. Acta Oncologica. 2019;58(10):1532-5.
133. Witulla B, Goerig N, Putz F, Frey B, Engelhorn T, Dörfler A, et al. On PTV definition for glioblastoma based on fiber tracking of diffusion tensor imaging data. PLoS One. 2020;15(1):e0227146-e.
134. Croteau D, Scarpace L, Hearshen D, Gutierrez J, Fisher JL, Rock JP, et al. Correlation between magnetic resonance spectroscopy imaging and image-guided biopsies: semiquantitative and qualitative histopathological analyses of patients with untreated glioma. Neurosurgery. 2001;49(4):823-9.

135. Matsumura A, Isobe T, Anno I, Takano S, Kawamura H. Correlation between choline and MIB-1 index in human gliomas. A quantitative in proton MR spectroscopy study. Journal of clinical neuroscience : official journal of the Neurosurgical Society of Australasia. 2005;12(4):416-20.
136. Pirzkall A, McKnight TR, Graves EE, Carol MP, Sneed PK, Wara WW, et al. MR-spectroscopy guided target delineation for high-grade gliomas. International journal of radiation oncology, biology, physics. 2001;50(4):915-28.
137. Cordova JS, Shu HK, Liang Z, Gurbani SS, Cooper LA, Holder CA, et al. Whole-brain spectroscopic MRI biomarkers identify infiltrating margins in glioblastoma patients. Neuro-oncology. 2016;18(8):1180-9.
138. Park I, Tamai G, Lee MC, Chuang CF, Chang SM, Berger MS, et al. Patterns of recurrence analysis in newly diagnosed glioblastoma multiforme after three-dimensional conformal radiation therapy with respect to pre-radiation therapy magnetic resonance spectroscopic findings. International journal of radiation oncology, biology, physics. 2007;69(2):381-9.
139. Czernicki T, Szeszkowski W, Marchel A, Gołębiowski M. Spectral changes in postoperative MRS in high-grade gliomas and their effect on patient prognosis. Folia Neuropathologica. 2009;47(1):43-9.
140. Zhou J, Tryggestad E, Wen Z, Lal B, Zhou T, Grossman R, et al. Differentiation between glioma and radiation necrosis using molecular magnetic resonance imaging of endogenous proteins and peptides. Nature Medicine. 2011;17(1):130-4.
141. Sagiyama K, Mashimo T, Togao O, Vemireddy V, Hatanpaa KJ, Maher EA, et al. In vivo chemical exchange saturation transfer imaging allows early detection of a therapeutic response in glioblastoma. Proceedings of the National Academy of Sciences. 2014;111(12):4542.
142. Jiang S, Eberhart CG, Lim M, Heo H-Y, Zhang Y, Blair L, et al. Identifying Recurrent Malignant Glioma after Treatment Using Amide Proton Transfer-Weighted MR Imaging: A Validation Study with Image-Guided Stereotactic Biopsy. Clinical cancer research : an official journal of the American Association for Cancer Research. 2019;25(2):552-61.
143. Mehrabian H, Myrehaug S, Soliman H, Sahgal A, Stanisz GJ. Evaluation of Glioblastoma Response to Therapy With Chemical Exchange Saturation Transfer. International Journal of Radiation Oncology*Biology*Physics. 2018;101(3):713-23.
144. Chan RW, Chen H, Myrehaug S, Atenafu EG, Stanisz GJ, Stewart J, et al. Quantitative CEST and MT at 1.5T for monitoring treatment response in glioblastoma: early and late tumor progression during chemoradiation. Journal of Neuro-Oncology. 2021;151(2):267-78.
145. Regnery S, Adeberg S, Dreher C, Oberhollenzer J, Meissner J-E, Goerke S, et al. Chemical exchange saturation transfer MRI serves as predictor of early progression in glioblastoma patients. Oncotarget; Vol 9, No 47. 2018.
146. Singh SK, Hawkins C, Clarke ID, Squire JA, Bayani J, Hide T, et al. Identification of human brain tumour initiating cells. Nature. 2004;432(7015):396-401.
147. Heddleston JM, Li Z, McLendon RE, Hjelmeland AB, Rich JN. The hypoxic microenvironment maintains glioblastoma stem cells and promotes reprogramming towards a cancer stem cell phenotype. Cell cycle (Georgetown, Tex). 2009;8(20):3274-84.
148. Li Z, Bao S, Wu Q, Wang H, Eyler C, Sathornsumetee S, et al. Hypoxia-inducible factors regulate tumorigenic capacity of glioma stem cells. Cancer cell. 2009;15(6):501-13.
149. Heddleston JM, Li Z, Lathia JD, Bao S, Hjelmeland AB, Rich JN. Hypoxia inducible factors in cancer stem cells. British Journal of Cancer. 2010;102(5):789-95.
150. Bao S, Wu Q, McLendon RE, Hao Y, Shi Q, Hjelmeland AB, et al. Glioma stem cells promote radioresistance by preferential activation of the DNA damage response. Nature. 2006;444(7120):756-60.
151. Eramo A, Ricci-Vitiani L, Zeuner A, Pallini R, Lotti F, Sette G, et al. Chemotherapy resistance of glioblastoma stem cells. Cell Death & Differentiation. 2006;13(7):1238-41.
152. Chen J, Li Y, Yu TS, McKay RM, Burns DK, Kernie SG, et al. A restricted cell population propagates glioblastoma growth after chemotherapy. Nature. 2012;488(7412):522-6.
153. Folkman J. Tumor angiogenesis: therapeutic implications. The New England journal of medicine. 1971;285(21):1182-6.
154. Pezzella F, Di Bacco A, Andreola S, Nicholson AG, Pastorino U, Harris AL. Angiogenesis in primary lung cancer and lung secondaries. European journal of cancer (Oxford, England : 1990). 1996;32a(14):2494-500.
155. Holash J, Maisonpierre PC, Compton D, Boland P, Alexander CR, Zagzag D, et al. Vessel cooption, regression, and growth in tumors mediated by angiopoietins and VEGF. Science (New York, NY). 1999;284(5422):1994-8.
156. Reiss Y, Machein MR, Plate KH. The role of angiopoietins during angiogenesis in gliomas. Brain pathology (Zurich, Switzerland). 2005;15(4):311-7.
157. Zagzag D, Amirnovin R, Greco MA, Yee H, Holash J, Wiegand SJ, et al. Vascular Apoptosis and Involution in Gliomas Precede Neovascularization: A Novel Concept for Glioma Growth and Angiogenesis. Laboratory Investigation. 2000;80(6):837-49.
158. Stratmann A, Risau W, Plate KH. Cell type-specific expression of angiopoietin-1 and angiopoietin-2 suggests a role in glioblastoma angiogenesis. The American journal of pathology. 1998;153(5):1459-66.
159. Rafat N, Beck G, Schulte J, Tuettenberg J, Vajkoczy P. Circulating endothelial progenitor cells in malignant gliomas. Journal of neurosurgery. 2010;112(1):43-9.
160. Farin A, Suzuki SO, Weiker M, Goldman JE, Bruce JN, Canoll P. Transplanted glioma cells migrate and proliferate on host brain vasculature: a dynamic analysis. Glia. 2006;53(8):799-808.
161. Vander Heiden MG, Cantley LC, Thompson CB. Understanding the Warburg effect: the metabolic requirements of cell proliferation. Science (New York, NY). 2009;324(5930):1029-33.
162. Warburg O, Wind F, Negelein E. THE METABOLISM OF TUMORS IN THE BODY. The Journal of general physiology. 1927;8(6):519-30.
163. Agnihotri S, Zadeh G. Metabolic reprogramming in glioblastoma: the influence of cancer metabolism on epigenetics and unanswered questions. Neuro-oncology. 2016;18(2):160-72.

164. Hardee ME, Zagzag D. Mechanisms of Glioma-Associated Neovascularization. The American journal of pathology. 2012;181(4):1126-41.
165. Akbari H, Macyszyn L, Da X, Bilello M, Wolf RL, Martinez-Lage M, et al. Imaging Surrogates of Infiltration Obtained Via Multiparametric Imaging Pattern Analysis Predict Subsequent Location of Recurrence of Glioblastoma. Neurosurgery. 2016;78(4):572-80.
166. Fei Q, Qian LX, Zhang YJ, Guo WJ, Bian XH, Yin L, et al. The Utility of Diffusion and Perfusion Magnetic Resonance Imaging in Target Delineation of High-Grade Gliomas. Biomed Res Int. 2020;2020:8718097.
167. Baker GJ, Yadav VN, Motsch S, Koschmann C, Calinescu AA, Mineharu Y, et al. Mechanisms of glioma formation: iterative perivascular glioma growth and invasion leads to tumor progression, VEGF-independent vascularization, and resistance to antiangiogenic therapy. Neoplasia (New York, NY). 2014;16(7):543-61.
168. Mehrabian H, Desmond KL, Soliman H, Sahgal A, Stanisz GJ. Differentiation between Radiation Necrosis and Tumor Progression Using Chemical Exchange Saturation Transfer. Clinical cancer research : an official journal of the American Association for Cancer Research. 2017;23(14):3667-75.
169. Larobina M, Murino L. Medical image file formats. J Digit Imaging. 2014;27(2):200-6.
170. Graham RNJ, Perriss RW, Scarsbrook AF. DICOM demystified: A review of digital file formats and their use in radiological practice. Clinical radiology. 2005;60(11):1133-40.
171. Li X, Morgan PS, Ashburner J, Smith J, Rorden C. The first step for neuroimaging data analysis: DICOM to NIfTI conversion. Journal of neuroscience methods. 2016;264:47-56.
172. Adams R, Bischof L. Seeded region growing. IEEE Transactions on Pattern Analysis and Machine Intelligence. 1994;16(6):641-7.
173. Soeda A, Hara A, Kunisada T, Yoshimura S-i, Iwama T, Park DM. The Evidence of Glioblastoma Heterogeneity. Scientific Reports. 2015;5(1):7979.
174. Perrin SL, Samuel MS, Koszyca B, Brown MP, Ebert LM, Oksdath M, et al. Glioblastoma heterogeneity and the tumour microenvironment: implications for preclinical research and development of new treatments. Biochemical Society transactions. 2019;47(2):625-38.
175. Hanif F, Muzaffar K, Perveen K, Malhi SM, Simjee SU. Glioblastoma Multiforme: A Review of its Epidemiology and Pathogenesis through Clinical Presentation and Treatment. Asian Pac J Cancer Prev. 2017;18(1):3-9.
176. Stensjøen AL, Solheim O, Kvistad KA, Håberg AK, Salvesen Ø, Berntsen EM. Growth dynamics of untreated glioblastomas in vivo. Neuro-oncology. 2015;17(10):1402-11.
177. Kelly PJ, Daumas-Duport C, Kispert DB, Kall BA, Scheithauer BW, Illig JJ. Imaging-based stereotaxic serial biopsies in untreated intracranial glial neoplasms. Journal of neurosurgery. 1987;66(6):865-74.
178. Unkelbach J, Schwahofer F, Menze B, Konukoglu E, Shih H. SU-E-T-486: Evaluation of the Fisher-Kolmogorov Glioma Growth Model for Radiotherapy Target Delineation. Medical physics. 2013;40:317.
179. Arzanforoosh F, Croal PL, van Garderen KA, Smits M, Chappell MA, Warnert EAH. Effect of Applying Leakage Correction on rCBV Measurement Derived From DSC-MRI in Enhancing and Nonenhancing Glioma. Front Oncol. 2021;11:648528-.

Appendices

Appendix A: DICOM Header for format conversion

DICOM Tag	DICOM Attribute	Copied/newly created
0008, 0008	Image Type	Copied
0008, 0012	Instance Creation Date	Newly created
0008, 0013	Instance Creation Time	Newly created
0008, 0020	Study Date	Copied
0008, 0021	Series Date	Newly created
0008, 0030	Study Time	Copied
0008, 0031	Series Time	Newly created
0008, 0050	Accession Number	Copied
0008, 0060	Modality	Copied
0008, 103e	Series Description	Newly created
0010, 0010	Patient Name	Copied
0010, 0020	Patient ID	Copied
0010, 0030	Patient Birth Date	Copied
0018, 0050	Slice Thickness	Copied
0020, 000d	Study Instance UID	Copied
0020, 000e	Series Instance UID	Newly created
0020, 0010	Study ID	Copied
0020, 0011	Series Number	Newly created
0020, 0013	Instance Number	Newly created
0020, 0032	Image Position (Patient)	Newly created
0020, 0037	Image Orientation (Patient)	Newly created
0020, 0052	Frame of Reference UID	Copied

Appendix B: The mean signal intensities of the biomarkers

	Patient 1	Patient 2	Patient 3	Patient 4	Mean
APT	0.0172	0.0218	0.0206	0.0224	0.0205
VSI	0.0361	0.0206	0.0202	0.0125	0.0224
rCBV	1.722	1.645	1.093	1.802	1.5655

Appendix C: Seed point analysis: VSI and rCBV volumes

Table C1: An overview of the distribution of volumes on VSI maps created during the seed point analysis.

Patient	Median signal intensity (VSI)	Number of seed points	Generated volumes	Intervolume DS
1	24.2	89	No volume (n=89)*	
2	21.2	185	Vol. 1 (n=157)* Vol. 2 (n=20) No volume (n=8)	$DS_{Vol1,Vol2}$ = 0.039
3	20.0	174	Vol. 1 (n=142)* No Volume (n=32)	
4	20.6	76	No volume (n=76)*	

*Volume that visually covers the suspicious region best.

Table C2: An overview of the distribution of volumes on rCBV maps created during the seed point analysis.

Patient	Median signal intensity (rCBV)	Number of seed points	Generated volumes	Intervolume DS
1	1658	17	Vol. 1 (n=2)* No volume (n=15)*	
2	1536	60	Vol. 1 (n=58)* No volume (n=2)	
3	1336	55	Vol. 1 (n=31)* Vol. 2 (n=5) Vol. 3 (n=5) Vol. 4 (n=1) No volume (n=13)	$DS_{Vol1,Vol2}$ = 0.003 $DS_{Vol1,Vol3}$ = 0.009 $DS_{Vol1,Vol4}$ = 0.007 $DS_{Vol2,Vol3}$ = 0.009 $DS_{Vol2,Vol4}$ = 0.003 $DS_{Vol3,Vol4}$ = 0.007
4	1496	29	Vol. 1 (n=2) No volume (n=27)*	

*Volume that visually covers the suspicious region best.

Appendix D: Seed point analysis: Seed point distance VSI and rCBV

Fig. D1: Evaluation of the distance and distribution of seed points and their corresponding volumes for VSI. The x-axis describes the distance of the seed points to the GTV center, whereas the y-axis describes the distribution of labelled seed points.

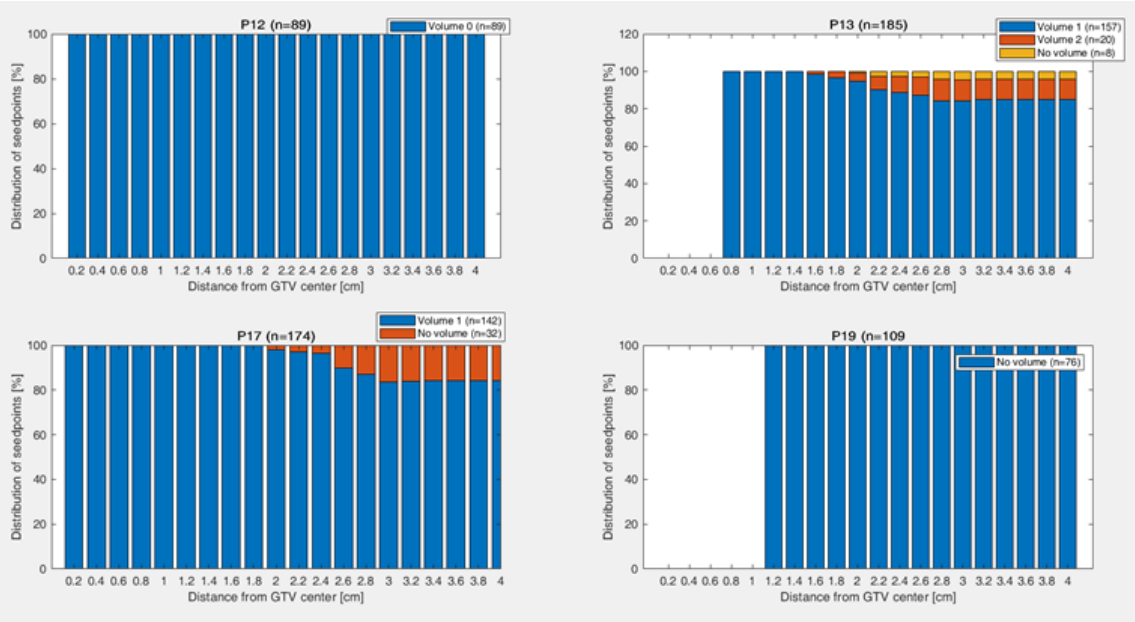

Fig. D2: Evaluation of the distance and distribution of seed points and their corresponding volumes for rCBV. The x-axis describes the distance of the seed points to the GTV center, whereas the y-axis describes the distribution of labelled seed points.

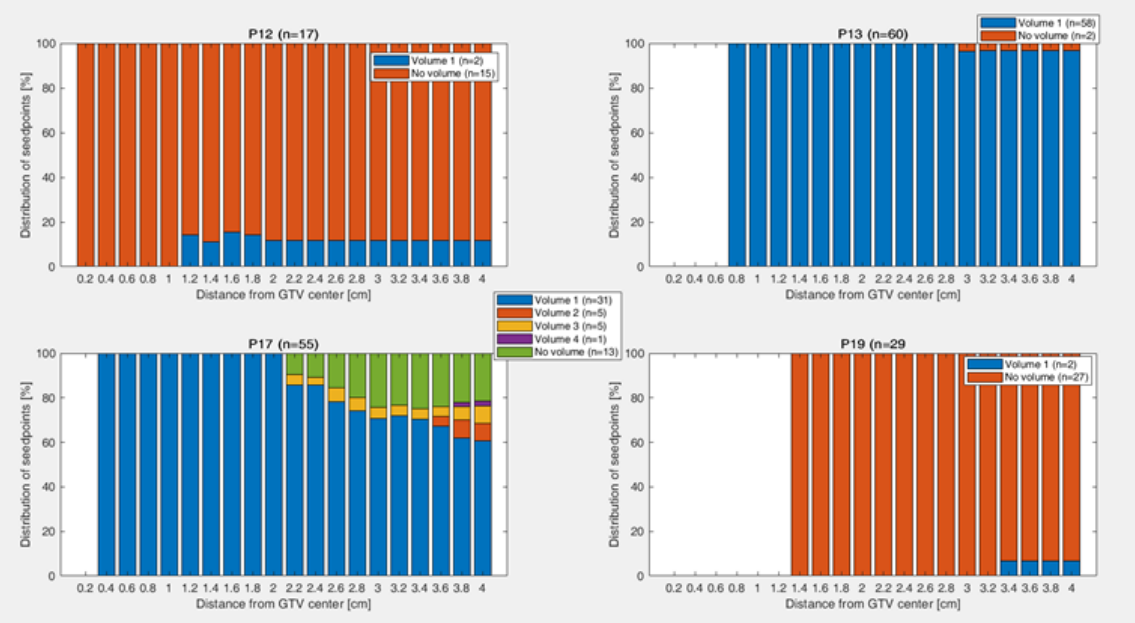

Appendix E

User's manual

Semi-automatic workflow for the generation of a biological CTV.

In this user's manual, a step-by-step guide is provided that explains how the workflow in MIM Maestro® can be used to generate a biological CTV that incorporates information from advanced MR imaging. The workflow *BioCTV_aMRI* creates a biological CTV based on high-risk regions detected on biomarker maps of amide proton transfer (APT), vessel size imaging (VSI) and relative cerebral blood volume (rCBV). Before initiation of the workflow can be initiated, it is important that the advanced MR biomarker maps have been introduced in MIM Maestro® and registered to the planning CT. Additionally, a GTV delineation should already be available.

1. Preparation in MIM Maestro®

Goal: Prepare the set-up for running the semi-automatic workflow.

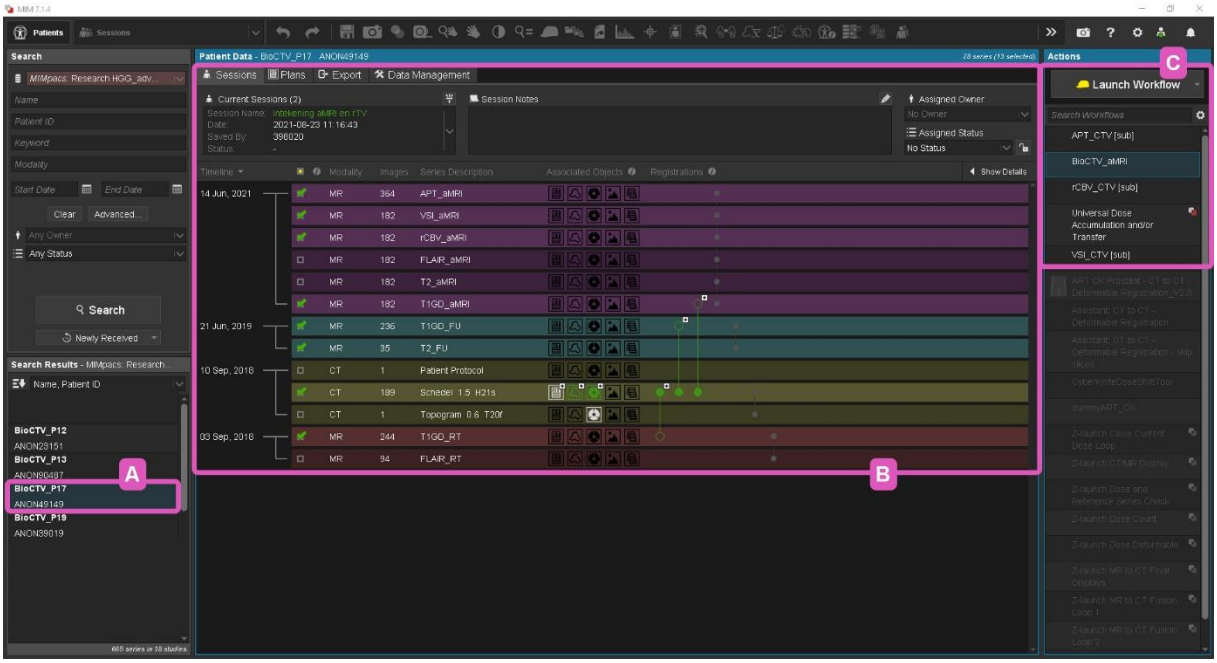

1. Open MIM Maestro® and select the patient with advanced MR biomarker maps in *Search Results* **(A)**.

2. Make sure the correct session is selected as *Current Session* in the *Sessions Overview* **(B)**. In a correct session, the GTV is already delineated and registration of the *T1GD_aMRI* from the advanced MR imaging session towards the planning CT has been performed.

   Note: As the advanced biomarker maps are co-registered to the T1GD_aMRI ●—●, registration of the T1GD_aMRI to the planning CT ○—● will ensure the biomarker maps to be registered to the planning CT as well.

3. Select *BioCTV_aMRI* in the *Actions bar* **(C)** and select *Launch Workflow.*

2. Image assignment

Goal: Assign the images to the Targets in the semi-automatic workflow.

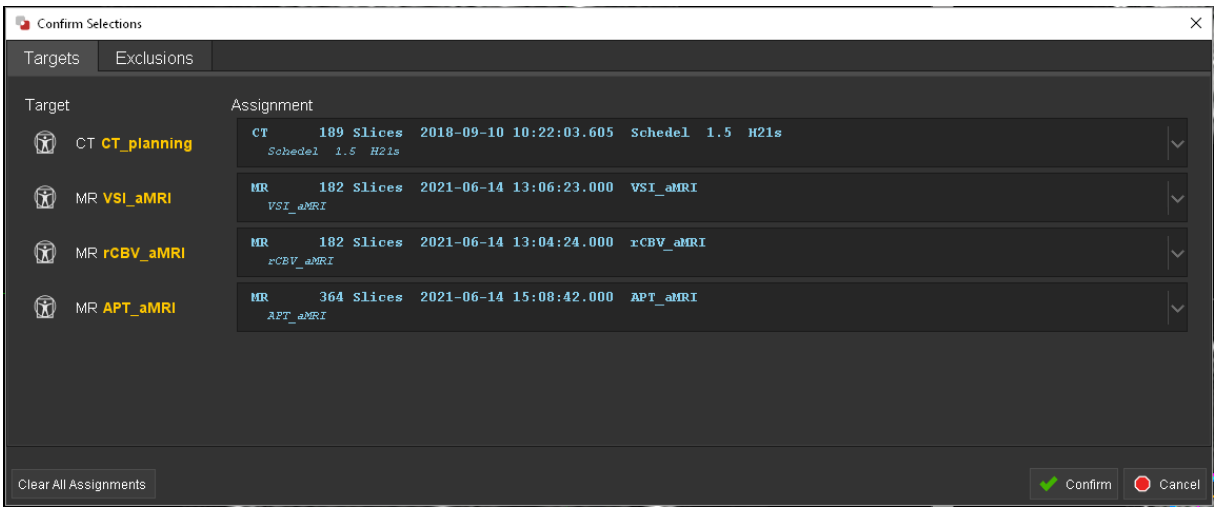

1. Check if the imaging assigned to the target is correct in the window *Confirm Selections.*

   Note: The workflow will automatically recognize the images most of the time and assign it to the corresponding Target. Manual adjustments might be needed when, for example, two CTs are available.

2. Select *Confirm* when the images are assigned correctly to the corresponding Targets.

Important: In the next step, the APT map will be shown. It is important to not scroll through the image yet as the workflow will automatically select an important voxel for the following step. If the slice has been changed, please go to *Step A* before continuing to *Step 3*.

3. Contouring on the biomarker map.

Goal: Create a contour for the high-risk region on the biomarker map.

Note: The images shown in this section are for the contouring of APT only. The steps for contouring on the VSI and rCBV map are similar to the steps below.

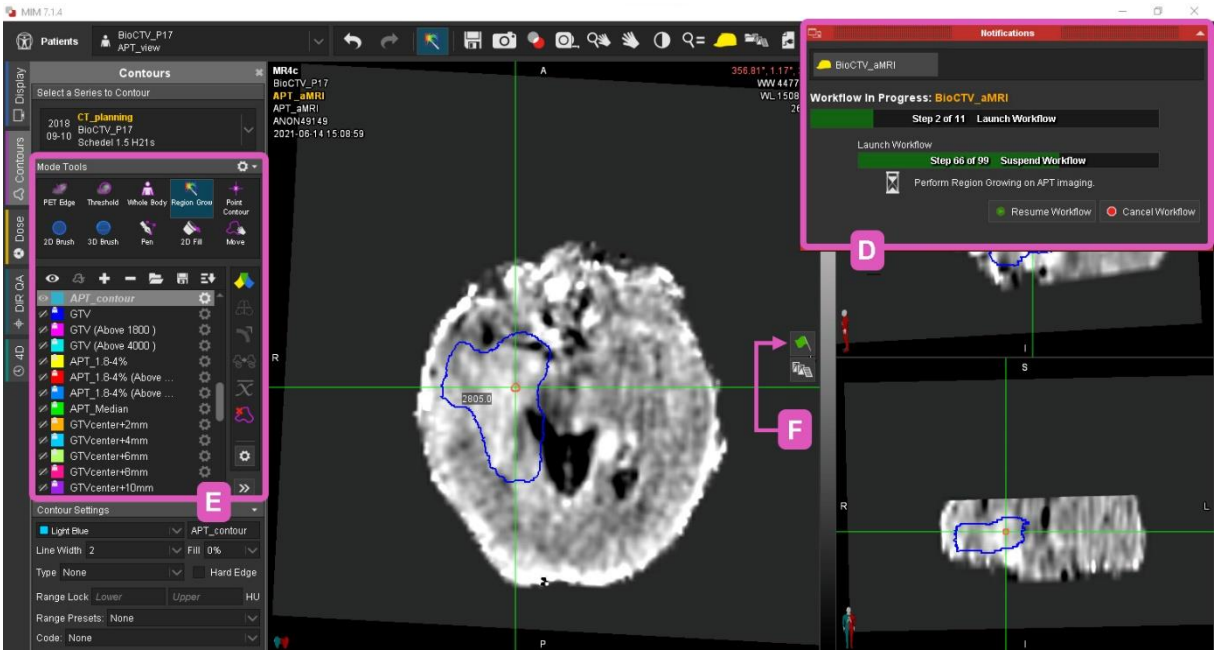

Note: An APT map is loaded and the cursor points towards a specific voxel within the GTV (dark blue contour). This is the automatically selected seed point for the region growing algorithm that will delineate the suspicious region on the map. If the slice has been changed (e.g. after scrolling), go to *Step A* before continuing.

Note: In *Notifications* **(D)**, an overview is shown of the progress in the workflow.

*Note: In the Mode Tools **(E)**, a vast amount of new contours have been created for this step, but will be deleted when this step is finished.*

1. Select *Start Region Grow at Localization Point*  ***(F)***.

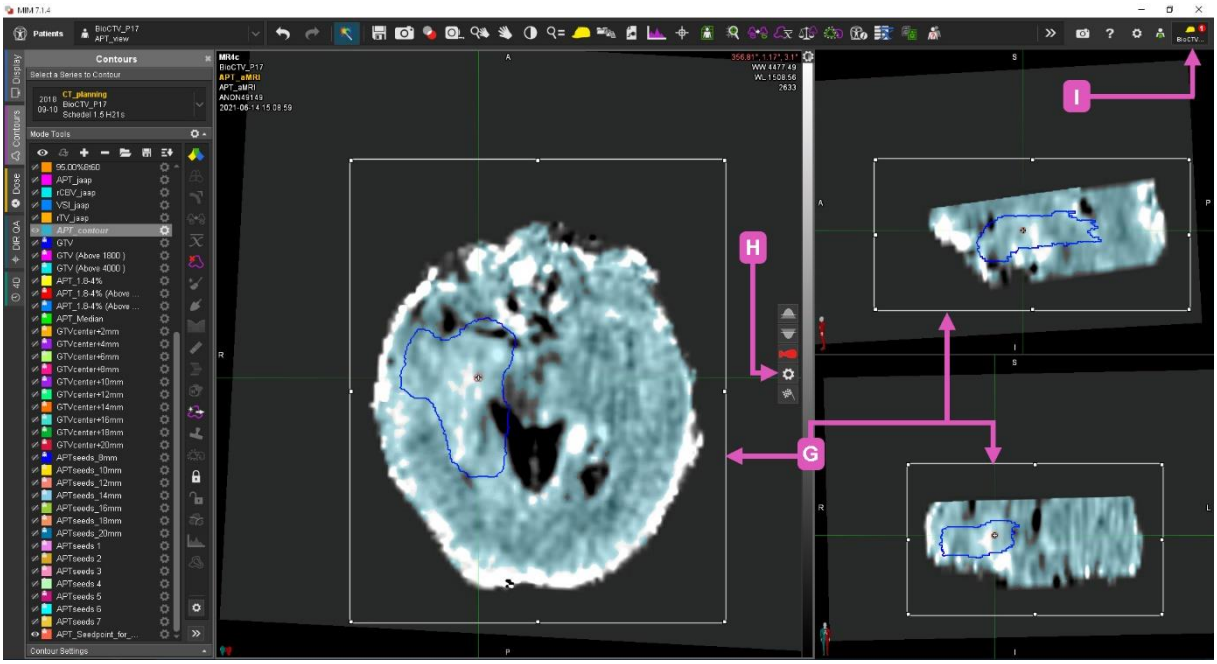

2. Drag the *Region of Interest Box* ***(G)*** in such way that it covers the entire brain in all three views.

   Note: The seed point for the region growing algorithm has now already been selected. Therefore, it is possible to scroll through the three views to ensure the entire brain is covered.

   Note: As can be seen on the sagittal and frontal view, the APT map does not show the entire brain in craniocaudal direction. This is a result of the advanced MR technique requiring a volume of interest.

3. Select *Region Grow Settings* ***(H)***.

Note: If the *Region Grow Settings window* does not pop up, it might be required to manually open the *Notifications bar* ***(I)***.

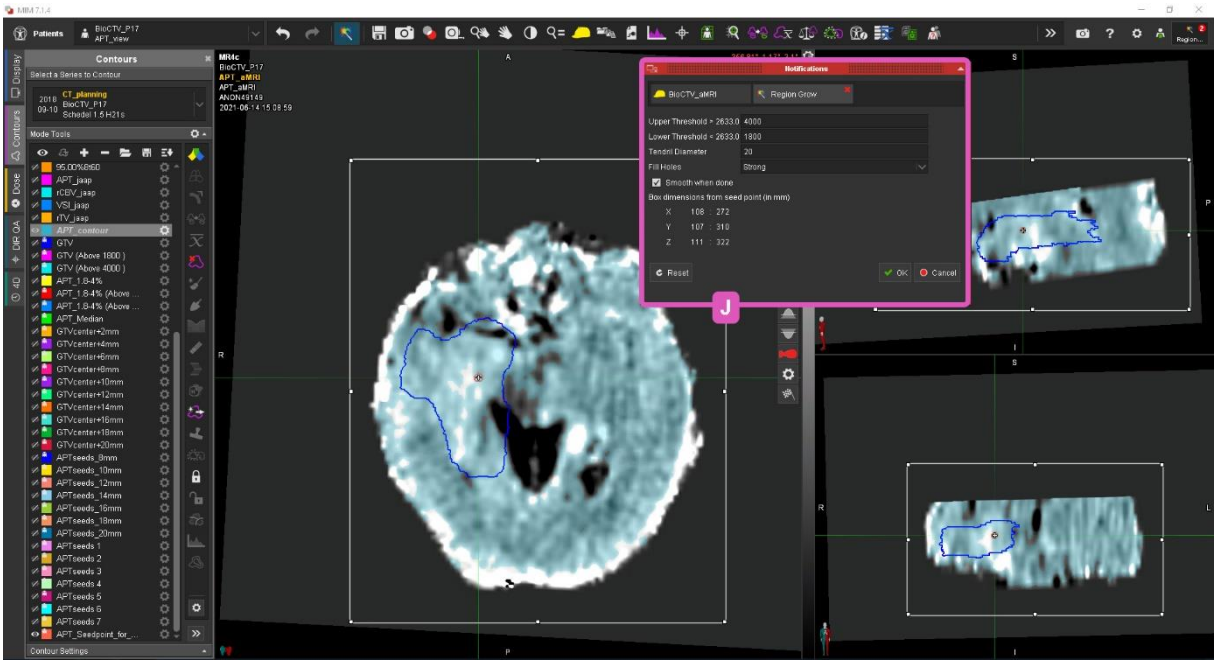

4. In the *Region Grow Settings* ***(J),*** choose the preferred input parameters (e.g. the ones proposed in *Chapter 8.3)* and select *OK*.

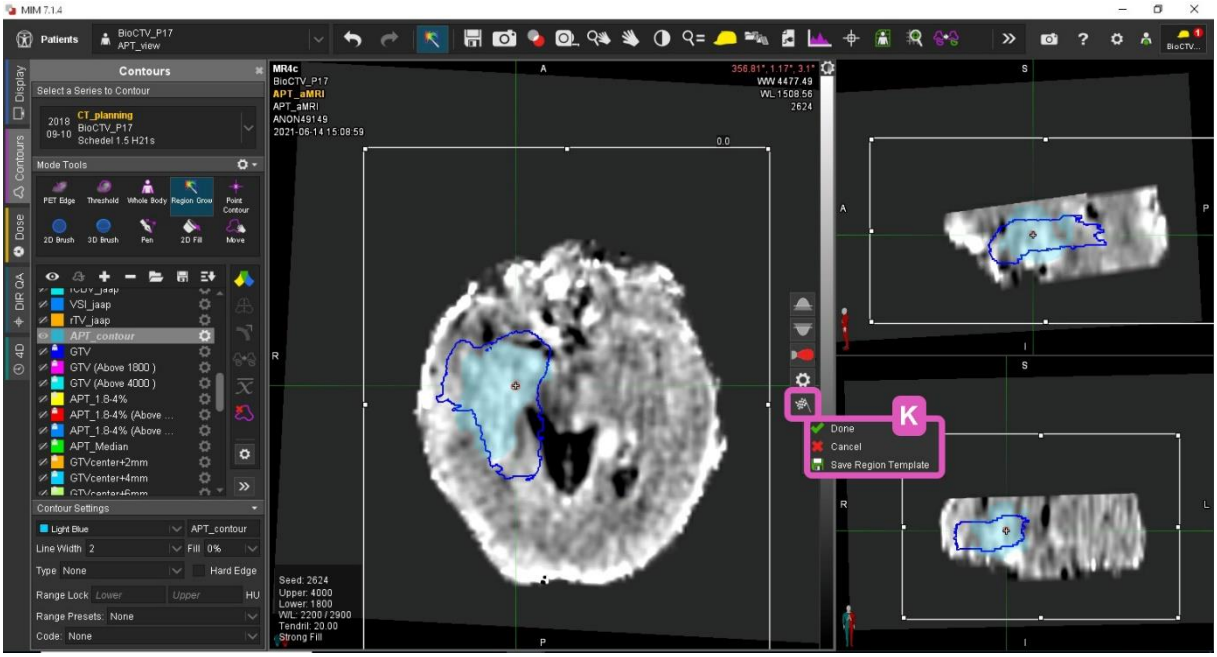

5. Select *Finish Region Grow* ***(K)*** and click *Done*.

Note: By selecting *Save Region Template,* the chosen input parameters can be stored in a template to improve time-efficiency. In *Step B,* the process of region growing using templates is explained.

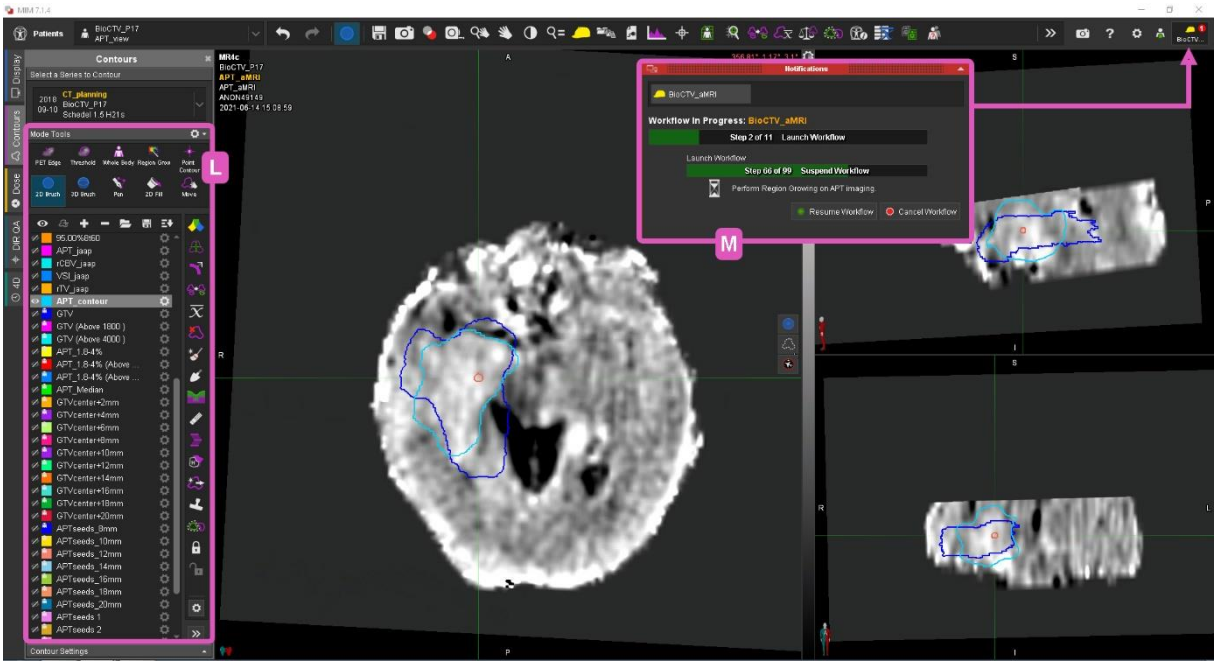

6. Manual adjustment of the *APT_contour (light blue)* can be performed in this step. The user can opt to include or exclude regions using tools in *Mode Tools* ***(L),*** e.g. with *2D Brush.*

7. When the high-risk region of the APT contour is accepted, select *Resume Workflow* in the *Notifications bar* ***(M).***

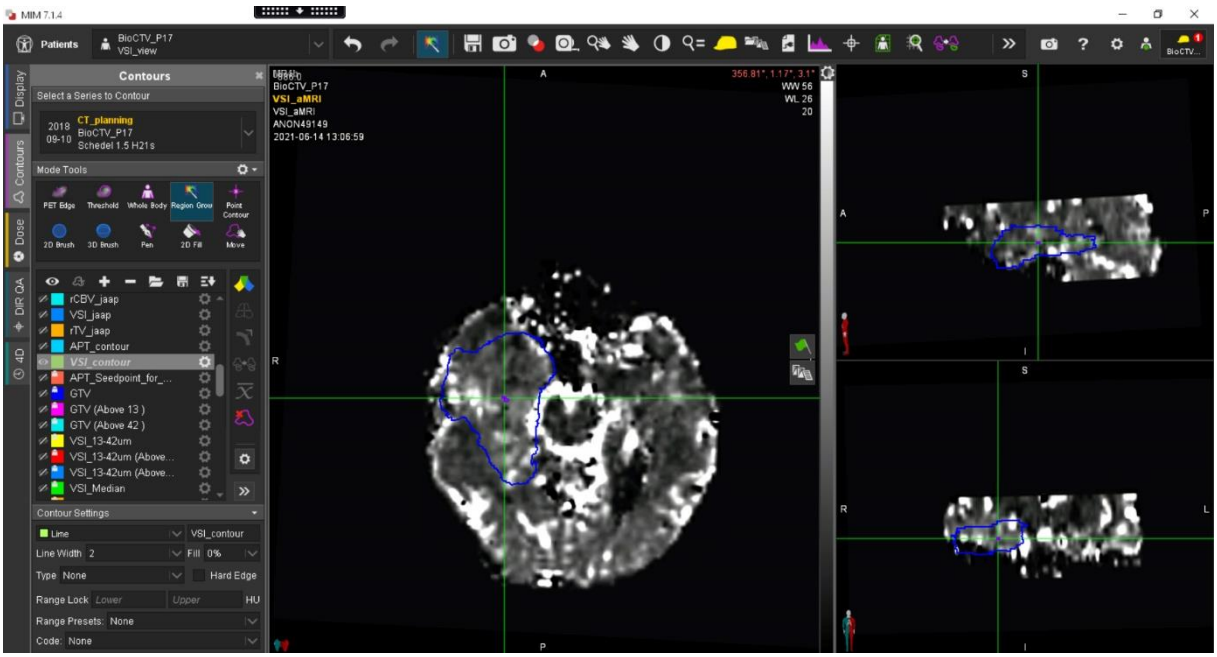

8. Repeat the steps from *Step 3 (1 - 7)* on the VSI map.

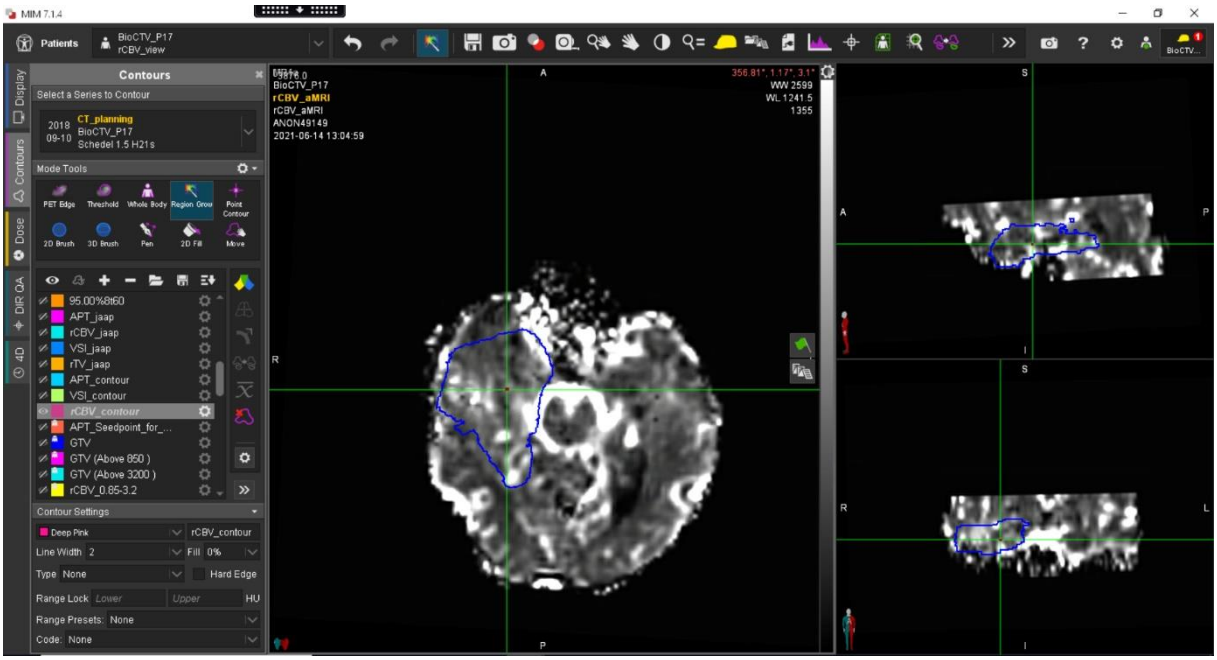

9. Repeat the steps from *Step 3 (1 - 7)* on the rCBV map.

4. Biological CTV generation

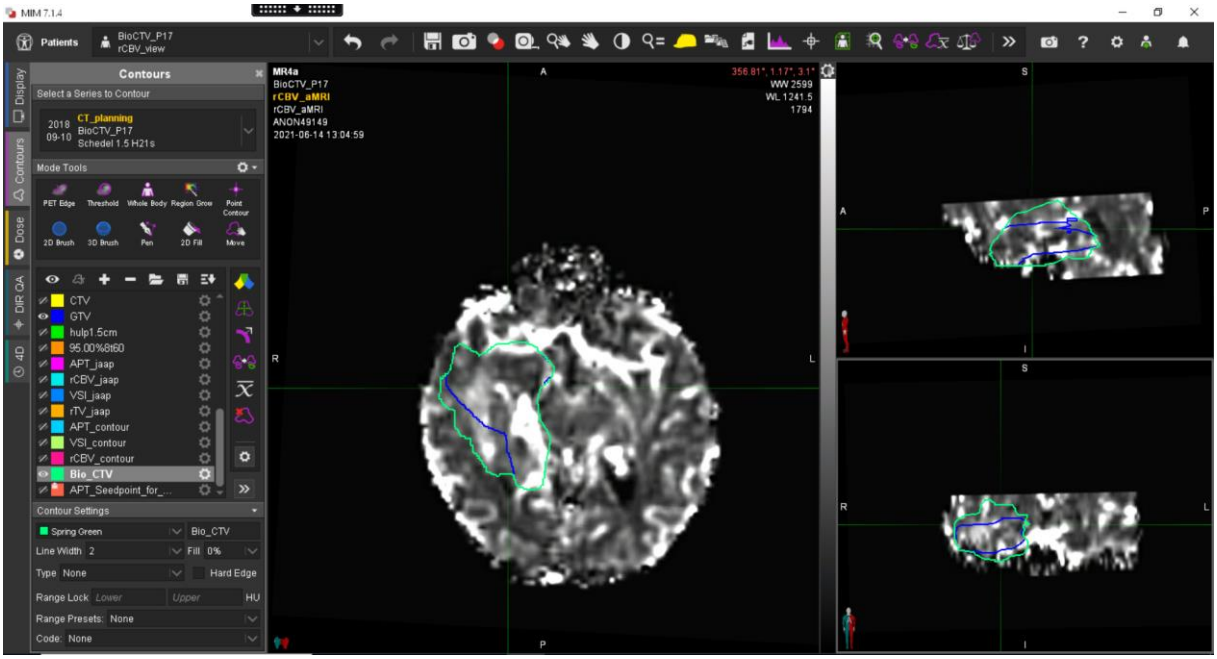

A biological CTV has been automatically created by union of the *GTV, APT_contour, VSI_contour* and *rCBV_contour.*

1. On the conventional MR imaging (T1-weighted, T2/FLAIR), the user can now further adjust the *Bio_CTV* for anatomical barriers or organs at risk as would be done in the conventional workflow.

A. Readjusting the cursor to the seed point location

Goal: To manually redirect the cursor to the correct seed point location for region growing.

> *Note The images used in this section show the APT maps. The steps to readjust the cursor for VSI and rCBV are similar as the steps presented in this section.*

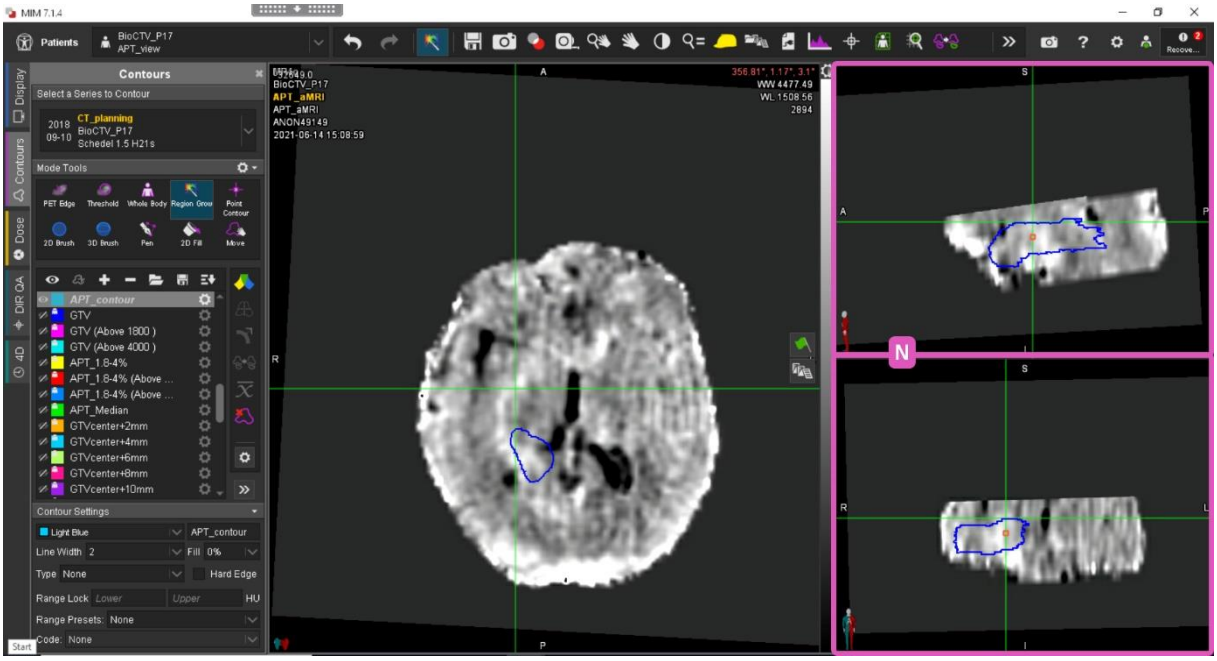

This step shows how to readjust the cursor to the automatically selected seed point if the slice has been changed (e.g. after scrolling). As can be seen on the sagittal and frontal view of the example above, the cursor has been moved in craniocaudal direction ***(N)***.

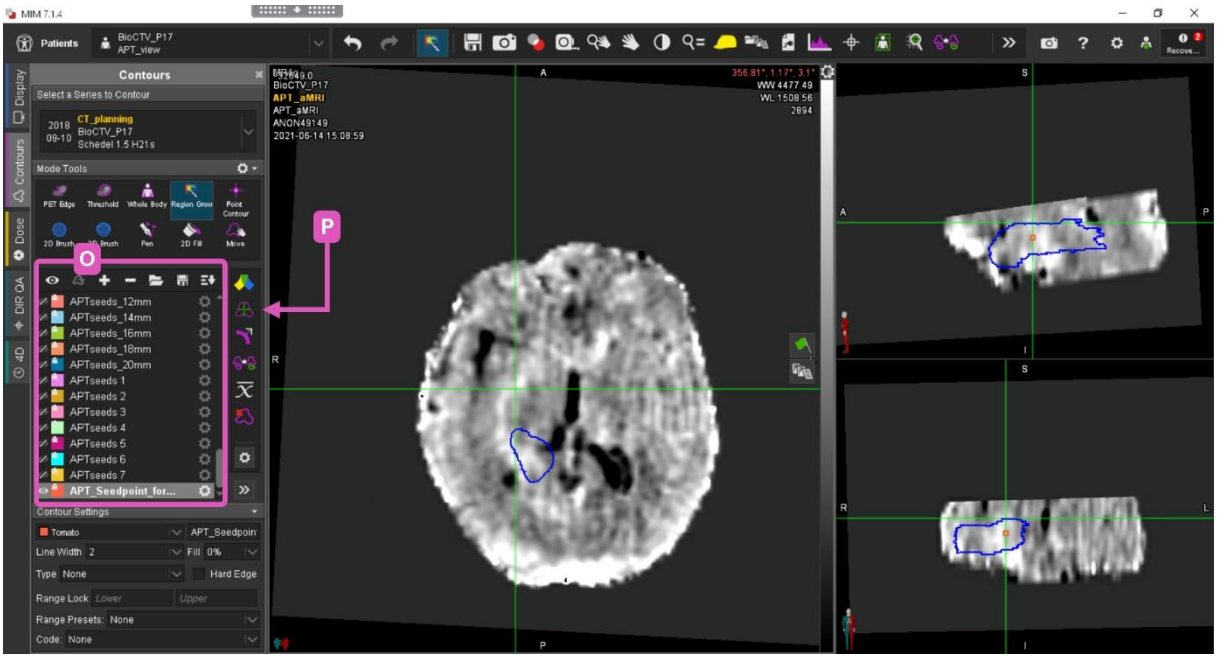

1. In the *Contour overview* ***(O)***, find and select the contour named *APT_Seedpoint_for_Region_Growing.*

   Note: On the VSI or rCBV map, select *VSI_Seedpoint_for_Region_Growing* or *rCBV_Seedpoint_for_Region_Growing*, respectively.

2. Select *Localize to Contour Centroid*  ***(P)***.

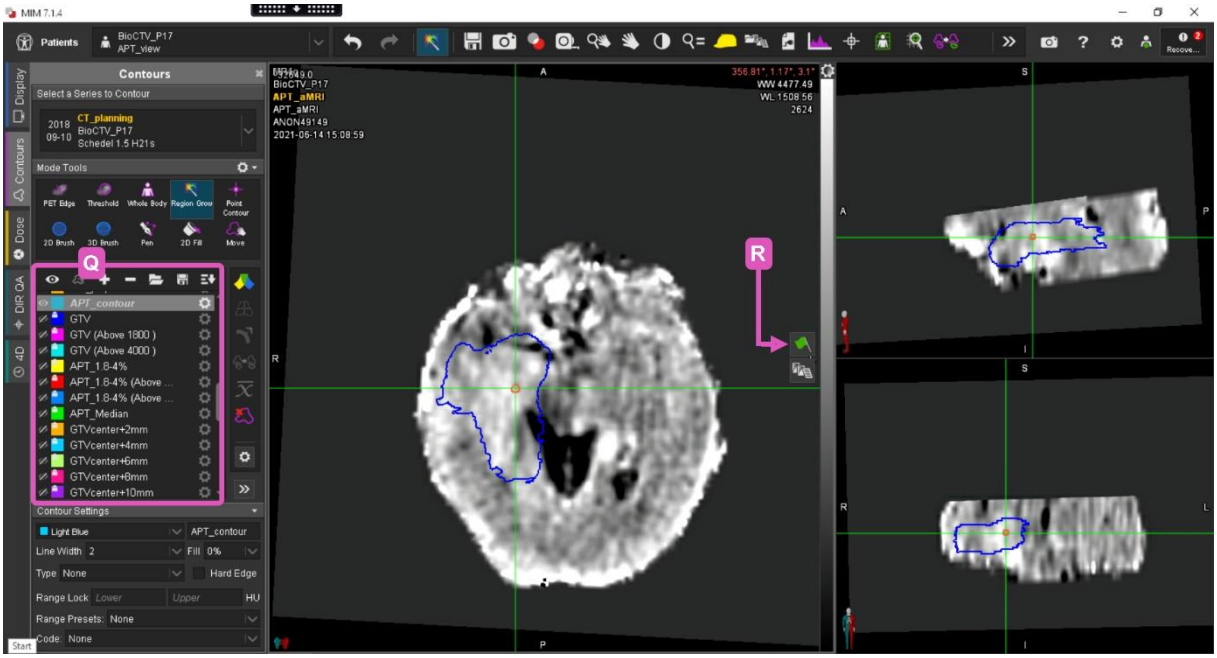

3. In the *Contour overview* ***(Q)****,* select *APT_contour.*

   Note: On the VSI or rCBV map, select *VSI_contour* or *rCBV_contour*, respectively.

4. Now, the cursor point at the correct seed point and the user can continue with *Step 3 (1) Start Region Grow at Localization Point*  ***(R)****.*

5. After manual adjustment (if needed), the user can select *Resume Workflow* in the *Notifications bar* to move on to the next step of the workflow.

B. Using region growing templates

Goal: To use templates with fixed input parameters for region growing to minimize human error and improve time-efficiency.

Step B can be used as an alternative for *Step 3*, but requires a region growing template to be already saved *(see Step 3).*

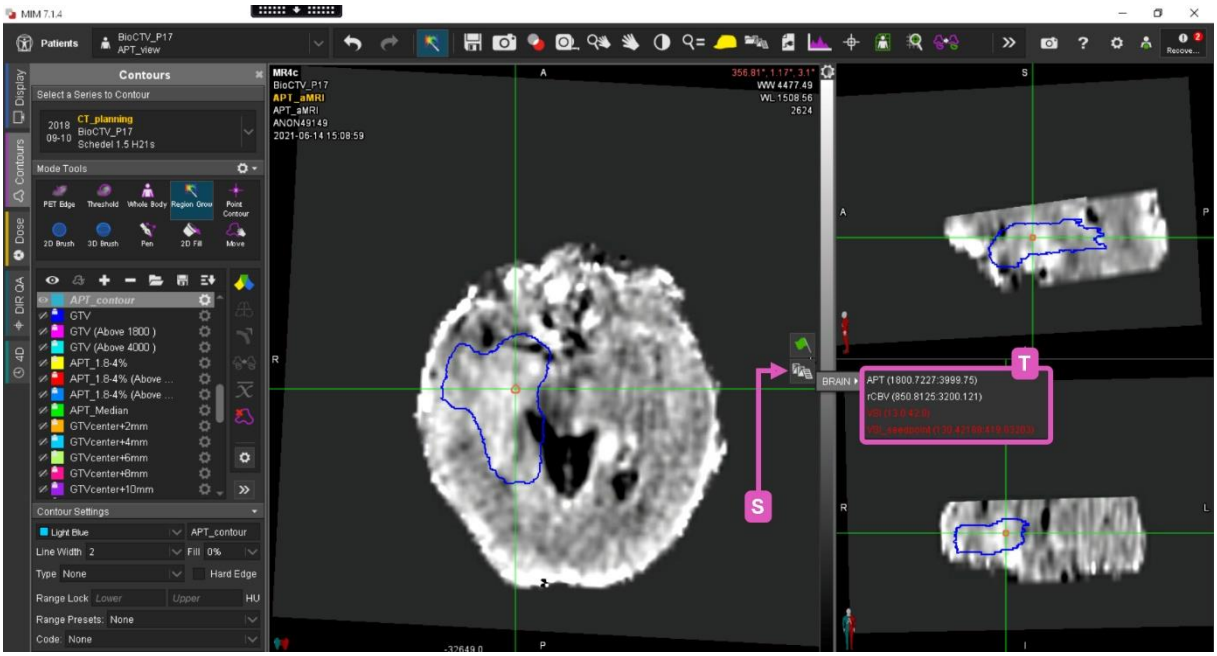

1. Select *Load Region Growing Templates*  ***(S)***

2. In the *pop-up window* ***(T),*** choose the fitting template (in this case APT).

3. Drag the *Region of Interest Box* ***(U)*** in such way that it covers the entire brain in all three views.

Note: The seed point for the region growing algorithm has now already been selected. Therefore, it is possible to scroll through the three views to ensure the entire brain is covered.

Note: As can be seen on the sagittal and frontal view, the APT map does not show the entire brain in craniocaudal direction. This is a result of the advanced MR technique requiring a volume of interest.

4. Select *Finish Region Grow* ***(V)*** and select *Done.*

Appendix F: Size comparison of the GTV, biological CTV and conventional CTV

Table F1: An overview of the (differences in) sizes of the GTV, biological CTV and conventional CTV.

Patient	Volume GTV [cc]	Volume biological CTV [cc]	Volume conventional CTV [cc]	Size difference [cc]	Size reduction of the CTV [%]
1	21.6	31.1	178.3	147.2	82.6
2	53.1	104.5	241.4	136.9	56.7
3	56.0	89.9	218.1	128.2	58.8
4	71.8	71.8	205.7	133.9	65.1

Appendix G: Dice similarity coefficients of the individual biomarkers.

Table G1: An overview of the DS between the individual high-risk regions contoured by the region growing algorithm.

Patient	$DS_{APT,VSI}$	$DS_{APT,rCBV}$	$DS_{VSI,rCBV}$
1	n/a	n/a	n/a
2	0.45	0.47	0.75
3	0.58	0.57	0.72
4	n/a	n/a	n/a

Appendix H: Coverage of the recurrence volume by the individual biomarkers.

Table H1: The distribution of the RV for each patient.

	Patient 1	**Patient 2**	**Patient 3**	**Patient 4**
1) GTV	93.0%	73.5%	46.6%	95.4%
2a) APT	2.0%	8.1%	1.7%	0.0%
2b) VSI	0.0%	0.2%	1.0%	0.0%
2c) rCBV	0.0%	4.4%	1.8%	0.0%
2d) APT + VSI	0.0%	0.1%	0.3%	0.0%
2e) VSI + rCBV	0.0%	5.8%	0.8%	0.0%
2f) APT + rCBV	0.0%	2.5%	0.7%	0.0%
2g) APT + VSI + rCBV	0.0%	0.7%	4.4%	0.0%
3) Not covered by the biological CTV	5.0%	4.8%	42.7%	4.6%
Total rTV	**100%**	**100%**	**100%**	**100%**

Table H2: The coverage of the individual biomarkers of the regions of the RV that go beyond the GTV. Note that the total can exceed 100%; this is due to the possibility of regions that fall within multiple biomarkers.

	Patient 1	**Patient 2**	**Patient 3**	**Patient 4**
APT	29.2%	43.0%	13.3%	0%
VSI	0%	25.4%	12.2%	0%
rCBV	0%	50.2%	14.4%	0%

Appendix I: Validation of the region growing algorithm.

Table I1: Comparison of the coverage of the RV by the manually delineated biological CTV and the biological CTV generated with the workflow.

	Coverage biological CTV (workflow)	Coverage biological CTV (manual)
Patient 1	95%	94%
Patient 2	95%	91%
Patient 3	57%	62%
Patient 4	95%	95%